

Inaugural dissertation
for
obtaining the doctoral degree
of the
Combined Faculty of Mathematics, Engineering and Natural Sciences
of the
Ruprecht - Karls - University
Heidelberg, Germany.

Presented by,
M.Sc., Opeyemi Ernest Oludada
Born in: Ikere Ekiti, Ekiti State, Nigeria.
Oral examination: 14th March, 2023.

**Characterization of human antibodies against
Plasmodium falciparum circumsporozoite protein
(PfCSP) epitopes**

Referees:

Prof. Dr. F. Nina Papavasiliou

Prof. Dr. Hedda Wardemann

DECLARATION

I hereby declare that this thesis is my original work and has not been submitted for examination or award of a degree at any other educational or degree-awarding institution. I further declare that all experiments, unless stated otherwise, were performed by me using the indicated resources between October 2018 and December 2022, in the laboratory of Prof. Dr. Hedda Wardemann, Division of B-Cell Immunology, German Cancer Research Centre (DKFZ), Heidelberg, Germany.

Heidelberg, 09/01/2023

Opeyemi Ernest Oludada

SUMMARY

Plasmodium falciparum malaria, a mosquito-borne, unicellular parasitic disease, remains a major health concern, particularly in the sub-Saharan Africa. Despite many attempts to develop effective malaria vaccines in recent decades, only one vaccine (RTS,S/AS01) targeting the pre-erythrocytic stage of the *Plasmodium falciparum* life cycle, has passed the Phase III clinical trial. However, the protective efficacy of this vaccine is low, and the protection is not long-lasting. Thus, a deeper understanding of the immune responses elicited by currently available vaccines and the identification of protective and non-protective B-cell epitopes are essential for the development of next-generation vaccine candidates that will elicit a robust and long-lasting humoral immune response against protective epitopes while avoiding the induction of non-protective antibodies. The vast majority of pre-erythrocytic malaria vaccines elicit antibodies that primarily target the *Plasmodium falciparum* circumsporozoite protein (PfCSP), a major protein on the surface of sporozoites with a basic structure consisting of the N-terminus (N-CSP), the junction (N-Junc), the central repeat motifs, and the C-terminus (C-CSP), which comprises a linker (C-linker) and a structured α -TSR subdomain that hosts almost all PfCSP T cell epitopes. While antibodies targeting the central repeat with or without cross-reactivity to the N-Junc or C-CSP have attracted much interest due to their promising protective capacity, little is known about the molecular dynamics, fine epitope specificity and the overall protective efficacy of antibodies specific for the N-Junc or the C-CSP domain.

To address these questions, I analyzed a large collection of human monoclonal antibodies (mAbs) against the N-Junc and C-CSP domains using a high-throughput single-cell immunoglobulin (Ig) gene repertoire analysis, following a three-dose immunization with *Plasmodium falciparum* radiation-attenuated sporozoites (*Pf* RAS). The naïve human B cell repertoire contains numerous anti-N-Junc and anti-C-CSP antibodies that undergo efficient affinity maturation and IgG class-switching, providing an explanation for the high immunogenicity of the N-Junc and C-CSP domains. Specificities for the N-Junc and C-CSP epitopes were found in both germline and mutated mAbs, and were frequently encoded by *IGHV3-23/IGLV1-47* and *IGHV3-21/IGLV3-1* or *IGLV3-21* gene combinations, respectively. With the exception of one mAb that recognized the C-linker subdomain, all C-CSP specific mAbs targeted the α -TSR subdomain, demonstrating the immunodominance of the α -TSR subdomain. However, while the N-Junc-specific mAbs showed a lower *Plasmodium falciparum* parasite inhibitory capacity than the cross-reactive mAbs, none of the C-CSP-specific mAbs showed parasite inhibition, regardless of their affinity, gene usage, and epitope specificity. Direct comparison of these antibodies in mice

showed that protection from blood stage parasitemia was limited only to C-CSP reactive mAb that cross-reacted with the central repeat domain and N-Junc.

Taken together, these findings highlight the molecular features associated with N-Junc and C-CSP specific antibodies at B cell repertoire level and provide supportive evidence that antibodies elicited specifically against the C-CSP domain, whether through natural malaria exposure or vaccine immunization, will not contribute to protection. Hence, to develop a broadly effective PfCSP-based subunit vaccine against *Plasmodium falciparum* malaria, careful consideration must be given to whether integrating the C-CSP domain into PfCSP-based immunogens is the optimal means of delivering T-cell epitopes. Instead, vaccine design should focus on the N-Junc and the conserved central repeat domains to elicit robust and cross-neutralizing antibodies.

ZUSAMMENFASSUNG

Malaria, eine durch den einzelligen Parasit *Plasmodium falciparum* verursachte Krankheit, ist nach wie vor ein großes Gesundheitsproblem, insbesondere in Afrika südlich der Sahara. Trotz zahlreicher versuche, in den letzten Jahrzehnten wirksame Malaria-Impfstoffe zu entwickeln, hat nur ein Impfstoff (RTS,S/AS01), der auf das prä-erythrozytäre Stadium des *Plasmodium falciparum* Lebenszyklus abzielt, die klinische Prüfung der Phase III bestanden. Die Schutzwirkung dieses Impfstoffes ist jedoch gering, und der Schutz ist nicht von langer Dauer. Daher sind ein tieferes Verständnis der durch die derzeit verfügbaren Impfstoffe ausgelösten Immunreaktionen und die Identifizierung von schützenden und nicht schützenden B-Zell-Epitopen für die Entwicklung von Impfstoffkandidaten der nächsten Generation unerlässlich. Dabei ist das Ziel eine robuste und langanhaltende humorale Immunreaktion gegen schützende Epitope auszulösen und gleichzeitig die Induktion von nicht schützenden Antikörpern zu vermeiden. Die überwiegende Mehrheit der prä-erythrozytären Malaria-Impfstoffe löst Antikörper aus, die in erster Linie gegen das *Plasmodium falciparum* circumsporozoite Protein (PfCSP), gerichtet sind ein Hauptprotein auf der Oberfläche von Sporoziten. Dieses weist eine Grundstruktur auf, die aus dem N-terminus (N-CSP), der Kreuzung (N-Junc), den zentralen Wiederholungsmotiven und dem C-terminus (C-CSP) besteht, wobei der linker (C-Linker) und eine strukturierte α -TSR-Subdomäne fast alle T-Zell-Epitope des PfCSP beinhaltet. Während Antikörper, die auf die zentrale Wiederholung mit oder ohne Kreuzreaktivität zum N-Junc oder C-CSP abzielen, aufgrund ihrer vielversprechenden Schutzwirkung auf großes Interesse gestoßen sind, ist nur wenig über die molekulare Dynamik, die feine Epitopspezifität und die allgemeine Schutzwirkung von Antikörpern bekannt, die für das N-Junc- oder das C-CSP-Epitop spezifisch sind.

Um diese Fragen zu klären, habe ich eine große Sammlung menschlicher monoklonaler Antikörper (mAbs) gegen die N-Junc- und C-CSP-Epitope mit Hilfe einer hochdurchsatz-einzelzell-Immunglobulin (Ig)-Genrepertoireanalyse nach einer dreifach-immunisierung mit strahlenabgeschwächten Sporoziten von *Plasmodium falciparum* (Pf RAS) analysiert. Das naive menschliche B-Zell-Repertoire enthält zahlreiche Anti-N-Junc- und Anti-C-CSP-Antikörper, die eine effiziente Affinitätsreifung und einen IgG-Klassenwechsel durchlaufen, was eine Erklärung für die hohe Immunogenität der N-Junc- und C-CSP-Domänen liefert. Spezifitäten für die N-Junc- und C-CSP-Epitope wurden sowohl in keimbahn- als auch in mutierten mAbs gefunden und wurden häufig von den Genkombinationen *IGHV3-23/IGLV1-47* bzw. *IGHV3-21/IGLV3-1* oder *IGLV3-21* kodiert. Mit Ausnahme einer mAb, die die C-Linker-Subdomäne erkannte, zielten alle C-CSP-spezifischen mAbs auf die α -TSR-Subdomäne ab, was die Immundominanz und Immunogenität der α -TSR-Subdomäne belegt.

Während jedoch die N-Junc-spezifischen mAbs eine geringere Hemmwirkung auf *Plasmodium falciparum*-parasiten zeigten als die kreuzreaktiven mAbs, zeigte keiner der C-CSP-spezifischen Antikörper eine Parasitenhemmung, unabhängig von ihrer Affinität, Genverwendung und Epitopspezifität. Ein direkter Vergleich dieser Antikörper in Mäusen zeigte, dass der Schutz vor Parasitämie im Blutstadium nur auf die C-CSP-reaktiven mAb beschränkt war, die mit der zentralen Wiederholungsdomäne und N-Junc kreuzreagierten.

Insgesamt unterstreichen diese Ergebnisse die molekularen Merkmale, die mit N-Junc- und C-CSP-spezifischen Antikörpern auf der Ebene des B-zell-repertoires assoziiert sind, und liefern stützende beweis dafür, dass Antikörper, die spezifisch gegen die C-CSP-domäne gebildet werden - sei es durch natürliche Malariaexposition oder Impfstoffimmunisierung - nicht zum Schutz beitragen. Um einen breit wirksamen PfCSP-basierten Untereinheiten-impfstoff gegen *Plasmodium falciparum* Malaria zu entwickeln, muss sorgfältig geprüft werden, ob die Integration der C-CSP-domäne in PfCSP-basierte immunogene das optimale Mittel zur Bereitstellung von T-Zell-Epitopen ist. Stattdessen sollte sich das Impfstoffdesign auf die N-Junc- und die konservierten zentralen Wiederholungsdomänen konzentrieren, um robuste und kreuzneutralisierende Antikörperantworten hervorzurufen.

TABLE OF CONTENTS

DECLARATION	1
SUMMARY	2
ZUSAMMENFASSUNG	4
LIST OF FIGURES	9
LIST OF TABLES	10
LIST OF ABBREVIATIONS	11
1.0 INTRODUCTION	15
1.1 Malaria: a global endemic disease.....	15
1.2 The life cycle of <i>Plasmodium falciparum</i> parasite	16
1.3 Immune response to <i>Plasmodium falciparum</i> malaria infection.....	17
1.3.1 Targeting the erythrocytic stage of <i>Plasmodium falciparum</i> malaria	17
1.3.2 Targeting the pre-erythrocytic stage of <i>Plasmodium falciparum</i> malaria.....	18
1.4 <i>Plasmodium falciparum</i> circumsporozoite protein (PfCSP): a major pre-erythrocytic stage antigen	19
1.4.1 PfCSP structure and functions	19
1.5 Recent advances in vaccines and monoclonal antibodies against PfCSP.....	20
1.6 B cell mediated immune response.....	22
1.6.1 Generation of B cell receptor (BCR)	22
1.6.2 Memory B cells	23
1.6.3 Antibody structure and functions	25
1.6.4 Human antibody repertoire diversity	26
2.0 STUDY OBJECTIVES	27
3.0 MATERIALS AND METHODS	28
3.1 Materials.....	28
3.1.1 ELISA capture and standard antibodies	28
3.1.2 ELISA secondary antibodies	28
3.1.3 FACS analysis antibodies & reagents	28
3.1.4 Recombinant mAbs used as controls	28
3.1.5 Antigens.....	28
3.1.6 Bacteria.....	29
3.1.7 Bacterial culture media and supplements.....	29
3.1.8 Chemicals, Buffers and Solutions.....	29
3.1.9 Cell lines	31
3.1.10 Cell culture media	31
3.1.11 Commercial kits.....	32

3.1.12 Enzymes and additives	32
3.1.13 Expression vectors.....	32
3.1.14 Nucleotides and nucleic acids	32
3.1.15 Instruments and consumables.....	32
3.1.16 Softwares	34
3.1.17 Web Resources.....	34
3.2 Methods	35
3.2.1 Human malaria immunization trial	35
3.2.2 Fluorescence-activated single-cell sorting (FACS)	35
3.2.3 cDNA synthesis from single cells by the Reverse Transcription-Polymerase Chain Reaction (RT-PCR).....	37
3.2.4 Human Ig gene transcripts amplification using semi-nested PCR.....	38
3.2.5 Next generation sequencing (NGS) of amplified human Ig gene transcripts	40
3.2.6 Sequence analysis of human Ig genes.....	41
3.2.7 Ig gene cloning and recombinant antibody expression	41
3.2.8 Specific PCR amplification of Ig genes.....	41
3.2.9 Purification of specific PCR products.....	42
3.2.10 Competent bacteria preparation	42
3.2.11 Eukaryotic expression vector preparation and <i>E. coli</i> transformation.....	43
3.2.12 Cloning vector and PCR amplicon restriction endonuclease digestion	43
3.2.13 Ligation and Transformation.....	44
3.2.14 Screening of successful bacterial colonies by PCR and Sanger sequencing.....	45
3.2.15 Sanger sequencing and colony PCR sequence analysis.....	46
3.2.16 Preparation/Purification of vector DNA (Plasmid preparation)	46
3.2.17 Expression of recombinant monoclonal antibodies.....	46
3.2.18 Recombinant monoclonal antibody purification	47
3.2.19 Reactivity and binding profile of monoclonal antibodies.....	47
3.2.20 Surface Plasmon Resonance (SPR)	50
3.2.21 Statistical analysis.....	50
4.0 RESULTS	51
4.1 Human malaria immunization trial and sample collection.....	51
4.2 Quality of anti-PfCSP serum antibody response after <i>Plasmodium falciparum</i> (<i>Pf RAS</i>) immunization	52
4.2.1 Strong anti-PfCSP serum antibody response	52
4.2.2 <i>Pf RAS</i> immunization induces strong anti-N-Junc, NANP, and C-CSP antibodies.....	53
4.3 B cell memory against PfCSP in response to <i>Pf RAS</i> immunization	54
4.3.1 <i>Pf RAS</i> immunization induces strong anti-PfCSP memory response.....	54

4.3.2 Immune cell sorting and amplification of Ig gene heavy and light chains	55
4.4 Ig gene characteristics of PfCSP reactive memory B cells and plasmablasts	56
4.4.1 PfCSP-reactive memory B cells are dominated by IgM	56
4.4.2 Somatic hypermutation (SHM) in PfCSP-reactive MBCs and plasmablasts.....	57
4.4.3 PfCSP-reactive memory B cells undergo clonal expansion following <i>Pf</i> RAS immunization.....	58
4.4.4 Strong enrichment of <i>IGH3-33</i> and <i>IGHV3-21</i> gene segments in PfCSP-reactive memory B cells	60
4.5 Reactivity, epitope specificity and functional characterization of PfCSP reactive MBCs monoclonal antibodies (mAbs)	61
4.5.1 PfCSP-reactive mAbs target N-Junc, NANP and C-CSP epitopes	62
4.5.2 Determination of the relative affinity of epitope-specific and cross-reactive mAbs	63
4.6 Affinity maturation, sub-epitope and strain specificity of C-CSP specific mAbs	65
4.6.1 Affinity maturation of VH3-21 mAbs is aided by threonine selection in the HCDR1. ..	65
4.6.2 C-CSP specific mAbs preferentially target distinct epitopes in the α -TSR sub-subdomain of C-CSP	66
4.6.3 C-CSP specific mAbs exhibit limited cross-reactivity	68
4.7 Protective capacity of N-Junc, C-CSP and cross-reactive mAbs.....	69
4.7.1 N-Junc and C-CSP specific mAbs showed poor parasite inhibitory capacity	69
5.0 DISCUSSION.....	72
5.1 Serum antibodies and memory B-cells generated after <i>Pf</i> RAS immunization	72
5.2 Signs of germinal center selection in PfCSP-reactive memory B cells	73
5.3 Enrichment of affinity-mature <i>IGHV3-33</i> and <i>IGHV3-21</i> encoded Ig genes in PfCSP-reactive memory B cells.....	74
5.4 PfCSP reactive mAbs preferentially target the C-CSP domain.....	75
5.5 Naïve human B cells contain numerous C-CSP-specific mAbs encoded by <i>IGHV3-21</i> gene segment.	76
5.6 C-CSP specific mAbs bind novel epitopes and exhibit limited cross-reactivity to other <i>Plasmodium falciparum</i> strains.	77
5.7 V λ 1-47/VH3-23 mAbs are highly reactive against the N-Junc.....	78
5.8 Antibody cross-reactivity to the N-Junc is mediated by affinity to NANP repeat	79
5.9 Efficient parasite inhibition is limited to PfCSP mAbs with dual-specificity for NANP, N-Junc and/or C-CSP domain.	79
6.0 OUTLOOK.....	82
7.0 REFERENCES	83
8.0 SUPPLEMENTARY DATA	94
9.0 ACKNOWLEDGEMENT	119

LIST OF FIGURES

Figure 1: <i>Plasmodium falciparum</i> life cycle.	17
Figure 2: Schematic representation of PfCSP (NF54 strain).....	20
Figure 3: Recombination of immunoglobulin heavy and light chains.....	23
Figure 4: B cell-mediated immune response	24
Figure 5: Schematic representation of an IgG1 antibody structure.	26
Figure 6: Schematic representation of the human malaria vaccine immunization trial (MAVACHE verification phase).....	51
Figure 7: Immunization with <i>Pf</i> RAS induces strong anti-PfCSP response.....	52
Figure 8: Strong antibody response against the N-Junc, NANP ₅ , and C-CSP domains.....	53
Figure 9: Strong induction of PfCSP-reactive MBCs in <i>Pf</i> RAS immunized volunteers.....	55
Figure 10: Ig gene sequence efficiency.....	56
Figure 11: Isotype distribution in PfCSP-reactive MBCs and plasmablasts.	57
Figure 12: <i>IGHV</i> somatic hypermutation (SHM) counts in PfCSP MBCs and plasmablasts.....	58
Figure 13: Clonal expansion in PfCSP-reactive MBCs and plasmablasts.....	59
Figure 14: <i>IGHV</i> gene usage in PfCSP-reactive MBCs and plasmablasts.....	61
Figure 15: ELISA binding profiles of PfCSP-reactive MBCs mAbs.	63
Figure 16: SPR affinity profiles of PfCSP reactive mAbs.	64
Figure 17: Gene segments associated with N-Junc and C-CSP specificity.	65
Figure 18: Threonine selection at position 33 of the HCDR1 in VH3-21 mAbs enhances affinity maturation.....	66
Figure 19: Epitope fine-specificity of C-CSP specific mAbs.....	68
Figure 20: Cross-specificity of C-CSP specific mAbs.	69
Figure 21: Protective capacities of N-Junc specific, C-CSP specific, and cross-reactive mAbs. 71	

LIST OF TABLES

Table 1: Antibody dilutions for flow cytometry cell staining	36
Table 2: Reagent concentrations used in the sort RHP mix per well	37
Table 3: RT master mix reagent concentrations per well for RT-PCR	37
Table 4: RT-PCR thermocycler program for reverse transcription of Ig gene transcripts	38
Table 5: Concentration of reagents for primary (1 ^o) semi-nested PCR reaction mix	39
Table 6: Secondary (2 ^o) semi-nested PCR reaction mix reagent concentration	39
Table 7: PCR thermocycler conditions for primary and secondary semi-nested PCR reaction mix	40
Table 8: Specific PCR reagent concentrations per well	42
Table 9 : Reagent volumes and concentrations per reaction for vector restriction digestion	44
Table 10: Reagent volumes and concentrations per reaction for restriction digestion of purified Ig genes.....	44
Table 11: Ligation reagent concentrations used per reaction	45
Table 12: Concentration of colony PCR reagents used per reaction	45
Table 13: Thermocycler conditions for colony PCR.....	46

LIST OF ABBREVIATIONS

7AAD	7-Aminoactinomycin D
ABTS	2,2'-azino-bis (3-ethylbenzthiazoline-6- sulphonic acid
AID	Activation-induced cytosine deaminase
Amp	Ampicillin
AmpR	Ampicillin resistance
AUC	Area under curve
B cell	Bone marrow derived cell
BCR	B cell receptor
BM	Bone marrow
bp	Base pairs
BSA	Bovine serum albumin
CaCl ₂	Calcium chloride
C-CSP	C-terminus of <i>Plasmodium falciparum</i> circumsporozoite protein
CD	Cluster of differentiation
cDNA	Complementary DNA
CDR	Complementarity determining region
CHMI	Controlled human malaria infection
CIP	Calf intestine phosphatase
CMV	Cytomegalovirus
CO ₂	Carbon dioxide
CSR	Class-switch recombination
C _μ	Constant μ
DAMPS	Danger-associated molecular patterns
ddH ₂ O	Double distilled water
dC	Deoxycytidine
DENV	Dengue virus
DMSO	Dimethyl sulfoxide
DNA	Deoxyribonucleic acid
dNTP	Deoxynucleotide triphosphate

DSB	Double-strand break
DTT	Dithiothreitol
dU	Deoxyuridine
EBV	Epstein-Barr virus
<i>E.coli</i>	<i>Escherichia coli</i>
EDTA	Ethylenediaminetetraacetic acid
EEF	Exoerythrocytic form
ELISA	Enzyme-Linked Immunosorbent Assay
EMBL	European Molecular Biology Laboratory
Fab	Fragment antigen-binding
FACS	Fluorescence-activated cell sorting
Fc	Fragment crystallizable
FcR	Fc receptor
FCS	Fetal calf serum
FDC	Follicular dendritic cell
FITC	Fluorescein isothiocyanate
FL-CSP	Full-length of <i>Plasmodium falciparum</i> circumsporozoite protein
FSC	Forward scatter
FWR	Framework region
GC	Germinal center
GPI	Glycophosphatidylinositol
h	Hour
HBsAg	Hepatitis B surface antigen
HC-04 cells	Human hepatocyte cells
HCDR	Heavy complementary-determining region
HIV	Human Immunodeficiency Virus
HEK cells	Human embryonic kidney cells
HRP	Horseradish peroxidase
HSC	Hematopoietic stem cell
Ig	Immunoglobulin

<i>IGHA</i>	Immunoglobulin heavy locus encoding IgA constant region
<i>IGHC</i>	Immunoglobulin heavy constant region
<i>IGHM</i>	Immunoglobulin heavy locus encoding IgM constant region
<i>IGHG</i>	Immunoglobulin heavy locus encoding IgG constant region
<i>IGHV</i>	Immunoglobulin heavy variable gene segment
i.v.	Intravenous
LB	Lysogeny broth
LPS	Lipopolysaccharide
mAbs	Monoclonal antibodies
MBCs	Memory B cells
MFI	Mean fluorescence intensity
min	Minute
MgCl ₂	Magnesium chloride
MZB	Marginal zone B cells
NANP repeat	Peptide/epitope consisting of asparagine-alanine-asparagine-proline
N-CSP	N-terminus of <i>Plasmodium falciparum</i> circumsporozoite protein
N-Junc	N-terminal junction of <i>Plasmodium falciparum</i> circumsporozoite protein
NK	Natural killer cells
NKT	Natural killer T cells
NGS	Next-generation sequencing
OD	optical density
PAMPS	Pathogen-associated molecular patterns
<i>Pb</i>	<i>Plasmodium berghei</i>
<i>Pb-PfCSP</i>	Transgenic <i>Pb</i> expressing the CSP of <i>Pf</i>
PBMC	Peripheral blood mononuclear cell
PBS	Phosphate-buffered saline
PCR	Polymerase chain reaction
PE	phycoerythrin
PEI	polyetherimide
<i>Pf</i>	<i>Plasmodium falciparum</i>

PFA	Paraformaldehyde
PfCSP	<i>Plasmodium falciparum</i> circumsporozoite protein
<i>Pf</i> SPZ	<i>Plasmodium falciparum</i> sporozoites
<i>Pf</i> RAS	<i>Plasmodium falciparum</i> radiation-attenuated sporozoites
PRRs	Pathogen recognition receptors
RAG	Recombination-activating gene
RHP	Random hexamer primers
RNA	Ribonucleic acid
rpm	Revolutions per minute
RPMI	Roswell Park Memorial Institute (medium)
RSS	Recombination signal sequences
RT	Reverse transcription
RTS,S	R: stands for the central repeat region of <i>Pf</i> CSP; T: stands for the T cell epitopes in the C-terminus of CSP; S: stands for the hepatitis B surface antigen (HBsAg)
sec	Second
SHM	Somatic hypermutations
SPR	Surface Plasmon Resonance
SS	Signal sequence
SSC	Sideward scatter
<i>Taq</i> polymerase	<i>Thermos aquaticus</i> polymerase
T cells	Thymus-derived cells
TCR	T cell receptor
TFH	T follicular helper cells
TSR	Thrombospondin-like type I repeat
VDJ	Variable, Diversity and Junctional segments
VH	Variable heavy chain
VL	Variable light chain
ZIKV	Zika virus

1.0 INTRODUCTION

1.1 Malaria: a global endemic disease

Malaria is a mosquito-borne parasitic disease transmitted to humans through the bite of an infected female *Anopheles* mosquito. It is caused by five *Plasmodium* parasite species: *Plasmodium falciparum*, *Plasmodium vivax*, *Plasmodium ovale*, *Plasmodium malariae*, and *Plasmodium knowlesi*^{12,13}. Of these, *Plasmodium falciparum* (*Pf*), the most common species in Africa, is responsible for most malaria-related deaths globally¹⁴⁻¹⁶. Early symptoms of malaria such as fever, headache, chills, and vomiting occur 7 to 15 days after the infection and, if left untreated, can lead to severe illness, coma, and death¹⁷. Despite the great progress that has been made in combating malaria through the use of various interventions that are now accessible, the disease still poses a significant threat to public health. According to the latest world malaria report, malaria cases increased from 227 million in 2019 to 241 million in 2020, with approximately 627,000 deaths in 2020, an increase of 69,000 from the previous year^{18,19}. The global malaria incidence and mortality rates for 2020 were 59 cases per 1000 people at risk and 15 deaths per 100,000 people at risk, respectively, indicating insufficient progress towards the global technical strategy targets of 35 cases per 1000 and 7.2 deaths per 100,000 people at risk¹⁹. Young children under the age of five bear the brunt of malaria deaths worldwide (67% of all malaria deaths in 2019). According to WHO, 94% of all malaria-related deaths in 2019 occurred in Africa, particularly in sub-Saharan regions²⁰, and many African countries continue to be plagued by the economic hardship of the disease.

Malaria is preventable and treatable through a number of ongoing initiatives. These include the use of insecticide-treated bed nets, chemoprophylaxis, fumigation, and pharmacological therapy. However, the eradication and treatment of malaria is hampered by the alarming increase in resistance to antimalarial drugs and insecticides. In addition to the above measures, the use of vaccines in the fight against malaria disease has been pursued for decades. The RTS,S/AS01 (Mosquirix™) vaccine is currently the only approved malaria vaccine²¹, although other promising candidates such as the recombinant subunit protein vaccine (R21/Matirx-M)^{22,23}, whole *Plasmodium falciparum* sporozoite-based vaccines^{10,24,25}, near full-length *Plasmodium falciparum* circumsporozoite protein vaccine²⁶⁻²⁸, and the blood stage vaccine targeting the *Plasmodium falciparum* reticulocyte-binding protein homolog 5 (*Pf* RH5)^{29,30}, are in pipeline. Although approved, RTS,S/AS01 confers only a short-lived protection paralleling to the rapid decrease of the antibody titers induced over time in malaria-endemic cohorts³¹⁻³⁵. It is

therefore evident that a deeper knowledge of the immune response to malaria is needed for the development of more effective malaria vaccines.

1.2 The life cycle of *Plasmodium falciparum* parasite

The *Plasmodium falciparum* parasite has a complex life cycle involving an alternation between female *Anopheles* mosquitoes and the vertebrate host (humans), as well as sexual and asexual reproduction in the mosquito and human host, respectively³⁶. The parasite is transmitted to humans when an infected female *Anopheles* mosquito feeds on human skin and injects a small number of sporozoites (a freely mobile form of the parasite residing in the salivary glands) into the skin (Figure 1A). The sporozoites quickly enter the bloodstream and migrate to the liver, where they can escape destruction from the host's immune system^{37,38}. Sporozoites that have made it to the liver sinusoids overcome the sinusoidal barrier and invade the hepatocyte³⁸, where they can begin their first differentiation by forming a parasitophorous vacuole³⁹. The sporozoites grow into multinucleate exoerythrocytic forms (schizonts) in the hepatocytes within 2 to several days, and later grow, divide several times and produce thousands of asexual first-generation merozoites (Figure 1B). The merozoites are released into the bloodstream after the infected hepatocytes rupture, resulting in a second asexual schizogony⁴⁰. After 48 hours of exponential replication, the erythrocyte is lysed, releasing new merozoites and pernicious waste products such as the pigment haemozoin (Figure 1C), which in turn triggers the clinical signs of malaria by activating macrophages and other immune cells. The asexual life cycle is maintained when the released merozoites invade new erythrocytes.

The sexual reproductive phase of the cycle begins when some merozoites develop into male and female gametocytes, which are subsequently taken up into the midgut of another female *Anopheles* mosquito during a blood meal^{41,42}. The transmission of gametocytes to mosquitoes is considerably enhanced by the fact that mature gametocytes can circulate in human blood for many days. The male and female gametocytes in the midgut of the mosquito use proteases to break out of the red blood cells and begin to differentiate into the eight microgametocytes and one macrogametocyte that will eventually unite to form the zygote⁴³. To develop into an oocyst, the zygote undergoes metamorphosis into a motile ookinete, which then penetrates the epithelial layer of the midgut wall. In the oocyst, the parasites complete their third cycle of asexual reproduction and release hundreds of sporozoites into the hemolymph⁴⁴. When the sporozoites

reach the salivary gland of a mosquito, they attach themselves to the gland and infect it. They remain there until they are transmitted to a new vertebrate host during a blood meal (Figure 1D).

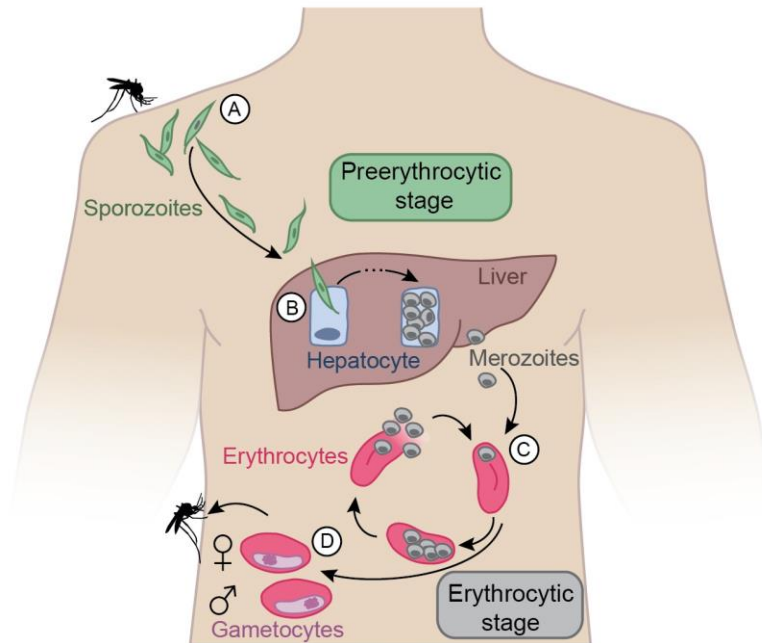


Figure 1: *Plasmodium falciparum* life cycle. (A) Sporozoites are injected into the skin during a blood meal from an infected female *Anopheles* mosquito. (B) The sporozoites invade the hepatocytes of the liver after migrating via the bloodstream. The parasite multiplies and develops into asexual merozoites in the hepatocytes, which then escape from the host cell through a membrane spot and enter the blood. (C) After entering the bloodstream, the merozoites attack erythrocytes, reproduce asexually, lyse the erythrocytes and infect new red blood cells, leading to exponential growth of the parasite and the appearance of malaria symptoms. (D) Male and female gametocytes are formed by the differentiation of some merozoites. When another female *Anopheles* mosquito feeds on an infected host during a blood meal, the gametocytes are taken up and carried to the next stage of their life cycle. Figure adopted from ⁴⁵.

1.3 Immune response to *Plasmodium falciparum* malaria infection

1.3.1 Targeting the erythrocytic stage of *Plasmodium falciparum* malaria

Vaccines targeting the blood stage of malaria aim to prevent the disease, rather than the infection in humans. Although no blood-stage vaccine has yet been licensed, there are a number of promising candidates currently being tested. These include the attenuated whole parasites and recombinant proteins subunit vaccines ⁴⁶. Blood-stage subunit vaccines currently in development primarily target immunodominant merozoite antigens such as the merozoite surface proteins (MSP1, MSP2 and MSP3), and apical membrane antigen 1 (AMA1). However, targeting these proteins have been associated with little or no protection due to the antigenic polymorphisms ⁴⁷⁻⁵². In addition, the reticulocyte-binding protein homolog 5 (*Pf* RH5) antigen has recently been

described as a potential malaria vaccine ²⁹. However, *Pf* RH5 is less immunogenic in natural infection and mediate less protection against malaria ⁵³.

Alternatively, antibodies directed against infected erythrocytes can prevent severe symptoms of clinical malaria ⁵⁴. In order to halt the progression of the asexual erythrocytic stages of *Plasmodium falciparum* life cycle, antibodies must recognize either merozoites or the variant surface antigens displayed in knob-like structures on the surface of infected erythrocytes ⁵⁵⁻⁵⁸. Although adaptive immunity via the antibody response against merozoite antigens probably plays a crucial role in immunity against *Plasmodium falciparum* malaria infection, only a few immunodominant antigens have been thoroughly studied ⁵⁴. Just recently, the first human neutralizing monoclonal antibodies against the blood stage *Pf* RH5 antigen were obtained and structurally characterized ³⁰. These antibodies inhibit the growth of *Plasmodium falciparum* parasite by inhibiting the formation of the *Pf* RH5-CyRPA-*Pf* RIPR complex and preventing *Pf* RH5 from binding to basigin (BSG) ³⁰. These data are strong evidences that epitope mapping and analysis of human monoclonal antibody responses against different erythrocytic stage antigens at the monoclonal level may be crucial for the identification of most promising protective epitopes that could be considered in the development of erythrocytic stage malaria vaccines.

1.3.2 Targeting the pre-erythrocytic stage of *Plasmodium falciparum* malaria

A roadblock in the life cycle of the malaria parasite occurs when the injected sporozoites cannot migrate into the hepatocytes and infect the cells. During a blood meal, about 10 to 100 *Plasmodium falciparum* sporozoites are injected under the skin ⁵⁹. It is hypothesized that even a single surviving *Plasmodium falciparum* sporozoite is sufficient to trigger an infection in the blood ⁶⁰. Thus, one of the hallmarks in the field of malaria vaccine research is to target the immune response to the pre-erythrocytic stage of *Plasmodium falciparum* and eliminate the parasites before reaching the symptomatic erythrocytic stage. More than half a century ago, experiments showed that rodents developed sterile immunity after exposure to sporozoites from infected mosquitoes that had been irradiated ⁶¹. The establishment of the erythrocytic-stage parasites was inhibited by radiation because it reduces the rate at which sporozoites undergo metamorphosis into exoerythrocytic forms and replicate in infected liver cells ^{62,63}. It was later observed that precipitation of a protein expressed on the surface of sporozoites could be mediated by incubating the sporozoites with serum samples from mice vaccinated with *Plasmodium falciparum* radiation-attenuated sporozoites (*Pf* RAS) ^{61,64}. This observation led to the identification of *Plasmodium falciparum* circumsporozoite protein (PfCSP), formerly known as *Pb44*, as the surface protein of

the sporozoites targeted by the antibodies, and causing the precipitation process and active inhibition of the parasites ⁶⁵⁻⁶⁸.

To acquire immunity against *Plasmodium falciparum* malaria parasite by targeting the PfCSP, the immune system must be repeatedly exposed to the parasite, either through natural infection or vaccination with PfCSP based vaccines, as immunity to the infection develops slowly over time ^{69,70}. However, this immunity will probably never develop into sterile immunity ^{54,56,71-73}. The slow acquisition of the natural immunity may be attributed to the poor immunogenicity of the protective epitopes encoded in the PfCSP ^{74,75}, or antigenic variation and degree of genetic polymorphism among strains of *Plasmodium falciparum* parasites ⁷⁶⁻⁷⁹. To develop a wide range of immunity, one must be exposed to different strains of the parasites for many years. Several variables, including the age of the host, the degree of exposure to the parasite and the dose of antigen presented, also influence how quickly immunity against *Plasmodium falciparum* parasites develops ⁸⁰⁻⁸³. Thus, due to the lack of sterile immunity and the resulting delay in the formation of protective natural immunity, there is an urgent need to develop safe and effective vaccines that provide long-term and sterile protection.

1.4 *Plasmodium falciparum* circumsporozoite protein (PfCSP): a major pre-erythrocytic stage antigen

1.4.1 PfCSP structure and functions

The PfCSP of human malaria species is the most abundant protein on the surface of sporozoites. It is encoded by 412 amino acids and consists of the N-terminal domain (N-CSP), which contains a highly conserved KLKQP amino acid motif (region I) that binds to the heparin sulphate proteoglycan during sporozoites adhesion to the hepatocytes ⁸⁴; the junction region (N-Junc), which is characterized by a small number of alternating NANP and NANP-like (KQPA, NPDP, NVDP) amino acid motifs that connect the N-CSP to the central repeats; the central repeat region with conserved repetitive asparagine-alanine-asparagine-alanine (NANP) motifs; and the C-terminal domain (C-CSP) (Figure 2). While the central NANP repeat region has been described to be the immunodominant B cell epitope ^{4,85-87}, the C-CSP domain has a 3D configuration and contains almost all T cell epitopes in PfCSP ^{88,89}. The C-CSP domain comprises a linker subdomain (C-linker) and a structured α -thrombospondin type-1 repeat (α -TSR), a highly polymorphic subdomain that bound to the cell membrane of sporozoites via a glycosylphosphatidylinositol (GPI) anchor, and harbors almost all the T-cell epitopes ^{4,84,88-97}.

Within the α -TSR subdomain of C-CSP are the polymorphic Th2R/Th3R epitopes, and the conserved region II-plus (RII+) ^{90,98} (Figure 2).

PfCSP is responsible for the development of sporozoites in mosquitoes and aids their motility and hepatocyte invasion in the mammalian host ⁹⁹⁻¹⁰⁵. It also promotes the maturation of oocysts and the budding of sporozoites within oocysts, which are both necessary steps in the development of sporozoites in mosquitoes ¹⁰². In addition to its role in hepatocyte invasion, PfCSP also plays a role in host tissue identification and enables sporozoites binding to liver cells in the mammalian host by binding to heparan sulphate proteoglycans (HSPGs) on different cell types ¹⁰⁶. Taken together, these findings highlight the importance of PfCSP in sporozoite motility and human hepatocyte invasion during infection, and underscore the promising role of T and B cell-mediated anti-PfCSP responses in suppressing sporozoite invasion and thus protecting against malaria.

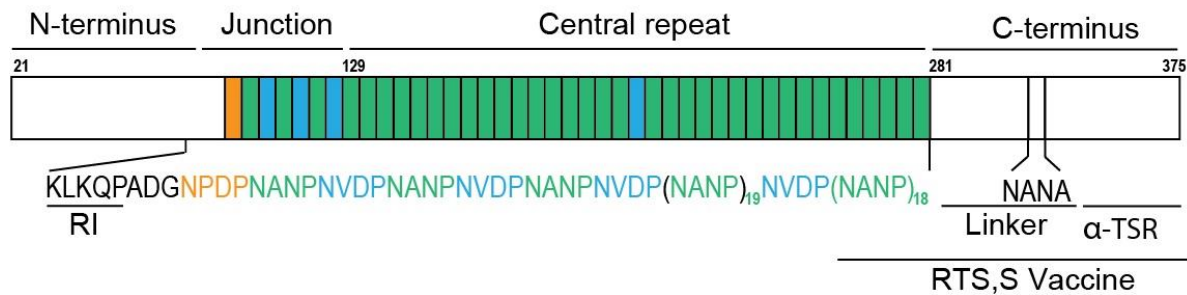


Figure 2: Schematic representation of PfCSP (NF54 strain). The PfCSP comprises of the N-terminal region (N-CSP), the junction (N-Junc), the central NANP repeat motifs (NANP), and the C-terminal (C-CSP) domain. Amino acid sequences of overlapping epitopes in the junction for protective antibodies ^{4,107,108} are represented in stick structures, labelled and colour-coded as NPDP (orange), NVDP (blue) and NANP (green). Epitopes targeted by RTS,S vaccine are underlined. Figure adapted from ⁴

1.5 Recent advances in vaccines and monoclonal antibodies against PfCSP

Pre-erythrocytic vaccine candidates in the clinical phase include radiation-attenuated sporozoites (*Pf* RAS) ^{10,109,110}, live sporozoites under chemoprophylaxis ^{24,111}, genetically attenuated parasites (GAP) ¹¹², nearly full-length recombinant PfCSP vaccine ²⁸ and epitope-based subunit vaccines ^{23,31,113}. Despite the success achieved with *Pf* RAS vaccine, in which the sporozoites have been exposed to random irradiation to enhance DNA damage and prevent them from replicating in the liver ^{10,110,114,115}, the need for exceptionally high numbers of sporozoites and the inability to induce long-term protection has prompted endless research into alternative vaccine development. RTS,S/AS01, the only malaria vaccine recommended by WHO ²¹, and the R21 vaccine ^{22,23,116} which is equivalent to the RTS,S vaccine without the excess of hepatitis B virus surface antigen (HBsAg), are subunit vaccines consisting of two components: 18.5 motifs of the

central NANP repeat and the entire C-terminus of PfCSP fused with HBsAg. However, recent Phase III clinical trials conducted in areas where malaria is endemic have shown that the protective efficacy of RTS,S/AS01 is between 25% and 55%^{31,32,117,118} and does not induce long-term protection¹¹⁷. While the protective efficacy of RTS,S is low and does not elicit a long-lasting memory response, clinical trials are currently being conducted with the R21/Matrix-M vaccine²³. Furthermore, vaccination with live sporozoites under chemoprophylaxis (pyrimethamine or chloroquine prophylaxis) has been shown in animal and human studies to mediate long-lasting protection against malaria infection by stopping the infection at the liver stage and eliminating the asexual parasites as soon as they start replicating in the erythrocytes^{24,25,111,119}. Although complete protection can be achieved with a few sporozoites, this approach is limited by the need to administer antimalarial drugs continuously during vaccination, and also raises serious safety concerns due to the parasites' ability to cause malaria disease. Thus, in light of the ineffectiveness of *Pf* RAS, RTS,S, and other currently available malaria vaccines, there is an urgent need to advance vaccine technology to enhance malaria prevention.

Another novel approach to malaria prevention and treatment is the use of isolated PfCSP-specific monoclonal antibodies (mAbs) as a drug therapy. Recently, recombinant mAbs against PfCSP were obtained from humans immunized with PfCSP-based vaccines^{1,5,8,9,86,107,108,120,121}. Their molecular characterization revealed that most potent anti-PfCSP mAbs showed high affinity and dual specificity (cross-reactive) for the central NANP repeat and the N-Junc, and were encoded by germline or mutated *IGHV3-33* and *IGKV1-5* gene segments with 8 amino acid long in the kappa complementarity determining region 3 (KCDR3)¹²⁰. Interestingly, two high affinity mAbs (CIS43 and L9) with dual specific for the central NANP repeat and the N-Junc, cloned from memory B cells of individuals immunized with *Pf* RAS, mediated sterile protection against malaria in recent human clinical trials^{122,123}. Ongoing research is being conducted with the intention of applying these findings to the formulation of an enhanced PfCSP-based vaccine. In summary, these findings demonstrate the importance of using monoclonal antibodies not only as drug therapy, but also as a template to identify protective and non-protective epitopes that could be included or excluded in the development of next-generation subunit vaccines against malaria.

1.6 B cell mediated immune response

1.6.1 Generation of B cell receptor (BCR)

The B cell antigen receptors (BCRs) are complex membrane-embedded multi-proteins on the surface of B cells that transmit signals important for the survival, differentiation, and activation of B cells in response to antigens. Consequently, humoral immunity may mount an immune response against unlimited array of antigens with radically different structural features. During B cell development in the bone marrow, B cells undergo site-specific somatic V(D)J recombination, a process that allows B cells to assemble complete antigen receptor genes from separately encoded germline variable (V), diversity (D) and junctional (J) segments. The V(D)J segments are randomly recombined into functional immunoglobulin (Ig) heavy (IgH) and Ig light (IgL: kappa (Igκ) or lambda (Igλ)) chains (Figure 3). Recombination begins with the generation of double-strand breaks (DSBs) by the recombination-activating genes (RAG1 and RAG2) at the boundary between variable heavy (VH) and diversity heavy (DH) and their corresponding recombination signal sequences (RSS), which results in the creation of hairpin-sealed coding ends and blunt signal ends^{124,125}. RSS consists of conserved heptamer (essential for recognition element) and nonameric sequences (consensus sequences: 5'-CACAGTG-3' and 5'-ACAAAACC-3', respectively) separated by 12 or 23 less conserved “spacer” nucleotide sequences in the DNA¹²⁶⁻¹²⁸.

Successful recombination of the heavy (*IGHV*, *IGHD* and *IGHJ*), kappa (*IGKV* and *IGKJ*) or lambda (*IGLV* and *IGLJ*) chain results in allelic exclusion, ensuring expression of only the rearranged productive alleles and the formation of BCRs and functional IgH and IgL (Igκ or Igλ) variable genes of a fully developed naive B cells^{129,130}. Furthermore, imprecise recombination of IgH and, to a lesser degree, IgL, have been shown to increase antigen-receptor diversity^{131,132}. Antigen stimulation of naive B cells in the B cell follicles of secondary lymphoid leads to further rounds of immunoglobulin diversification. During diversification and affinity maturation, B cells can undergo class-switch recombination (CSR), somatic hypermutation (SHM) and clonal expansion in their Ig gene sequences during germinal center formation¹³³⁻¹³⁵, which in return promotes antibody affinity maturation and memory B cell formation¹³⁶⁻¹³⁸.

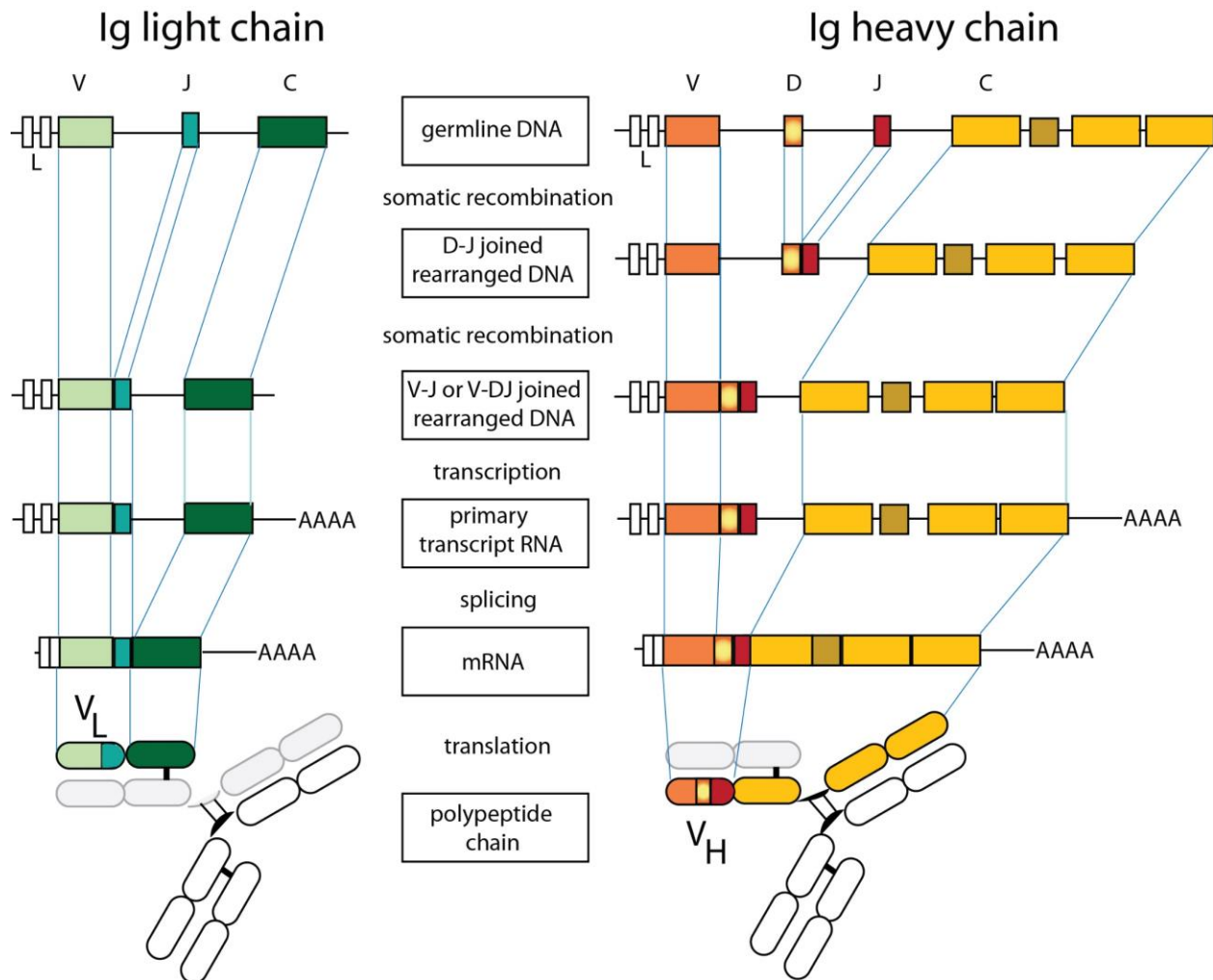


Figure 3: Recombination of immunoglobulin heavy and light chains. During the recombination process of the heavy chain gene locus, two unrelated gene segments, D and J, recombine to form DJ, which then combines with a third unrelated gene segment, V, to form VDJ. Segments of V and J are randomly recombined to generate VJ in the light chain locus. After being sorted out as functional and non-autoreactive, they become the BCRs of a fully developed naive B cell. Figure adopted from ¹³⁹

1.6.2 Memory B cells

Memory B cells (MBCs) are defined as subsets of the total B cell pool that have already been exposed to antigens and have developed antigen-specific BCRs ^{140,141}. Upon antigen recognition and binding, naïve B cells undergo BCR-mediated activation and migrate to the borders of B and T cell follicles in the secondary lymphoid organs, where they form long-lasting interactions with T cells and primed to receive helper signals from their cognate CD4+ T cells (Figure 5A) ^{142,143}. After interacting with T cells, a subset of the B cells migrates to the medullary chords of the lymph nodes, where they differentiate into short-lived, antibody-secreting plasmablasts ¹⁴⁴. The other subset of the activated B cells returns to the follicle, where they can rapidly divide and form the germinal center (GC). During BCR diversification in the dark zone of

the germinal center, the B cells undergo not only somatic hypermutation (SHM) ¹⁴⁵, but also isotype class switching and clonal expansion to increase their affinity for their cognate antigens (Figure 5B) ¹⁴⁶. The existence of clonally expanded and/or clonally related cells within the antigen-specific population is an important indicator of antigen-specific selection ^{147,148}. During clonal expansion, the average affinity of antibodies for antigens increases and the B cells elicit a stronger immune response to the already known antigens. Upon completing the cell cycle in the dark zone, the B cells exit the dark zone and migrate to the light zone, where they are subjected to affinity selection by interacting with the follicular dendritic cells (FDCs) and antigen-specific T follicular helper cells (TFH cells). B cells with high affinity for the cognate antigen proliferate and further differentiate into long-lived, antibody-secreting plasma cells, while others return to the germinal center and become MBCs (Figure 5C) ^{142,143,149}.

Long-lived plasma cells and MBCs are the two major subsets of B cells responsible for immunological memory ¹⁵⁰. While long-lived plasma cells are fully developed antibody-secreting cells that live for years in bone marrow, MBCs are peripherally distributed cells that respond quickly to a re-encounter with the same antigen (Figure 5D) ^{143,151,152,153}. Other features of MBCs include somatic mutation of high affinity B cell receptors which makes them more specific ¹⁵⁴⁻¹⁵⁷.

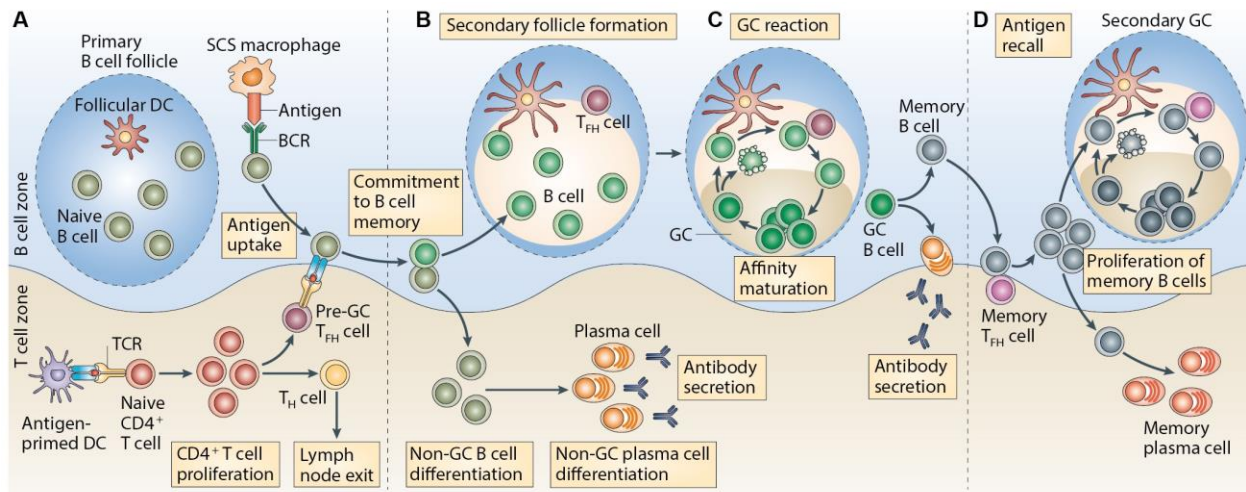


Figure 4: B cell-mediated immune response. (A) Macrophages of the subcapsular sinus (SCS) B cell zone capture all antigen upon antigen exposure or protein vaccination and deliver it to naive follicular B cells. Upon antigen recognition, the B cells become activated, take up the antigen, process it, and present it to the T cells in the draining lymph node. (B) B cell class switching, clonal expansion, and non-GC dependent antibody secreting B cells progress in the lymph nodes' extrafollicular zones. After the secondary follicle is formed, B cells, TH cells, and FDCs congregate to form a germinal center (GC). (C) Affinity maturation of B cells occurs during the GC reaction as a result of Ig gene diversity and selection by FDCs and Tfh cells. B cells undergo terminal differentiation after the GC, becoming either memory B cells or plasma cells that secrete antibodies (D) In the subsequent antigen encounter, memory B and TFH cells might take part, seeding new GCs. Figure adopted from ¹⁴³.

1.6.3 Antibody structure and functions

Antibody, an immunoglobulin (Ig) superfamily and a secreted form of BCR obtained from the splicing of the transmembrane domain of BCR, has similar structural motifs to BCRs and act extrinsically on B cells to enhance their antibody-mediated effector functions. Like BCRs, antibodies consist of two identical IgH and IgL chains covalently linked by disulfide bridges, with an additional disulfide bridge connecting the two heavy chains in the hinge region (Figure 4) ¹⁵⁸⁻¹⁶⁰. The structure of both heavy and light chains consists of variable amino-terminal region and a constant carboxy-terminal region ¹⁶¹⁻¹⁶⁵.

The structure of antibody is divided into two fragments: the antigen-binding fragment (Fab) and the fragment of crystallizable (Fc), each of which serves a different purpose in antibodies interaction with antigens (Figure 5). The effector actions are mediated by the Fc fragment, which binds to the Fc receptor (FcR) expressed on immune and non-immune cells and activates other immune mediators such as the complement system ¹⁶³. The constant region of the light chain in humans can be either kappa (60% of B cells) or lambda (40% of B cells) ¹⁶⁶. In contrast, the constant region of the heavy chain produces different isotypes, including IgD, IgM, IgE, IgA (subclasses 1 and 2), and IgG (subclasses 1-4), each of which is encoded by δ , μ , ϵ , α and γ , constant region genes, respectively ^{167,168}. The IgG1 subclass is the most abundant, followed by IgG2, IgG3, and finally IgG4. Class switch recombination is responsible for the production of IgG, IgA, and IgE, while alternative splicing of a shared parent mRNA transcript of the heavy chain locus is responsible for the expression of IgM and IgD ^{169,170}. IgA may be released as a dimer or a monomer ¹⁷¹, whereas IgM forms pentamers in serum ¹⁷². All other isotypes of antibodies are monomeric ¹⁶⁷. Once an antibody binds to its cognate antigen, the isotype of the antibody determines what the antibody can do next. The binding efficiency of lower-affinity antibodies might benefit greatly from the fact that certain antibody isotypes can multimerize, increasing the number of antigen binding sites and, therefore, their avidity. Sequence variability in heavy and light chain variable domains is centered in three loops called hypervariable regions or complementary-determining regions (CDRs). Each variable domain is composed of three CDRs and four frame-work regions (FWRs), each of which is a less variable-sheet framework area.

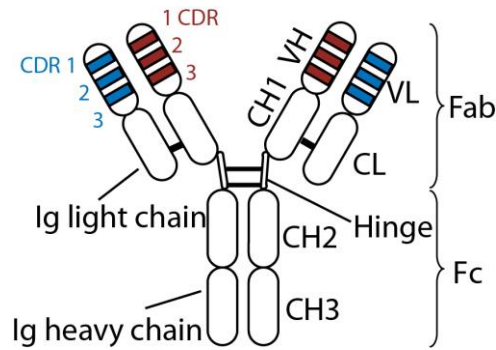


Figure 5: Schematic representation of an IgG1 antibody structure. Antibodies are polypeptides with four chains of different lengths, two of which are heavy (maroon) and two light (blue) chains. Heavy and light chains they are connected by disulfide bridges (thick black lines). Disulfide bridges also connect the two heavy chains at the hinge region (black). Variable regions (VH and VL) that are essential for the complementarity determining region (CDR) are coloured maroon and blue, respectively. The effector-mediating Fc region and the antigen-binding Fab region are both necessary for effective antibody function. Figure adapted from ¹³⁹.

1.6.4 Human antibody repertoire diversity

Humans Ig gene repertoire is the product of multiple B cell developmental stages, each of which features its own variable heavy (*IGHV*) and variable light (VL: *IGKV* or *IGLV*) selection and assembly mechanisms. Two major mechanisms of antibody diversification mediated by activation-induced deaminase (AID) enzyme and VH region invasion have been described in mice and human tissues ^{173,174}. In the antibody diversification process, it is proposed that AID mediates the transfer of homologous sequences between the rearranged VDJ gene and other VH genes. There are seven families of human *IGHV* genes (containing fifty-one unique VH sequences) and sixteen families of human VL (*IGKV* or *IGLV*) genes, both of which can be selected at random ¹⁷⁵. Three frame-work regions (FWRH 1, 2 and 3) and the first two CDRs (CDRH1 and CDRH2) of the heavy chains are encoded in each germline of the VH sequences, while the VL germline sequences are encoded by the three FWRs of the light chain (FWRL1, 2 and 3), CDRL1 and 2 and part of the CDRL3.

A recent repertoire analysis of a large panel of IgM-bearing B cell sequences from the cord blood neonates and peripheral blood of healthy human adults revealed that the *IGHV* genes in neonates and adults' repertoire are preferentially encoded by *IGHV1*, *IGHV2*, *IGHV3* and *IGHV4* Ig genes, and together accounted for 94.5% in neonate's repertoire and 99.9% in adult repertoire. Only 5.5% and 0.1% *IGHV5*, *IGHV6* and *IGHV7* encoded Ig genes were found in neonate and adults' repertoire, respectively ¹⁷⁶. These results provide a baseline frequency of *IGHV* gene usage for estimating Ig genes that are enriched in response to infectious diseases or vaccination. However, it is currently unknown how diverse an Ig gene repertoire needs to be to ensure competent and long-lasting humoral immunity against infectious diseases.

2.0 STUDY OBJECTIVES

The overall goal of this study was to functionally assess the memory B cell formation and quality of antibodies generated specifically against the understudied PfCSP N-Junc and C-CSP domains, with direct relevance for the design of an improved PfCSP-based malaria vaccine capable of eliciting long-lasting humoral immunity against *Plasmodium falciparum* malaria.

The specific aims are:

Aim 1: To define the Ig gene features of PfCSP-reactive memory B cells and plasmablasts at cellular level by assessing their isotype, somatic hypermutation, clonality and gene segment usage.

Aim 2: To analyze the selection, epitope specificity, affinity, and diversity of N-Junc and C-CSP specific mAbs derived from PfCSP-reactive memory B cells.

Aim 3: To determine parasite inhibitory capacity of N-Junc and C-CSP specific mAbs

3.0 MATERIALS AND METHODS

3.1 MATERIALS

3.1.1 ELISA capture and standard antibodies

Goat anti-human IgG Fc-fragment

Jackson ImmunoResearch Laboratories, Cambridgeshire, United Kingdom.
Sigma Aldrich, Steinheim, Germany

Human IgG1, κ Isotype Control
(from human myeloma plasma)

3.1.2 ELISA secondary antibodies

Goat anti-human IgG, Fc γ (HRP-conjugated)

Jackson ImmunoResearch Laboratories, Cambridgeshire, United Kingdom

Goat anti-human IgM, Fc5 μ (HRP-conjugated)

Jackson ImmunoResearch Laboratories, Cambridgeshire, United Kingdom

3.1.3 FACS analysis antibodies & reagents

7-aminoactinomycin (7-AAD)

Invitrogen GmbH, Karlsruhe, Germany

Mouse anti-human CD19 (BV786-conjugated)

BioLegend GmbH, Fell, Germany

Mouse anti-human CD21 (PE-Cy7conjugated)

BioLegend GmbH, Fell, Germany

Mouse anti-human CD27 (PE-conjugated)

BD Biosciences GmbH, Heidelberg, Germany

Mouse anti-human IgG (BV510-conjugated)

BD Biosciences GmbH, Heidelberg, Germany

Mouse anti-human IgM (BV421-conjugated)

BD Biosciences GmbH, Heidelberg, Germany

Mouse anti-human IgD (APC-H7-conjugated)

BD Biosciences GmbH, Heidelberg, Germany

Mouse anti-human CD38 (BV605-conjugated)

BD Biosciences GmbH, Heidelberg, Germany

3.1.4 Recombinant mAbs used

as controls

ED38 (Highly poly-reactive mAb)

11

JB40 (Mildly poly-reactive mAb)

3

2A10 (Chimeric antibody mAb)

1,85

mGO53 (non-poly-reactive mAb)

3

1710 (C-CSP specific mAb)

5

1512(C-CSP specific mAb)

9

3.1.5 Antigens

FL-CSP (NF54 strain) for ELISA

European Molecular Biology Laboratory (EMBL), Heidelberg, Germany

FL-CSP (7G8 strain) for ELISA

Kindly provided by Prof. Jean P. Julien, the hospital for sick children research institute, Toronto, Canada

Biotinylated FL-CSP (NF54 strain) for cell sorting

Kindly provided by Prof. Jean P. Julien, the Hospital for sick children research institute, Toronto, Canada

N-CSP

European Molecular Biology Laboratory (EMBL), Heidelberg, Germany

N-Junc

Peptide Specialty Laboratories GmbH (PSL), Heidelberg, Germany

NANP₅

Peptide Specialty Laboratories GmbH (PSL), Heidelberg, Germany

NANP ₁₀	Peptide Specialty Laboratories GmbH (PSL), Heidelberg, Germany
C-CSP	European Molecular Biology Laboratory (EMBL), Heidelberg, Germany
α-TSR	Kindly provided by Prof. Jean P. Julien, the hospital for sick children research institute, Toronto, Canada
C-linker	Peptide Specialty Laboratories GmbH (PSL), Heidelberg, Germany
DNA sodium salt from salmon testes	Sigma Aldrich Chemie GmbH, Steinheim, Germany
Human recombinant insulin	Sigma Aldrich Chemie GmbH, Steinheim, Germany
Lipopolysaccharides (LPS)	Sigma Aldrich Chemie GmbH, Steinheim, Germany

3.1.6 Bacteria

Escherichia coli DH10B

Clontech Inc., Palo Alto, CA, USA

3.1.7 Bacterial culture media and supplements

LB agar (35 g/L)

Sigma Aldrich Chemie GmbH, Steinheim, Germany

Lysogeny broth (LB) (25 g/L)

Sigma Aldrich Chemie GmbH, Steinheim, Germany

Ampicillin (100 mg/ml)

Sigma Aldrich Chemie GmbH, Steinheim, Germany

3.1.8 Chemicals, Buffers and Solutions

2-Mercaptoethanol, 50 mM

Life Technologies GmbH, Karlsruhe Germany
Carl Roth GmbH & Co. KG, Karlsruhe, Germany

2-propanol (≥ 99.5 %)

6x loading buffer gel electrophoresis

60 % (w/v) sucrose

50x TAE Buffer

1 mM cresol red

1% BSA Buffer (Serum ELISA)

AppliChem GmbH, Darmstadt, Germany

4% BSA buffer (Antigen ELISA)

1X PBS + 1% BSA

ABTS self-made buffer

1X PBS + 4% BSA

0.1 M citric acid

0.2 M disodium phosphate

1 ABTS tablet/91 ml ABTS Buffer

ABTS tablets

Roche diagnostisch GmbH, Mannheim, Germany

Acetic acid (CH₃COOH)

Sigma Aldrich Chemie GmbH, Steinheim, Germany

Ammonium chloride (NH₄Cl₂)

Sigma Aldrich Chemie GmbH, Steinheim, Germany

Ammonium sulfate ((NH₄)₂SO₄)

Sigma Aldrich Chemie GmbH, Steinheim, Germany

Bovine serum albumin fraction V (BSA)

Carl Roth GmbH & Co. KG, Karlsruhe, Germany

Calcium chloride (CaCl ₂)	Sigma Aldrich Chemie GmbH, Steinheim, Germany
Citric acid (C ₆ H ₈ O ₇) (≥ 99.5 %)	Sigma Aldrich Chemie GmbH, Steinheim, Germany
Coomassie Brilliant Blue G-250	BioRad Laboratories GmbH, München, Germany
Coomassie De-staining Buffer	100 ml methanol 400 ml acetic acid 500 ml deionized water
Coomassie Incubation Buffer	50% (v/v) methanol 2% (v/v) phosphoric acid 17% (m/v) ammonium sulfate ad 1000 ml deionized water 0.66 g Coomassie Brilliant Blue G-250/1l
Coomassie Staining Buffer	0.66 g Coomassie Brilliant Blue G-250/1l 1l Coomassie Incubation buffer
Criterion™ TGX™ Precast Gels	BioRad Laboratories GmbH, München, Germany
Cytochalasin D	Sigma Aldrich Chemie GmbH, Steinheim, Germany
Dimethyl sulfoxide (DMSO)	Sigma Aldrich Chemie GmbH, Steinheim, Germany
Disodium phosphate (Na ₂ HPO ₄)	Sigma Aldrich Chemie GmbH, Steinheim, Germany
ELISA blocking buffer (concentration ELISA)	1x PBS 0.05% (v/v) Tween®20 1 mM EDTA
ELISA development solution	1 µl/ml 30% H ₂ O ₂ ABTS solution
ELISA washing solution	1x PBS 0.05% (v/v) Tween®20
Elution buffer pH 3 (antibody purification)	0.1 M Glycine
Ethanol	Sigma Aldrich Chemie GmbH, Steinheim, Germany
Ethidium bromide (C ₂₁ H ₂₀ BrN ₃)	Sigma Aldrich Chemie GmbH, Steinheim, Germany
Ethylenediaminetetraacetic acid (EDTA)	Carl Roth GmbH & Co. KG, Karlsruhe, Germany
GIBCO™ 10x PBS (pH 7.4)	Life Technologies GmbH, Karlsruhe Germany
GIBCO™ 1x PBS (pH 7.4)	Life Technologies GmbH, Karlsruhe Germany
GIBCO™ Trypan Blue Stain 0.4%	Life Technologies GmbH, Karlsruhe Germany
Glycerol (C ₃ H ₈ O ₃)	Carl Roth GmbH & Co. KG, Karlsruhe, Germany
Glycine (C ₂ H ₅ NO ₂)	Sigma Aldrich Chemie GmbH, Steinheim, Germany

H ₂ O ₂	Th. Geyer GmbH & Co. KG, Renningen, Germany
Methanol (CH ₃ OH) (≥ 99.9%, p.a)	Carl Roth GmbH & Co. KG, Karlsruhe, Germany
Neutralization buffer pH 9.0 (antibody purification)	1M Tris
Paraformaldehyde (PFA)	Alfa Aesar, Thermo Fisher (Kandel) GmbH, Germany
Percoll®	GE Healthcare Life Sciences, Freiburg, Germany
Polyethyleneimine (PEI)	Sigma Aldrich Chemie GmbH, Steinheim, Germany
Protein G Sepharose™ Fast Flow	GE Healthcare Life Sciences, Freiburg, Germany
Regeneration Solution (10 mM Glycine-HCl, pH 2.1)	Cytiva Europe GmbH, Freiburg im Breisgau, Germany
SeaKem® LE Agarose	Cambrex Inc., Rockland, ME, USA
Sodium chloride (NaCl)	Sigma Aldrich Chemie GmbH, Steinheim, Germany
Sucrose (C ₁₂ H ₂₂ O ₁₁)	Carl Roth GmbH & Co. KG, Germany
SYBR™ green staining solution (100x)	Life Technologies GmbH, Karlsruhe Germany
T4 DNA Ligase Reaction Buffer (10X)	New England Biolabs GmbH, Frankfurt am Main, Germany
Triton X-100	Sigma Aldrich Chemie GmbH, Steinheim, Germany
Trizma® base (C ₄ H ₁₁ N ₀₃)	Sigma Aldrich Chemie GmbH, Steinheim, Germany
Tween® 20 (C ₅₈ H ₁₁₄ O ₂₆)	Carl Roth GmbH & Co. KG, Germany

3.1.9 Cell lines

HEK-293F	Life Technologies GmbH, Karlsruhe, Germany
----------	--

3.1.10 Cell culture media

Gibco™ DMEM	Life Technologies GmbH, Karlsruhe Germany
Gibco™ HEPES	Life Technologies GmbH, Karlsruhe Germany
Gibco™ L-glutamine	Life Technologies GmbH, Karlsruhe Germany
Gibco™ MEM	Life Technologies GmbH, Karlsruhe Germany
Gibco™ PenStrep	Life Technologies GmbH, Karlsruhe Germany
Gibco™ RPMI	Life Technologies GmbH, Karlsruhe Germany
Gibco™ RPMI with L-glutamine	Life Technologies GmbH, Karlsruhe Germany
Gibco™ Trypsin EDTA 1x	Life Technologies GmbH, Karlsruhe Germany
Human serum	Haema, Berlin, Germany
FreeStyle293 Expression media	Thermo Fisher Scientific Inc., Karlsruhe, Germany
EX-CELL® 293 Serum-Free Medium	Thermo Fisher Scientific Inc., Karlsruhe, Germany

3.1.11 Commercial kits

NucleoBond® Xtra Midi / Maxi

Macherey-Nagel GmbH & Co. KG, Düren, Germany

NucleoSpin® 96 PCR Clean-Up

Macherey-Nagel GmbH & Co. KG, Düren, Germany

NucleoSpin® Gel and PCR Clean-up

Macherey-Nagel GmbH & Co. KG, Düren, Germany

NucleoSpin® Plasmid Kit

Macherey-Nagel GmbH & Co. KG, Düren, Germany

3.1.12 Enzymes and additives

3.1.12.1 Cloning

Agel, BsiWI, Sall, XhoI

New England Biolabs GmbH, Frankfurt am Main, Germany

Cutsmart buffer 10x

New England Biolabs GmbH, Frankfurt am Main, Germany

T4 DNA Ligase

New England Biolabs GmbH, Frankfurt am Main, Germany

T4 DNA Ligase buffer 10x

New England Biolabs GmbH, Frankfurt am Main, Germany

3.1.12.2 RT and PCRs

10x PCR buffer

Quiagen AG, Hilden, Germany

5x First strand buffer (RT)

Life Technologies GmbH, Karlsruhe, Germany

DTT

Life Technologies GmbH, Karlsruhe, Germany

Hotstart *Taq* DNA polymerase

Quiagen GmbH, Hilden, Germany

NP-40

Sigma Aldrich Chemie GmbH, Steinheim, Germany

Nuclease free water

Eppendorf AG, Hamburg, Germany

RNAasin®

Promega Inc., Madison, WI, USA

RT buffer

Life Technologies GmbH, Karlsruhe, Germany

SuperScript™ III Reverse Transcriptase

Life Technologies GmbH, Karlsruhe, Germany

Taq DNA polymerase

Quiagen AG, Hilden, Germany

3.1.13 Expression vectors

Vectors (with γ 1-, κ - and λ -chain C regions)

Kind gift of Dr. J. Ravetch, Rockefeller University, New York City, USA

3.1.14 Nucleotides and nucleic acids

1kb Plus DNA marker

New England Biolabs GmbH, Frankfurt am Main, Germany

Desoxynucleotide Triphosphates (dNTPs)

Life Technologies GmbH, Karlsruhe, Germany

Oligonucleotides

MWG Biotech AG, Ebersberg, Germany

Random Hexamer Primers

Roche Diagnostics GmbH, Mannheim, Germany

3.1.15 Instruments and consumables

1.5 ml reaction tubes

Sarstedt AG, Nümbrecht, Germany

2 ml reaction tubes

Sarstedt AG, Nümbrecht, Germany

13 ml tubes (Bacteria inoculation)

Sarstedt AG, Nümbrecht, Germany

15 ml falcon tube

Costar Inc., Corning, Action, MA, USA

50 ml falcon tube

Costar Inc., Corning, Action, MA, USA

Cornical flasks	Sigma Aldrich Chemie GmbH, Steinheim, Germany
96-well Multiply®-PCR plate	Sarstedt AG, Nümbrecht, Germany
96-well skirted twintech PCR plate	Eppendorf AG, Hamburg, Germany
Alpha Imager™ 1220	Alpha Innotech Corporation Inc., San Leandro, CA, USA
Aluminum foil seal	4titude, Surrey, UK
AxioObserver Z1 fluorescence microscope	ZEISS Microscopy, Oberkochen, Germany
BD Aria II™	BD Biosciences GmbH, Heidelberg, Germany
BD LSR II™	BD Biosciences GmbH, Heidelberg, Germany
BD Microlance™ 3 30G x 1/2"	BD Biosciences GmbH, Heidelberg, Germany
BioPhotometer	Eppendorf AG, Hamburg, Germany
Bio-Spin® chromatography columns	Bio-Rad Inc., Hercules, CA, USA
Cell culture 48-well plate	TPP, Trasadingen, Switzerland
Cell culture 96-well plate	TPP, Trasadingen, Switzerland
Cell culture 96-well plate (transparent bottom)	TPP, Trasadingen, Switzerland
Cell culture dish (150 mm)	BD Biosciences GmbH, Heidelberg, Germany
CellStar sterile serological pipettes 2 ml,	Greiner Bio-One GmbH, Frickenhausen, Germany
5 ml, 10 ml, 25 ml, 50 ml	Eppendorf AG, Hamburg, Germany
Centrifuge 5180R (rotor A-4-81)	Eppendorf AG, Hamburg, Germany
Centrifuge 5417R (rotor F-45-30-11)	Thermo Electron GmbH, Langenbold, Germany
Clean bench HERAsafe KS12	Thermo Electron GmbH, Langenbold, Germany
CO ₂ Incubator CB210	Binder GmbH, Tuttlingen, Germany
Cover slips	Menzel-Gläser GmbH, Braunschweig, Germany
CryoTube™ Vials	Thermo Fisher Scientific Inc., Darmstadt, Germany
Domed 12-cap strips (PCR tube strips)	Bio-Rad Laboratories GmbH, München, Germany
Electrophoresis chamber D3 (horizontal)	Thermo Scientific Inc., Rochester, NY, USA
ELISA plates (96-well, flat bottom)	Costar Inc., Corning, Action, MA, USA
ELISA plates (384-well)	Costar Inc., Corning, Action, MA, USA
FluoNunc Plates	Costar Inc., Corning, Action, MA, USA
FrameStar® 384	4titude, Surrey, UK
Heraeus B5042 (Bacteria incubator)	Kendro Laboratory Products, Weaverville, NC, USA
Inoculating loops/needles, polystyrene	Sarstedt, Nümbrecht, Germany
Leica DM2000 LED	Leica Microsystems GmbH Wetzlar, Germany
M1000Pro plate reader	Tecan, Crailsheim, Germany
Mastercycler® ep Gradient S	Eppendorf AG, Hamburg, Germany
Mastercycler® Pro 384	Eppendorf AG, Hamburg, Germany
Microscopy slides	Carl Roth GmbH & Co. KG, Karlsruhe, Germany
Microscopy slides (8-well)	Medco GmbH, München, Germany
Microwave	Panasonic AG, Hamburg, Germany
MiniVE vertical electrophoresis unit	Höfer Inc., Holliston, MA USA

Multichannel Pipet-Lite® LTS 2-20 µl,
20-200 µl, 100-1200 µl
Multipipette plus
Multitron Pro (Bacteria shaker)
Nanodrop™ 1000
Neubauer Counting Chamber by Marienfeld

Omnican® 50 Insulin Syringes, 12 mm
30 G
PC
Petri dishes (100 mm)

Pipetboy acc

Pipet-Lite® LTS 0.1-2 µl, 2-20 µl,
20-200 µl, 100-1000 µl
Polypropylene tubes (15 ml, 50 ml)
Polystyrene round bottom tube (5 ml)
with cell strainer cap
Safety-Lancet
Safety-Multifly®
Slide-A-Lyzer® Mini Dialysis Devices
S-Monovette® EDTAK
SpectraMax 190 Microplate Reader
Stemi 2000 Stereomicroscope
Stuart® Gyro rocker SSL3

T75 cm² flask
Thermomixer comfort
Vortex genie 2
Water bath with thermostat

Wax seal

3.1.16 Softwares

FlowJo v10.0
GraphPad Prism 9.1.2
Adobe Illustrator® CS5
Microsoft® Office 2011
Rstudio version 4.1.0

3.1.17 Web Resources

Clustal Omega
Ensemble Genome Browser
Expasy SIB Bioinformatics Resource Portal
IMGT®
NCBI Ig Blast
PlasmoDB

Rainin Instrument Inc. LLC, Woburn, MA, USA

Eppendorf AG, Hamburg, Germany
Infors HT, Bottmingen, CH
Thermo Scientific Inc., Wilmington, DE, USA
Carl Roth GmbH & Co. KG, Karlsruhe,
Germany
B. Braun Medical Ltd, Sheffield, UK

LG Electronics Lenovo PC
Greiner Bio-One GmbH, Frickenhausen,
Germany
Integra Biosciences GmbH, Fernwald,
Germany
Rainin Instrument Inc. LLC, Woburn, MA, USA

Sarstedt AG, Nümbrecht, Germany
BD Biosciences GmbH, Heidelberg, Germany

Sarstedt, Nümbrecht, Germany
Sarstedt, Nümbrecht, Germany
Thermo Scientific, Rockford, IL, USA
Sarstedt, Nümbrecht, Germany
Molecular Devices Inc., Sunnyvale, CA, USA
ZEISS Microscopy, Oberkochen, Germany
Sigma Aldrich Chemie GmbH Steinheim,
Germany
BD Biosciences GmbH, Heidelberg, Germany
Eppendorf AG, Hamburg, Germany
Scientific Industries Inc., Bohemia, NY, USA
JULABO Labortechnik GmbH, Seelbach,
Germany
4titude, Surrey, UK

Treestar Systems Inc., Ashland, USA
GraphPad Software Inc., La Jolla, USA
Adobe Inc., San Jose, CA, USA
Microsoft GmbH, Stuttgart, Germany
RStudio, Inc., Boston, MA USA

<http://www.ebi.ac.uk/Tools/msa/clustalo/>
<http://www.ensembl.org/index.html>
<http://expasy.org/>
<http://www.imgt.org/>
<http://www.ncbi.nlm.nih.gov/igblast/>
<http://plasmodb.org/plasmo/>

3.2 METHODS

3.2.1 Human malaria immunization trial

The sera, repertoire data, and monoclonal antibodies analyzed in this thesis were from the clinical Phase I malaria vaccine immunization trial (MAVACHE-verification phase) carried out by Prof. Dr. Benjamin Mordmüller and colleagues at the Institute of Tropical Medicine, Tübingen, Germany ¹⁰. While serum samples were collected 28, 55 and 83 days post third immunization, blood samples for peripheral blood mononuclear cells (PBMCs) isolation were taken 14, 35 and 63 days after the third immunization. The Ethics Committee of the Faculty of Medicine and the University Clinics of the University of Tübingen gave their approval. The research was conducted in accordance with the standards of the Declaration of Helsinki. The clinical trial was registered in the EudraCT database (<https://clinicaltrials.gov/ct2/show/study/NCT02704533>). Serum samples obtained were used to measure anti-PfCSP serum antibody titers by ELISA. PBMCs were used to isolate PfCSP reactive memory B cells (MBCs) and plasmablasts at a single-cell level using flow cytometry. Paired functional Ig genes were obtained from isolated cells.

3.2.2 Fluorescence-activated single-cell sorting (FACS)

For flow cytometric analysis and single cell sorting of PfCSP-reactive MBCs and plasmablasts, frozen PBMCs were rapidly thawed at 37 °C and transferred to a 50 ml Falcon tube containing 30 ml pre-warmed RPMI medium. The cells were centrifuged at 4 °C for 8 min at a centrifugation speed of 1400 rpm and the supernatant discarded. The cell pellets were resuspended in 1 ml cold FACS buffer (2% FCS in 1x PBS) and transferred to 1.5 ml eppendorf tubes. The tubes were centrifuged at 3500 rpm at 4 °C for 5 minutes. The supernatants were then aspirated and the cell pellets were kept on ice. Biotinylated full-length PfCSP (strain NF54) was a kind gift from Dr. Jean-Philippe Julien (The Hospital for Sick Children Research Institute, Toronto, Canada). Cells on ice were resuspended in 100 µl FACS buffer containing 20 µg/ml biotinylated PfCSP and incubated for 30 minutes on ice. After incubation, cells were washed with 1 ml of cold FACS buffer and centrifuged at 3500 rpm at 4 °C for 5 minutes. The supernatants were discarded and the cell pellets were resuspended in 100 µl of antibody staining cocktail (diluted in FACS buffer) containing the antibodies listed in Table 1 and incubated on ice for additional 30 minutes. Biotin was detected with streptavidin FITC (1:1000 dilution). After incubation, cells were washed with 1 ml FACS buffer, centrifuged at 3500 rpm at 4 °C for 5 minutes and resuspended in 100 µl of FACS buffer containing membrane impermeable dye 7-aminoactinomycin (7-AAD; from Invitrogen) diluted to 1:400. Cells were incubated on ice for 10

min, washed with 1 ml FACS buffer, resuspended in 400 µl FACS buffer, and filtered through FACS falcon tubes. Cell sample staining analysis and single cell sorting were carried out using FACS Ariall (BD) with the FACSDiVa software version 8.0.1 (BD). Cell doublets were gated out using FSC-H/W and SSC-H/W. PfCSP-reactive MBCs were defined and sorted as 7AAD-CD19+CD27+IgG+CSP+, 7AAD-CD19+CD27-IgG+CSP+ or 7AAD-CD19+CD27+IgG-CSP+ cells. Plasmablasts were defined and sorted as 7AAD-CD19+CD27+CD38+. The above-mentioned gates were defined using 50,000 recorded cells due to sample limitations. An OR gate was set up between PfCSP memory B cells and plasmablasts to sort individual cells. Because the software's index sorting option was turned on during sorting, sorted cells could be identified subsequently for each of the two populations. Sorting was performed into 384-well plates containing 2 µl of sort RHP mix (Table 2). The sort RHP mix contained NP-40 to aid cell lysis, DTT to denature RNA secondary structures, RNasin to inhibit RNase and RHP to bind to RNA and prime reverse transcription (Table 2). Upon completion of the sort, the plates were immediately placed on dry ice to preserve the contents and then transported to a -80 °C freezer for long-term preservation and storage.

Table 1: Antibody dilutions for flow cytometry cell staining

Mouse anti-human antibody	Clone	Catalogue no	Manufacturer	Dilution
CD19-BV786	HIB19	13-0199-82	BioLegend	1:10
CD27-PE	M-T271	555441	BD Biosciences	1:5
IgG-BV510	G18-145	563247	BD Biosciences	1:20
CD38-BV605	HB7	562665	BD Biosciences	1:20
IgM-BV421	G20-127	562618	BD Biosciences	1:20
IgD-APC-H7	IA6-2	561305	BD Biosciences	1:20
CD21-PE-Cy7	Bu32	354912	BioLegend	1:20

Table 2: Reagent concentrations used in the sort RHP mix per well

Reagent	Concentration	Volume (μ l)
Nuclease free water	-	1.4813
DTT	100mM	0.1000
NP-40	10%	0.1375
RHP	300 ng/ μ l	0.1375
RNAsin	40 U/ μ l	0.0938
PBS	10X	0.0500
Total		2.0000

3.2.3 cDNA synthesis from single cells by the Reverse Transcription-Polymerase Chain Reaction (RT-PCR)

To facilitate denaturation of the RNA secondary structure, the frozen PCR plates were thawed on ice and incubated at 68 °C for 60 seconds. The plates were placed back on ice after incubation, and 2 μ l of a RT master mix was added. The RT master mix contained 1X RT buffer, DTT to denature the RNA secondary structures, dNTP for synthesis, RNAsin as an RNase inhibitor and SuperScript III, a monkey murine leukaemia virus (M-MLV) derived reverse transcriptase for the enzymatic reaction (Table 3). The reaction was carried out according to the steps and conditions in Table 4.

Table 3: RT master mix reagent concentrations per well for RT-PCR

Reagent	Concentration	Volume (μ l)
Nuclease free water	-	0.6375
RT buffer	5X	0.8000
DTT	100mM	0.3000
dNTP	25 mM each	0.1375
RNAsin	40 U/ μ l	0.0563
SuperScript III	200 U/ μ l	0.0688
Total		2.0000

Table 4: RT-PCR thermocycler program for reverse transcription of Ig gene transcripts

Step	Temperature	Time	Cycles
RNA denaturation	42 °C	5 min	1
Annealing of hexamers	25 °C	10 min	1
Reversal transcription	50 °C	60 min	1
End of reaction	94 °C	5 min	1

3.2.4 Human Ig gene transcripts amplification using semi-nested PCR

A nested PCR technique with primary and secondary PCRs for each locus^{166,177} was used to amplify Ig genes from the heavy, kappa and lambda loci. In the primary (1^o) PCR, 1 µl of synthesized cDNA was used as template in 3 different PCRs, with a separate specific primer set designed to recognize the leader region (5' primer) and the constant region (3' primer) of each locus (heavy, kappa or lambda; Supplementary Table 5). The heavy, kappa, and lambda loci were amplified separately, and the amplification efficiency of the heavy locus was increased by double PCRs, resulting in two heavy, one kappa, and one lambda reaction. The concentrations of the PCR reagents are given in Table 5. For the secondary PCR (2^o), 1 µl of the resulting amplicon from the primary PCR was used as template. Primers used in the secondary PCR are bar-coded and bind precisely to the V and J gene segment of the corresponding heavy, kappa, and lambda loci (Supplementary Table 6). The concentrations of the PCR reagents for the secondary PCR are given in Table 6. The conditions for the primary and secondary PCR reactions are listed in Table 7. Gel electrophoresis on a 2% agarose gel was used to assess whether heavy and kappa/lambda amplicons were successfully amplified. To determine the exact sequence of the amplified Ig transcripts, the matched heavy and light chains were sent to Eurofins Genomics GmbH for Illumina sequencing. cDNA preparation and Ig gene transcripts amplification were carried out by Julia Gartner.

Table 5: Concentration of reagents for primary (1°) semi-nested PCR reaction mix

Reagent	Concentration	Volume (μl)
Nuclease free water	-	7.5950
Buffer	10X	1.0000
5' primer sets	50 μM	0.1300
3' primer sets	50 μM	0.1300
dNTPs	25 mM each	0.1000
HotStart <i>Taq</i>	200 U/μl	0.0450
Template	5 U/μl	1.0000
Total		10.0000

Table 6: Secondary (2°) semi-nested PCR reaction mix reagent concentration

Reagent	Concentration	Volume (μl)
Nuclease free water	-	7.7900
Buffer	10X	1.0000
5' primer sets	50 μM	0.0325
3' primer sets	50 μM	0.0325
dNTPs	25 mM each	0.1000
HotStart <i>Taq</i>	200 U/μl	0.0450
Template	5 U/μl	1.0000
Total		10.0000

Table 7: PCR thermocycler conditions for primary and secondary semi-nested PCR reaction mix

Step	Temperature			Duration	Cycles
	Heavy	Kappa	Lambda		
HotStart <i>Taq</i> activation	94 °C	94 °C	94 °C	15 min	1
Denaturation of DNA	94 °C	94 °C	94 °C	30 sec	50
Primer annealing	58 °C	58 °C	60 °C	30 sec	50
Elongation	72 °C	72 °C	72 °C	55 sec (1°) or 45 sec (2°)	50
End of reaction	72 °C	72 °C	72 °C	10 min	1

3.2.5 Next generation sequencing (NGS) of amplified human Ig gene transcripts

Next-generation Illumina sequencing was performed on the resulting amplicons of the Ig genes. To do this, 1 µl of DNA from each well of the secondary PCR plate corresponding to a matrix and an Ig gene locus (heavy, kappa or lambda) were pooled. The pooled DNA was purified using the NucleoSpin Gel and PCR Clean-up Kit (Macherey-Nagel GmbH), a silica membrane-based DNA binding kit, according to the manufacturer's instructions. Subsequently, the ratio of absorbance at OD₂₆₀/OD₂₈₀ and CD₂₆₀/OD₂₃₀ was used to determine the purity and concentration of the purified DNA product using a NanoQuant plate in a Tecan M1000 Pro plate reader. Size exclusion of the DNA product was then performed by running the purified sample on a 4% agarose gel at 80 V for 6 hours. Appropriate bands corresponding to the expected amplicon size for each locus were excised and purified using the NucleoSpin Gel and PCR Clean-up Kit (Macherey-Nagel GmbH) according to the manufacturer's instructions. After purity and concentration determination with the Tecan M1000 Pro plate reader, the resulting purified products were used for library preparation with the TruSeq Nano DNA LT Kit (Illumina). For this purpose, the purified DNA products were first heated at 70 °C for 10 minutes and immediately placed on ice. Subsequently, the Illumina adapters were ligated with the resulting amplicons as described in the TruSeq Nano DNA LT Kit manual. The ligated DNA products were further purified and DNA purity and concentration were measured as before. The efficiency of adapter ligation was determined by qPCR using the KAPA Library Quant Kit (Roche) according to the manufacturer's instructions. Samples were then sent to Eurofins Genomics for Illumina MiSeq300 sequencing. All library preparation steps were kindly carried out by Julia Gärtner and Dorien Foster (DKFZ).

3.2.6 Sequence analysis of human Ig genes

Using the Pandaseq tool ¹⁷⁸, paired-end reads from Illumina sequencing were first assembled (Pandaseq parameters: $t = 0.8$, maximum length = 550, and minimum length = 320). To establish a balanced base composition during sequencing, the assembled sequences were matched to the genome of bacteriophage PhiX in order to eliminate the PhiX sequences introduced to the sample prior to sequencing. The assembled reads were processed and analyzed using the bioinformatics pipeline, sciReptor (version 8.0.1, github.com/b-cell-immunology/sciReptor) ¹⁷⁸. Following this, IgBLAST analysis, with alignment to the reference library ¹⁷⁹, was used to assign single reads to the corresponding well barcodes, and annotations were made to V, D, and J segments as well as somatic hypermutations, constant segments, framework regions (FRWs), and complementarity determining regions (CDRs). The flow cytometry index data together with the meta-information were connected with the sequence information and saved in a structured DBeaver database. R programming language ^{180,181} was used for the subsequent sequence visualization and analysis.

3.2.7 Ig gene cloning and recombinant antibody expression

Following sequence analysis of sorted PfCSP-reactive memory B cells, specific Ig genes were cloned into human AbVec2.0-*IGHG1*, AbVec1.1-*IGKC* and AbVec1.1-*IGLC2*-XhoI expression vectors ¹⁶⁶.

3.2.8 Specific PCR amplification of Ig genes

To clone the heavy and light chain DNA amplicons of the Ig genes into corresponding AbVec2.0-*IGHG1* and AbVec1.1-*IGKC* or AbVec1.1-*IGLC2*-XhoI expression vectors, a second PCR was performed with primers to introduce an AgeI restriction site at the 5' end of the heavy and light chain amplicons and a Sall, BsiWI, and XhoI restriction sites at the 3' end of the heavy, kappa, and lambda chains, respectively (see Supplementary Table 7 for primers). 2 ul of 1st PCR product were used as a template for amplification in the presence of PCR mix (reagents and concentrations are listed in Table 8. Using thermocycler program listed in Table 7, PCR was performed and the amplification of Ig genes was validated by gel electrophoresis (2% gel).

Table 8: Specific PCR reagent concentrations per well

Reagent	Concentration	Volume (μ l)
Nuclease free water	-	29.4
Hotstart <i>Taq</i> Buffer	10X	4.0
5' primer sets	50 μ M	2.0
3' primer sets	50 μ M	2.0
dNTPs	25 mM each	0.4
HotStart <i>Taq</i>	5 U/ μ l	0.2
Template	-	2.0
Total		40.0

3.2.9 Purification of specific PCR products

The PCR products were purified according to manufacturer's instructions using the NucleoSpin® 96 PCR Clean-Up Kit from Macherey-Nagel GmbH. Briefly, the PCR product was initially adjusted to a volume of 100 μ l and added to 2x its' volume worth of binding buffer (Buffer NT). The mix was transferred to the membrane embedded wells of NucleoSpin® 96 PCR Clean-Up Kit and allowed to flow through by vacuum processing. Following this, 900 μ l of Buffer NT1 was added (2x) to the wells in order to wash it and allowed to flow through by vacuum processing. Next, 75 μ l of pre-warmed (70°C) elution buffer (Buffer NE) was added to the wells and incubated at room temperature for 5 minutes. The eluate was collected in a 96 well plate by vacuum processing for 10 minutes.

3.2.10 Competent bacteria preparation

Cloning was carried out with the *Escherichia coli* (*E. coli*) DH10B strain. The *E. coli* strain was streaked onto an LB agar plate and incubated at 37 °C overnight. A single colony from the LB plate was inoculated into 5 ml of sterilized Lysogeny Broth medium (LB medium) and incubated at 37 °C overnight, with shaking at 180 rpm. At the start of the next day, 800 μ l of the overnight grown culture was added to 500 ml of LB medium and incubated at 37 °C with shaking at 180 rpm. *E. coli* DH10B strain was cultured to an OD₆₀₀ and kept on ice for 30 mins. After 30 mins on ice, the cells were centrifuged at 4000 rpm at 4 °C for 20 mins, and the resulting pellet was reconstituted into 80 ml of 0.1 M CaCl₂. The bacterial cells were again centrifuged at 4000 rpm at 4 °C for 20 min and dissolved in a 50 ml solution of 0.1 M CaCl₂ in 15% glycerol. 50 μ l to 100

μl aliquots of the competent bacteria were stored at -80 °C. Transformation efficiency was determined by transforming different amounts of DNA (0.1 to 20 ng) into competent bacteria and counting the resulting colonies.

3.2.11 Eukaryotic expression vector preparation and *E. coli* transformation

Chemically competent *E. coli* strain DH10B was incubated for 30 minutes on ice with 1 ng of AbVec2.0-*IGHG1* (Addgene # 80795), AbVec1.1-*IGKC* (Addgene # 80796) and AbVec2.1-*IGLC2* (Addgene # 80797) vectors carrying the human Igγ1, Igκ and Igλ constant regions. The bacterial cells were heat shocked at 42 °C for 45 seconds and re-suspended into 100 μl of pre-warmed LB medium, which were then incubated at 37 °C for 1 hour with gentle shaking. On LB agar plates containing ampicillin at a concentration of 100 μg/ml, 80-100 μl of the transformed cells were plated. The plates were incubated overnight at 37 °C. The transformed bacteria were selected with an ampicillin resistance cassette on the expression vectors. One colony per vector was used to inoculate a 5 ml LB + 5 μl ampicillin starter culture, which was then incubated overnight at 37 °C and 180 rpm. Subsequently, 500 μl of this starter culture was used to inoculate a 200 ml culture, which was incubated overnight at 37 °C and 180 rpm. The vectors were purified using the NucleoBond® Xtra Maxi Kit from Macherey-Nagel GmbH according to the manufacturer's instructions. Nanodrop technology was used to calculate the DNA concentration.

3.2.12 Cloning vector and PCR amplicon restriction endonuclease digestion

The purified AbVec2.0-*IGHG1*, AbVec1.1-*IGKC* and AbVec2.1-*IGLC2* vectors, as well as the PCR-obtained amplicons of the heavy, kappa, and lambda chains of the Ig genes, were double-digested with the corresponding enzymes (Heavy: Agel-HF/Sall-HF, Kappa: Agel-HF/BsiWI-HF, Lambda: Agel-HF/XhoI, Table 9 and 10) overnight at 37 °C. Each vector reaction mix was incubated with 5 μl calf intestinal phosphatase (CIP) for 1 hour at 37 °C to prevent re-ligation. The phosphatase was then inactivated by heating it at 60 °C for 30 minutes. All PCR products, including the amplicons of the heavy, kappa, and lambda chains of the Ig genes obtained by PCR, which had been digested, were purified using a NucleoSpin® 96 PCR Clean-Up Kit from Macherey-Nagel GmbH (as previously described in 3.2.9). The Nanodrop™ 1000 was used to determine the final plasmid concentrations, and the efficiency and integrity of the linearized plasmids were evaluated by transforming them into DH10B *E. coli* bacteria.

Table 9 : Reagent volumes and concentrations per reaction for vector restriction digestion

Reagent	Volume (μ l)	Final concentration
Vector	X	100 μ g per 400 μ l
NEB CutSmart buffer (10X)	40	1X
Age1-HF	10	200 units per reaction
Second Enzyme	10	200 units per reaction
Nucelase-free H₂O	X	
Total	400	

Table 10: Reagent volumes and concentrations per reaction for restriction digestion of purified Ig genes

Reagent	Volume (μ l)	Final concentration
Purified digested product	40	
NEB CutSmart buffer (10X)	5	1X
Age1-HF	0.05	20 U per reaction
2nd Enzyme	0.05	20 U per reaction
Nuclease-free H₂O	4.9	
Total	50	

3.2.13 Ligation and Transformation

The digested PCR amplicons (heavy and kappa or lambda) were ligated using T4 DNA ligase to the corresponding linearized cloning vectors (Table 11), and incubated overnight at 16 °C. At the beginning of the next day, 5 μ l of the ligation mixtures were mixed with 10 μ l of competent bacteria and incubated on ice for 30 minutes. The ligation reaction mixture was then heat shocked at 42 °C for 45 seconds and incubated with 100 μ l of lysogenic broth (LB) in a rotator for 1 hour at 37 °C. Transformation efficiency was determined by plating the ligation mixture onto a LB agar plate and incubating overnight at 37 °C.

Table 11: Ligation reagent concentrations used per reaction

Reagent	Concentration	Volume (μ l)
Digested PCR amplicon	8 ng/ μ l	7.5
Ligation buffer	10X	1.0
Linearized vector	25 ng/ μ l	1.0
T4 DNA ligase	400 U/ μ l	0.5
Total		10.0

3.2.14 Screening of successful bacterial colonies by PCR and Sanger sequencing

To determine whether cloning was successful, three bacterial colonies were randomly selected and added to a PCR mix (Table 12) to determine the correct insertion of the heavy, kappa or lambda amplicon ligated to the corresponding cloning vectors. For all the three vectors, a 5' primer (Absence) which binds to a vector sequence upstream of the inserted PCR product was used. Primers binding to the constant regions of human Ig γ 1 (IgG-Internal primer), Igk (Ck494 primer) and Ig λ (hCl-057 primer), were used as 3' primers. Using the thermocycler program listed in Table 13, PCR was performed on the selected colonies and the expected sizes of 650 bp for Ig γ 1, 700 bp for Igk and 590 bp for Ig λ were validated on a 2% agarose gel. To rule out the presence of PCR-based point or frameshift mutations, the PCR products were sequenced (Sanger sequencing by Eurofin Genomics GmbH). A list of primer sequences can be found in Supplementary Table 8.

Table 12: Concentration of colony PCR reagents used per reaction

Reagent	Concentration	Volume (μ l)
Nuclease free water	-	21.825
Buffer (Qiagen Hotstar Taq)	10X	2.5
5' primer	50 μ M	0.2
3' primer	50 μ M	0.2
dNTPs	25 mM each	0.125
Qiage Taq polymerase	5 U/ μ l	0.15
Total		25.0

Table 13: Thermocycler conditions for colony PCR

Step	Temperature	Time	Cycle
HotStart <i>Taq</i> activation	94 °C	5 min	1
Denaturation of DNA	94 °C	30 sec	27
Primer annealing	58 °C	30 sec	27
Elongation	72 °C	60 sec	27
End of reaction	72 °C	10 min	1

3.2.15 Sanger sequencing and colony PCR sequence analysis

The template replication primer used for Sanger sequencing was 5' Absence. The resulting sequences (from Eurofin Genomics GmbH) were analysed using a pipeline algorithm that checked for parameters such as frameshift mutations, stop codons, ori-alignment, insert length (350-380 bp) and the presence of a leader sequence. In addition, the secondary PCR sequences were compared to the colony PCR sequences using the free online IgBLAST tool ¹⁷⁹ to ensure a perfect match. Sequences that deviated in any way from what was expected in the secondary PCR were ignored and the PCR output from the corresponding backup plate was sent for sequencing instead.

3.2.16 Preparation/Purification of vector DNA (Plasmid preparation)

Successful bacterial colonies with correct sequences were inoculated into 5 ml LB medium containing 75 µg/ml ampicillin and incubated overnight at 37 °C with a 180 rpm shaker. After incubation, the bacterial culture was centrifuged at 4000 rpm for 15 minutes and the pellet was used to isolate the DNA using a Macherey-Nagel NucleoSpin® Plasmid Kit according to the manufacturer's instructions. The DNAs was eluted with 160 µl elution buffer and the concentration was determined using a Nanodrop. The plasmids were frozen at -20 degrees Celsius until further use.

3.2.17 Expression of recombinant monoclonal antibodies

FreeStyle™ 293-F cells were seeded at a density of 1.5×10^6 cells/ml in 5 ml FreeStyle™ 293 Expression Medium (Gibco) and incubated in a shaker at 180 rpm, 37 °C and 8% CO₂ for 24 hours prior to transfection. The next day, the cells were inoculated with 7.5 µg of heavy and light chain plasmids, and the tubes were incubated in the shaker for 5 minutes. Following this, 75 µl of

sterile 0.6 mg/ml polyethyleneimine (PEI), a cationic polymer that condenses DNA into positively charged particles, was added to each cell culture and incubated overnight at 37 °C, 8 % CO₂ and 180 rpm shaking. The next day, 5 ml of pre-warmed serum-free EX-CELL[®] 293 medium supplemented with 800 M L-glutamine was added to the cells and incubated for 5 days at 37 °C, 8 % CO₂ and 180 rpm shaking. At the end of the incubation period, the cell culture tubes were centrifuged at 4000 rpm and 4 °C for 20 minutes. The supernatant was carefully transferred to a new 15 ml Falcon tube and stored at 4 °C until use.

3.2.18 Recombinant monoclonal antibody purification

The recombinant antibodies were purified with protein G Sepharose beads. The beads were collected in a volume of 75 µl per 10 ml of antibody supernatant and rinsed with 20 ml of cold PBS. The beads were then centrifuged at 2000 rpm for 20 min at 4 °C. The PBS was discarded, and the resulting pellet was resuspended in an appropriate volume of PBS (500 µl per antibody), mixed vigorously, added to the antibody supernatants, and rotated overnight at 4 °C in a tube rotator. On the next, the tubes were centrifuged at 2,000 rpm for 20 min at 4 °C to remove the supernatant, leaving the pallet. The pallets were resuspended in 1 mL of cold PBS, transferred to a calibrated biospin column to run through the column, and washed twice with 1 ml cold PBS. The antibodies were then eluted with 200 ul of 0.1 M glycine (pH 3.0) into five different eppendorf tubes containing 20 ul of 1 M Tris (pH 8.0). Antibody concentration was measured using Nanodrop technology. After purification, the antibodies were dialyzed overnight in PBS using the Slide-A-Lyzer[®] Mini Dialysis Kit (Thermo Scientific) according to the manufacturer's instructions.

3.2.19 Reactivity and binding profile of monoclonal antibodies

3.2.19.1 Enzyme-linked immunosorbent assay (ELISA)

The Enzyme-Linked Immunosorbent Assay (ELISA) is a quantitative and qualitative biochemical and immunological assay used to quantify antigens, proteins, and glycoproteins in biological samples. The ELISA was used to determine the reactivity and specificity of the serum samples and the mAbs obtained against different PfCSP antigens. It was also used to quantify the concentration of antibodies in cell supernatant or purified antibodies.

3.2.19.2 Antibody concentration quantification (concentration ELISA)

Goat anti-human IgG Fc fragment (Jackson, 109-005-098) diluted 1:500 in PBS was used to coat high-binding 96-well ELISA plates (Corning) and then incubated overnight at 4 °C. The

next day, plates were washed three times with deionized water and blocked with 200 μ l/well blocking solution (1x phosphate-buffered saline (PBS) containing 0.05% (v/v) Tween20 and 1 mM EDTA) for 1 hour. Serial dilutions were prepared from the cell culture supernatants on a 96-well plate, starting with a 1:25 dilution in PBS and proceeding through 7 dilution steps of 1:2.5. Similarly, two dilution series of a human IgG1, κ -isotype control (Sigma, 15154-1MG) were prepared with 1 and 3 μ g/ml as starting concentrations. After washing three times with deionized water, 50 μ l of each diluted sample and standards were transferred to the ELISA plate and incubated for 1 hour at room temperature (RT). After 1 hour of incubation, the ELISA plates were washed three times with deionized water and incubated for another 1 hour with 50 μ l/well of horseradish peroxidase (HRP)-conjugated mouse anti-human IgG (Jackson Immuno Research, 115-035-008) diluted to 1:1000 in PBS. Plates were washed 6 times with deionized water and developed with 100 μ l/well H_2O_2 diluted in ABTS solution (1:1000). Absorbance was measured at 405 nm using a Tecan M1000Pro plate reader and antibody concentrations were calculated from the absorbance of the human IgG standard.

3.2.19.3 Serum and monoclonal antibodies antigen-specific ELISA

Full-length PfCSP (FL-CSP- 0.4 μ g/ml) or PfCSP-derived peptides/domains (N-CSP, Junc, NANP₅, NANP₁₀, C-CSP, α -TSR and C-linker and peptides (P1-14) covering the α -TSR subdomain- all at 2 μ g/ml) were coated onto high-binding 384-well plates (Corning) and incubated overnight at 4 $^{\circ}C$. The next day, plates were washed three times with a Tecan plate washer, blocked with 50 μ l/well 4% BSA (serum ELISA) or 1% BSA in PBS (antigen ELISA for mAbs) and incubated at room temperature for 1 hour at RT. Starting with a 1:200 dilution in 1% BSA (serum ELISA) or a concentration of 4 μ g/ml diluted in 1X PBS (antigen ELISA for mAbs), the samples were serially diluted at 1:4 in PBS in four steps. After 1 hour of incubation, plates were washed three times with 1X PBS-T and 15 μ l/well of serially diluted samples were added and incubated for 1.5 hours at RT. Antibodies were detected with goat anti-human IgG (Serum samples and mAbs) or IgM secondary antibody (Serum samples) coupled to horseradish peroxidase (HRP) diluted 1:1,000 in blocking buffer and then detected with a 2,2'-azino-bis(3-ethylbenzothiazole-6-sulfonic acid) diammonium (ABTS) substrate (Roche Diagnostics) diluted 1:1,000 in hydrogen peroxide (Tecan). Optical density (OD) at 405 nm was determined using an M1000Pro plate reader (Tecan). GraphPad Prism 9.1.2 was used for plotting and AUC calculation. 2A10¹ and mGO53³ were used as positive and negative controls, respectively. A list of peptide and protein sequences can be found in Supplementary Table 9.

3.2.19.4 Poly-reactivity ELISA

A polyreactive ELISA was performed as described^{1,120}. Insulin (10 µg/ml; Sigma Aldrich), lipopolysaccharide (LPS; 10 µg/ml; Sigma Aldrich) and double-stranded DNA (dSDNA; 20 µg/ml; Sigma Aldrich) were coated onto 384-well polystyrene plates (Corning) with high binding capacity and incubated at 4 °C overnight. The plates were washed three times with deionized water using a Tecan plate washer. The ELISA plates were incubated with blocking buffer (1x PBS, 0.05% (v/v) Tween20, and 1 mM EDTA) for one hour at room temperature. The plates were then loaded with 1:4 serially diluted (initial concentration of 1 µg/ml in 1x PBS) mAbs and incubated for 1.5 hours at room temperature. mAbs were detected with a goat anti-human IgG secondary antibody (Jackson Immuno Research) coupled to horseradish peroxidase (HRP) diluted 1:1,000 in blocking buffer and then detected with a 2,2'-azino-bis (3-ethylbenzothiazole-6-sulfonic acid) diammonium (ABTS) substrate (Roche Diagnostics) diluted 1:1,000 in hydrogen peroxide (Tecan). Optical density (OD) at 405 nm was determined using an M1000Pro plate reader (Tecan). GraphPad Prism 9.1.2 was used for plotting and AUC calculation. mAbs were designated as polyreactive when they recognized at least two of the three structurally distinct antigens. mAbs ED38¹¹ and JB40¹¹ were used as highly and mildly polyreactive mAbs, respectively, and mGO53¹ was used as a negative control.

3.2.19.5 Blocking ELISA

The procedure for the blocking ELISA was the same as for the mAbs antigen ELISA, with the following modifications. After 1 hour of blocking, plates were loaded with 1:2 serially diluted (initial concentration of 64 µg/ml in 1x PBS) mAbs and incubated for 1.5 hours at room temperature. Without washing the plates, 0.5 µg/ml of biotinylated mAb 1710⁵ or mAb 1512⁹ was added to compete with the incubated mAbs for 15 minutes at room temperature. The plates were then washed and incubated with streptavidin-HRP (1:1,000 dilution in blocking buffer). Detection of bound biotin-1710 or biotin-1512 was determined with 2,2'-azino-bis-(3-ethylbenzothiazoline-6-sulfonic acid) diammonium (ABTS) substrate (Roche Diagnostics) diluted 1:1000 in hydrogen peroxide. Optical density (OD) at 405 nm was determined using an M1000Pro plate reader (Tecan). GraphPad Prism 9.1.2 was used for plotting and AUC calculation.

3.2.20 Surface Plasmon Resonance (SPR)

Surface plasmon resonance (SPR) is an instrument that identifies a wide range of samples, such as mAbs, proteins, and small compounds, in a high-throughput, real-time, and label-free manner. SPR was used to determine the binding affinity of mAbs to PfCSP-derived N-Junc and NANP₅ peptides or the C-CSP protein. Measurements were performed using a BIACORE T200 (GE Healthcare) equipped with an S CM5 series sensor chip (GE Healthcare). The running buffer consisted of 10 mM HEPES mixed with 150 mM NaCl, 0.02% Tween20, and 0.05% BSA at a pH of 7.4. A human antibody Fab capture kit (GE Healthcare) was used to immobilize anti-human IgG on the sensor chip by amine coupling according to the manufacturer's instructions. PfCSP-reactive mAbs and an irrelevant mAb, mGO53³, were captured at the same concentrations in the sample and reference flow cells, respectively. Running buffer at a rate of 10 μ l/min was used to stabilize both flow cells for 20 min after collection. A series of concentrations (0, 0.015, 0.09, 0.55, 3.3, and 20 M) of resuspended peptides (N-Junc and NANP₅) or C-CSP protein were injected into the running buffer. Each injection was followed by a 60-second association and a 180-second dissociation at a flow rate of 30 μ l/min and a temperature of 25°C. After all the runs, both flow cells were regenerated with 3 MgCl₂. BIACORE T200 software version 2.0 was used to perform the steady state kinetic analysis and data fitting for the 1:1 binding model.

3.2.21 Statistical analysis

GraphPad Prism (version 9.1.2) and RStudio (version 4.2.2)¹⁸⁰ were used to analyze the data from the experiments. Plots were generated using GraphPad Prism 9.1.2, Adobe Illustrator CS6 v16.0.3, and R's ggplot2 package. Parametric or non-parametric tests were applied accordingly and are indicated in the figure legends. GraphPad Prism (version 9.1.2) was used for all statistical analysis. P-values (*P < 0.05; **P < 0.01; ***P < 0.001; ****P < 0.0001) were indicated in the graphs and figure legends.

4.0 RESULTS

4.1 Human malaria immunization trial and sample collection

To investigate anti-PfCSP B cell responses at the polyclonal and monoclonal levels, I analyzed serum samples and human peripheral blood mononuclear cells (PBMCs) from volunteers who had participated in a Phase I malaria vaccination clinical trial (MAVACHE verification phase) conducted by Prof. Dr. Benjamin Mordmüller and colleagues at the Institute of Tropical Medicine in Tübingen, Germany. In this study, 12 healthy, malaria-naïve European volunteers were intravenously immunized with 900,000 radiation-attenuated, aseptic, purified, cryopreserved *Plasmodium falciparum* sporozoites (Pf RAS), on day 0, 7, and 28 (Figure 6) ¹⁰. Serum samples corresponding to days 28 (III+28), 55 (III+55) and 83 (III+83), and PBMCs from days 14 (III+14), 35 (III+35) and 63 (III+63) after the last immunization were analyzed and reported in this thesis.

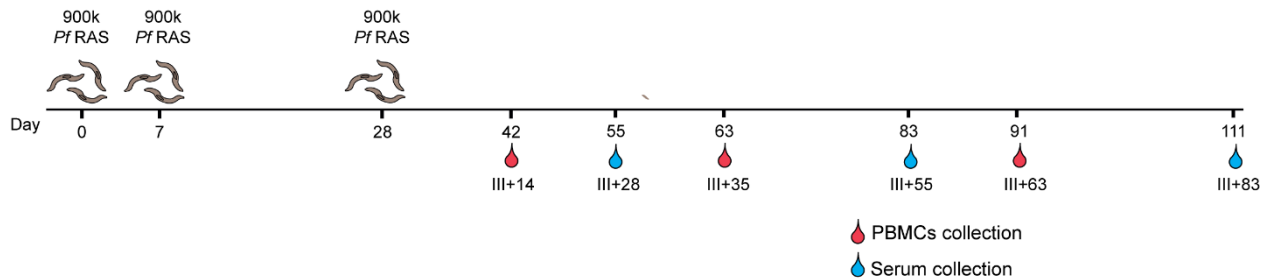


Figure 6: Schematic representation of the human malaria vaccine immunization trial (MAVACHE verification phase). 900.000 radiation-attenuated *Plasmodium falciparum* sporozoites (Pf RAS) were administered intravenously to 12 malaria-naïve healthy European volunteers. Blood samples for PBMCs isolation were collected 14, 35 and 63 days after the last immunization. Serum samples were collected 28, 55 and 83 days after the third immunization, after the third immunization. Collection times for PBMCs and serum samples are depicted by the red and blue arrows, respectively. The clinical study was conducted by Prof. Dr. Benjamin Mordmüller and colleagues at the Institute of Tropical Medicine in Tübingen, Germany ¹⁰.

4.2 Quality of anti-PfCSP serum antibody response after *Plasmodium falciparum* (Pf RAS) immunization

4.2.1 Strong anti-PfCSP serum antibody response

To assess the strength and PfCSP domain preference of the antibody response after *Pf* RAS immunization, I measured the IgM and IgG titers against the full length PfCSP (hereafter referred as FL-CSP) by ELISA in all available serum samples (Figures 7A and 7B). The antibody response curve (OD values) and the area under the curve (AUC) were plotted as a measure of antibody binding magnitude. Of note, serum samples corresponding to III+55 time point for volunteers M1.050 and M1.086 were not available. Compared to placebo recipients, anti-FL-CSP IgM and IgG antibody titers were higher in all immunized volunteers (Figure 7A). The average IgM and IgG decreased over time with considerable variability amongst the volunteers (Figure 7B). Nevertheless, three volunteers (M1.063, M1.064, and M1.086) showed a stable IgG titer over the course of the three time points. Taken together, these data demonstrate that *Pf* RAS immunization elicits a strong anti-PfCSP serum antibody response.

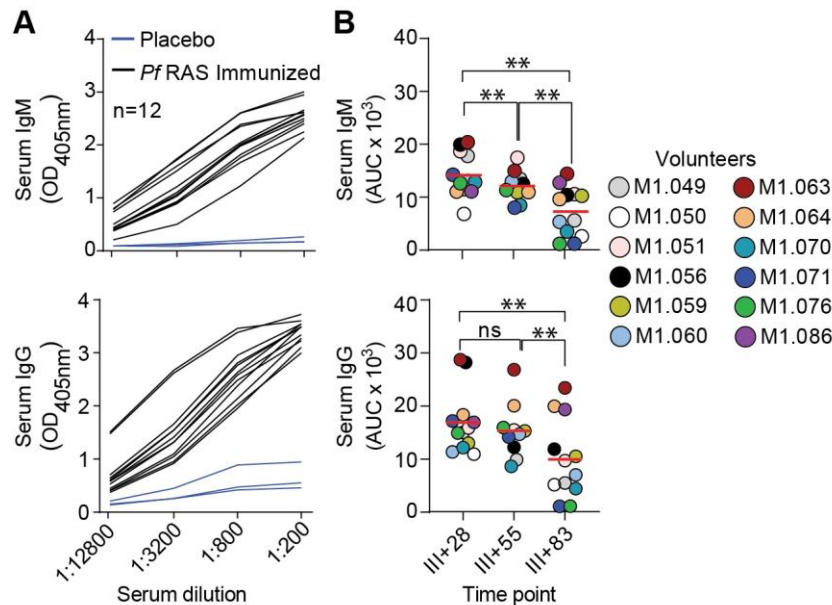


Figure 7: Immunization with *Pf* RAS induces strong anti-PfCSP response. (A) Serum IgM (top) and IgG (bottom) response (OD values) against FL-CSP in immunized (black lines; n=12) and placebo (blue lines; n=3) volunteers. **(B)** Anti-FL-CSP serum IgM (top) and IgG (bottom) antibody titers in immunized volunteers at indicated time points (III+28, III+55 and III+83). Each circle represents ELISA area under the curve (AUC) values for indicated volunteers. Horizontal red lines in **(B)** indicate mean values. **P < 0.01, Wilcoxon test **(B)**. Data are representative of two independent experiments.

4.2.2 *Pf* RAS immunization induces strong anti-N-Junc, NANP, and C-CSP antibodies

To determine binding of the induced humoral antibody response against PfCSP subdomains, I measured IgM and IgG titers against peptides covering the N-terminus (hereafter referred as N-CSP), the junctional epitope (hereafter referred as N-Junc), a representative of the central repeat with five repetitive motifs of the tetrapeptide asparagine-alanine-asparagine-proline (hereafter referred as NANP₅), and the entire C-terminus (hereafter referred as C-CSP) at different serum dilutions. The AUC was calculated as a measure of antibody binding strength. When compared to anti-N-Junc, NANP₅, or C-CSP titers, IgM and IgG antibody titers against the N-CSP domain were overall low in all volunteers (Figure 8A), demonstrating the poor immunogenicity of the N-CSP domain. Although the IgG response was strongest against NANP₅, strong anti-N-Junc and C-CSP titers were also detected (Figure 8A), suggesting that these epitopes are also immunodominant B cell epitopes that could be targeted in response to *Pf* RAS immunization. Similar to anti-FL-CSP titers, the average IgM and IgG titers against the three epitopes decreased over time after the third immunization (Figure 8B). Only one volunteer (M1.063) showed a stable anti-NANP₅ IgG titer over time. Thus, repeated immunization with *Pf* RAS induced a strong anti-PfCSP antibody response with parallel targeting of N-Junc, NANP repeat, and C-CSP epitopes at the polyclonal level.

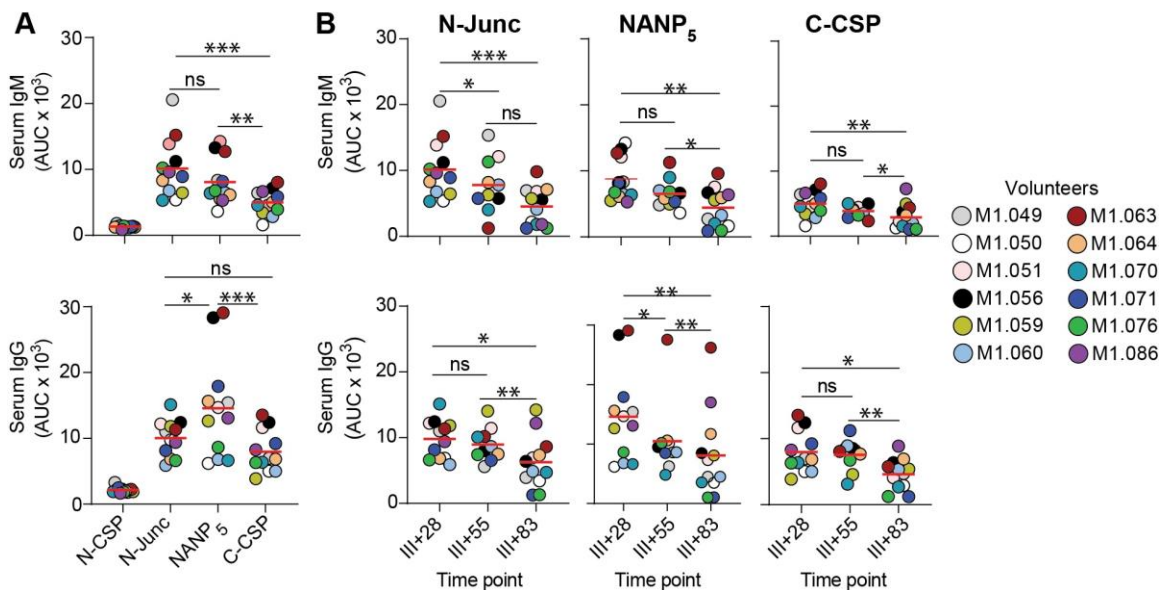


Figure 8: Strong antibody response against the N-Junc, NANP₅, and C-CSP domains. (A) AUC of serum IgM (top) and IgG (bottom) antibodies binding to indicated PfCSP-derived peptides (N-CSP, N-Junc and NANP₅) and C-CSP domain. (B) AUC of serum IgM (top) and IgG (bottom) antibody binding to N-Junc (left), NANP₅ (middle) and C-CSP (right) epitopes at indicated time points (III+28, III+55 and III+83). Each circle represents ELISA area under the curve (AUC) values for individual volunteers indicated in different colours. Horizontal red lines in (A) and (B) indicate mean values. **P* < 0.05, ***P* < 0.01, ****P* < 0.001, Wilcoxon test (A) and (B). Data are representative of two independent experiments.

4.3 B cell memory against PfCSP in response to *Pf RAS* immunization

4.3.1 *Pf RAS* immunization induces strong anti-PfCSP memory response

To determine the frequency of live PfCSP-reactive CD19+CD27+ memory B cells and total CD27+CD38+ plasmablasts, I performed flow cytometric analyses on PBMCs from all volunteers 14, 35 and 63 days after the third immunization (Figure 9A). Recombinantly expressed biotinylated FL-CSP was used to detect PfCSP reactive memory B cells (PfCSP MBCs). Notably, PBMCs from volunteers M1.064, M1.059 and M1.086 corresponding to timepoints III+14, III+35 and III+63, respectively, were not available. Compared to the non-exposed volunteers, *Pf RAS* immunized volunteers had a significantly higher mean frequency of PfCSP-reactive MBCs, which decreased after the third immunization, with variability amongst the volunteers (Figure 9B). Fourteen days after the third immunization, the frequency of PfCSP-reactive MBCs in 3 volunteers (M1.051, M1.056 and M1.071) accounted for more than 1.5% of all memory B cells, indicating a strong anti-PfCSP memory response in these volunteers. The average frequency of PfCSP-reactive MBCs at III+14 time point was similar to that observed at III+7 time point in volunteers who received live sporozoites (*PfSPZ*) under chemoprophylaxis¹²⁰, but higher than the average frequency observed in naturally exposed African volunteers¹.

Only 3 volunteers (M1.070, M1.071 and M1.086) showed considerably higher plasmablast frequencies compared to non-exposed volunteers (Figure 9C). A mean plasmablast frequency of 0.9% among all B cells was already measured in malaria-naïve European volunteers, demonstrating a constant background B-cell response in humans. In summary, these data show that immunization with *Pf RAS* elicited a strong anti-PfCSP MBC response.

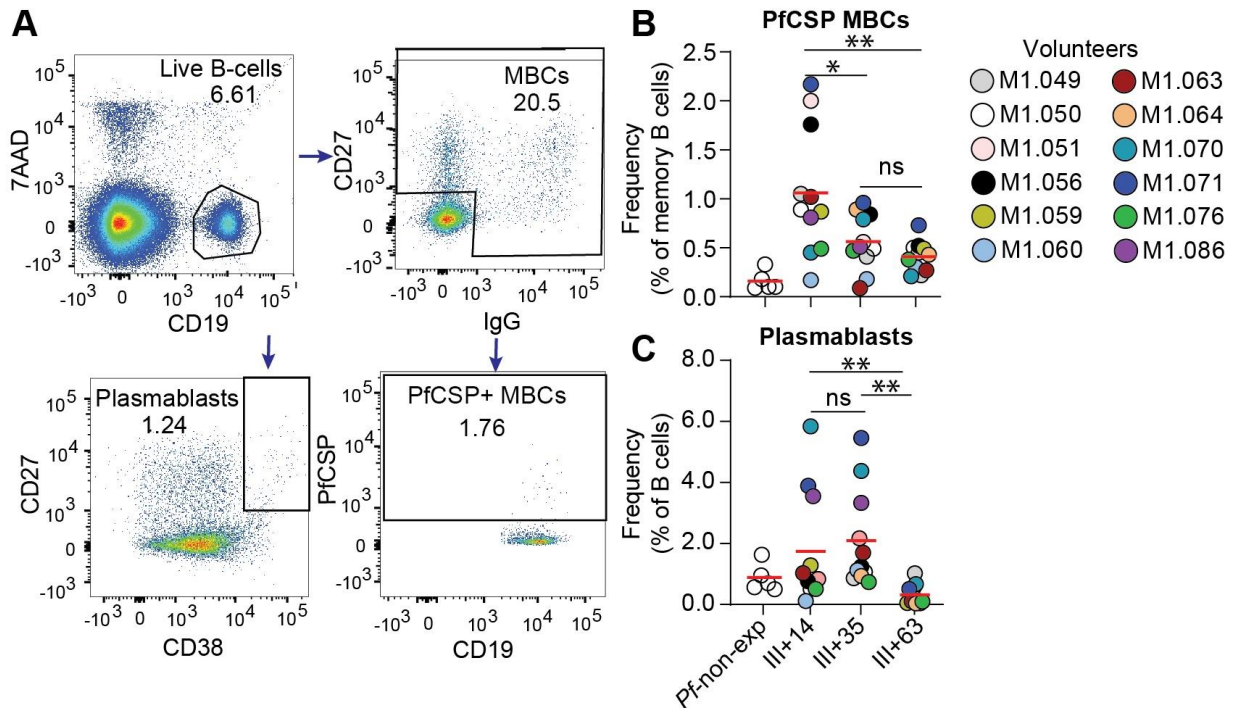


Figure 9: Strong induction of PfcSP-reactive MBCs in Pf RAS immunized volunteers. (A) Flow-cytometric cell staining and single-cell isolation strategy for PfcSP-reactive MBCs and plasmablasts from all volunteers and time points. (B and C) PfcSP-reactive MBCs (B) and plasmablasts (C) frequencies in PBMCs of indicated volunteers at indicated time points (III+14, III+35, and III+63). Each circle represents individual volunteers indicated in different colours. Plasmodium falciparum-non-exposed (Pf-non-exp; open circles) volunteers shown for comparison. Horizontal red lines in (B) and (C) indicate mean values. *P < 0.05, **P < 0.01, Wilcoxon test (B) and (C).

4.3.2 Immune cell sorting and amplification of Ig gene heavy and light chains

To assess the molecular features associated with the anti-PfcSP immune response, I isolated 3,676 single PfcSP-reactive MBCs using biotinylated FL-CSP (*Pf* NF54 strain), and 6,372 total plasmablasts (combined total cell number: 10,048 cells) from PBMCs of all volunteers corresponding at all available time points. The phenotypic information of the sorted cells was linked to the position of the cell on the plate using index sorting algorithm, which allows identification of populations by their original position. 8,404 cells, comprising 3394 single PfcSP memory B cells and 5,010 plasmablasts were processed for Ig RT-PCR amplification and next generation sequencing (NGS; Figure 10A). Using hexamer primers, the total RNA was reverse transcribed, and the resulting cDNA was used as template for the PCR amplification of Ig gene heavy and light chains. Miseq Illumina sequencing platform were used to bulk-sequence the resulting amplicons.

Paired IgH and Igκ/Igλ gene sequences for both PfCSP reactive MBCs and plasmablasts were obtained at high average efficiency of 55% and 51%, respectively (Figure 10A and 10B). This resulted in average amplification and sequencing efficiencies of 65%, 44% and 30% Ig heavy, kappa and lambda genes, respectively, for PfCSP reactive MBCs, and of 58%, 46% and 28% Ig heavy, kappa and lambda genes, respectively, for plasmablasts (Figure 10B). A total of 1,884 and 2,539 paired Ig gene sequences of PfCSP-reactive MBCs and plasmablasts, respectively, were analyzed and reported in this study (Supplementary Table 1).

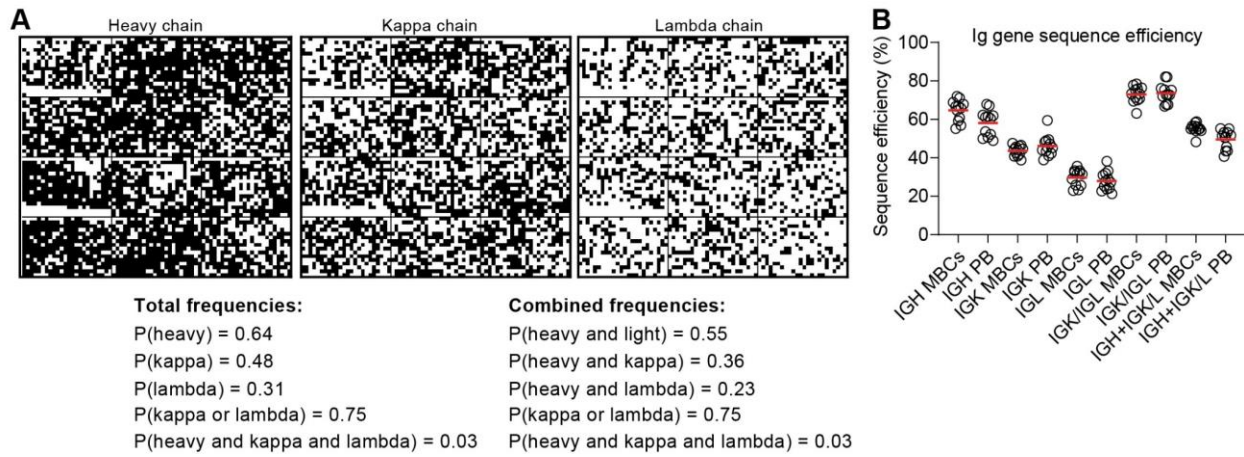


Figure 10: Ig gene sequence efficiency. (A) Representative heatmap illustrating sequence +ve (black) or sequence -ve (white) in the secondary IgH, Igκ and Igλ sequences. (B) Sequence efficiencies of Ig genes derived from PfCSP MBCs and plasmablasts. Data in (A) are sequence efficiencies of 6 out of the 12 volunteers from one matrix. The horizontal red lines in (B) indicate the mean value.

4.4 Ig gene characteristics of PfCSP reactive memory B cells and plasmablasts

4.4.1 PfCSP-reactive memory B cells are dominated by IgM

To assess the isotype distribution of PfCSP-reactive MBCs and plasmablasts after *Pf*RAS immunization, I analyzed the immunoglobulin heavy constant (*IGHC*) regions in all Ig gene sequences. Whereas anti-PfCSP MBC response was dominated by B cells expressing *IGHM* genes over *IGHG*, with near absence of *IGHA* in all volunteers, *IGHA* genes were expressed by nearly 50% of plasmablasts in most volunteers (Figure 11A). Nonetheless, in both PfCSP memory B cells and plasmablasts, there was no discernible change in the frequency of B cells expressing *IGHM*, *IGHG*, and *IGHA* genes over time. (Figure 11B, Supplementary Figure 1). The average

frequency of *IGHM* and *IGHG* gene usage in PfCSP-reactive MBCs was comparable to the observed frequency in live PfSPZ-exposed volunteers after the last immunization¹²⁰. Overall, these results show that IgM memory B cells are continuously recruited in response to PfCSP after PfRAS immunization.

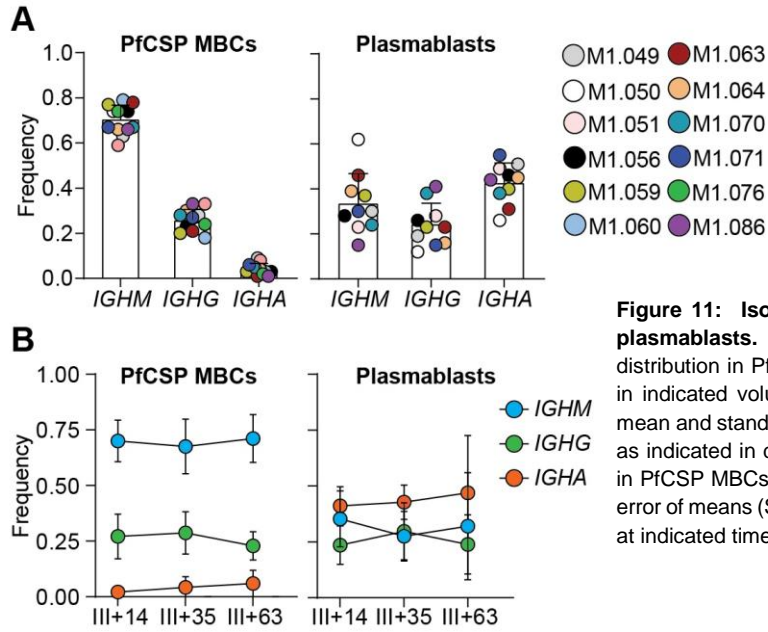


Figure 11: Isotype distribution in PfCSP-reactive MBCs and plasmablasts. (A) *IGHC* constants (*IGHM*, *IGHG* and *IGHA*) distribution in PfCSP-reactive MBCs (left) and plasmablasts (right) in indicated volunteers (pooled timepoints). Bar graphs show the mean and standard deviation, the circles mark individual volunteers as indicated in different colours. **(B)** Change in isotype distribution in PfCSP MBCs (left) and plasmablasts (right) over time. Standard error of means (SEMs) amongst volunteers are indicated per isotype at indicated timepoints.

4.4.2 Somatic hypermutation (SHM) in PfCSP-reactive MBCs and plasmablasts

To determine the mutation status of isolated memory B cells, I analysed the somatic hypermutation (SHM; in base pair) counts in the variable regions of immunoglobulin heavy (*IGHV*) locus of PfCSP-reactive MBCs and compared to the isolated plasmablasts. The vast majority of the PfCSP-reactive MBCs and plasmablasts carried mutations in their heavy chains, which were overall higher in plasmablasts (Supplementary Figure 2). A large number of PfCSP-reactive MBCs were encoded by low mutation 14 days after the last immunization (III+14), and the average mutation count increased over time, indicating the participation of PfCSP-reactive MBCs in the germinal center response (Figure 12A). Interestingly, PfCSP-reactive MBCs expressing *IGHG* genes continued to accumulate mutations over the three time points (Figure 12B), suggesting that class-switched IgG cells were continuously selected and participated in the germinal center response for affinity maturation. In summary, these results demonstrate that PfCSP-reactive memory B cells actively participated in germinal center responses after PfRAS immunization.

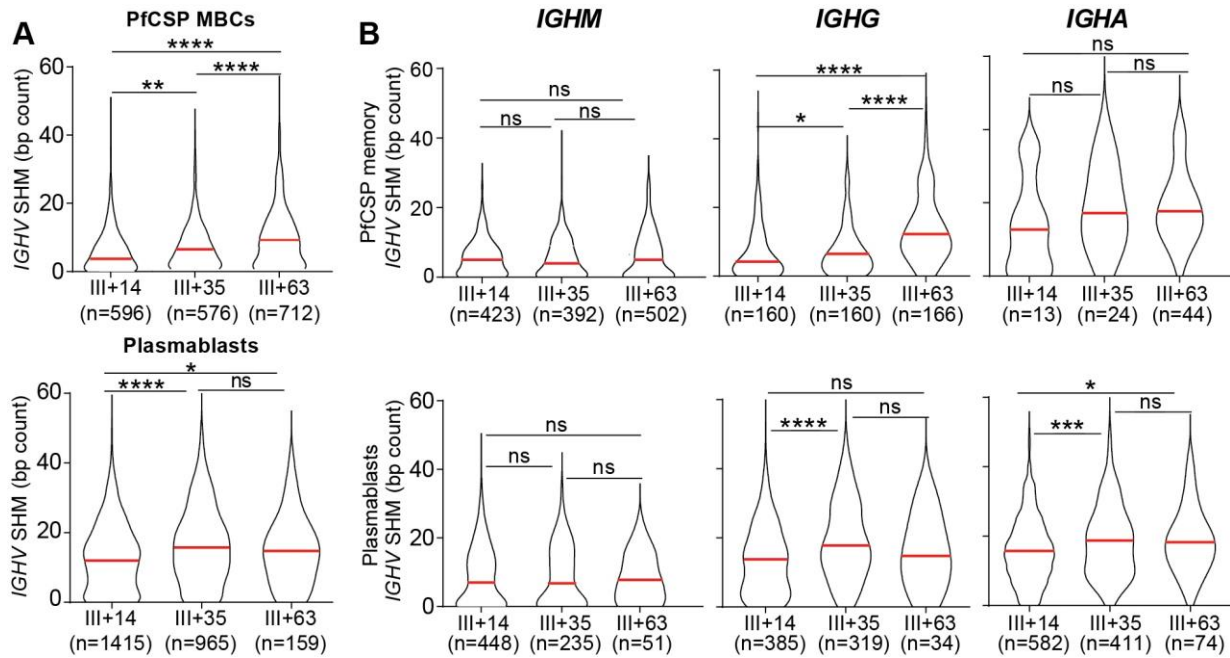


Figure 12: IGHV somatic hypermutation (SHM) counts in PfcSP-reactive MBCs and plasmablasts. (A) PfcSP-reactive MBCs (top) and plasmablasts (bottom) IGHV SHM counts (bp) after three *Pf* RAS immunizations from all volunteers. **(B)** IGHV SHM base pair counts of *IGHM* (left), *IGHG* (middle) and *IGHA* (right) in PfcSP MBCs (top) and plasmablasts (bottom) in immunized volunteers. Data shown in (A) and (B) are from pooled volunteers. Horizontal red lines in (A) and (B) indicate mean SHMs. * $P < 0.05$, ** $P < 0.01$, *** $P < 0.001$, **** $P < 0.0001$ Two tailed Mann-Whitney test (A) and (B).

4.4.3 PfcSP-reactive memory B cells undergo clonal expansion following *Pf* RAS immunization

To determine the extent of focused B-cell response against PfcSP, I assess the degree of clonal expansion in PfcSP-reactive MBCs and plasmablasts in all volunteers and available timepoints. Clonally expanded B cell clusters were identified and defined as B cells with the same *IGV* (*IGHV* and *IGKV/IGLV*) and *IGJ* (*IGHJ* and *IGKJ/IGLJ*) genes, same heavy and light CDR3 length, and similar CDR3 nucleotide sequences with shared or non-shared somatic hypermutations.

The degree of clonal expansion was overall higher in PfcSP-reactive MBCs than in the plasmablasts (Figure 13A), possibly because the plasmablasts were isolated using a non-antigen-specific approach. The expanded PfcSP-reactive MBCs expressing *IGHM* and *IGHG* genes had higher mutation counts compared to the non-expanded cells (Figure 13B), suggesting that they were selected for affinity maturation in the germinal center. Nevertheless, the frequency of clonally expanded cells in PfcSP-reactive MBCs continued to decrease with time in most volunteers, resulting in less than 12% clonal lineages sixty-three days after the third immunization (Figure

13C). To identify clonal overlap between the PfCSP memory B cells and plasmablasts, I evaluated the expression of CD38, an activation marker, in the expanded PfCSP-reactive MBCs (Figure 13D). The memory B cell (CD27+CD38-) and plasmablast (CD27+CD38+) phenotypes were both present in a series of memory B cell clusters in all but one volunteer (M1.070), demonstrating that some of the expanded precursor B cells differentiated into both memory B cells and plasmablasts¹²⁰. Taken together, these data show that the PfCSP memory B cells induced in these volunteers after *Pf* RAS immunization were clonally expanded, and also highlight that a single progenitor B cell can emerge from the germinal center and differentiate into memory B cells and plasmablasts.

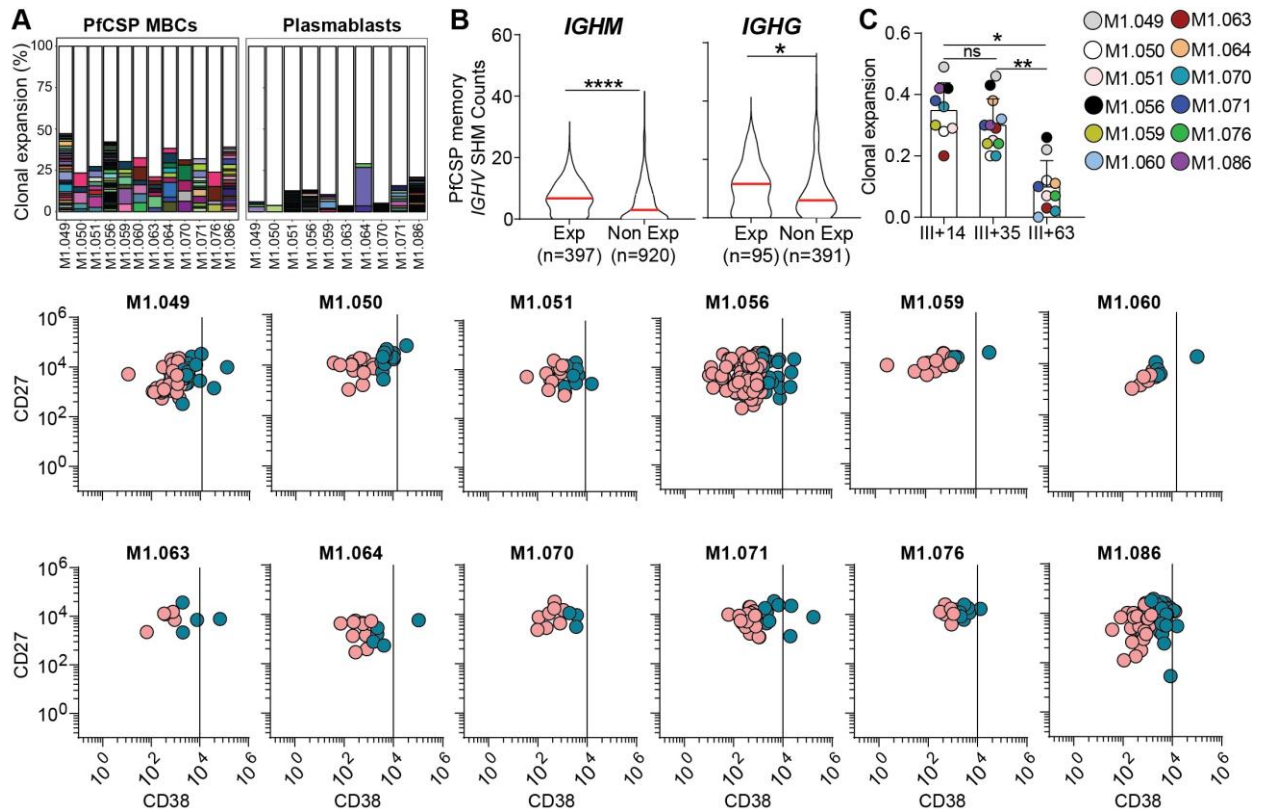


Figure 13: Clonal expansion in PfCSP-reactive MBCs and plasmablasts. (A) Degree of clonal expansion in PfCSP memory B cells (left) and plasmablasts (right) after three *Pf* RAS immunizations in indicated volunteers. Individual cell clusters are coloured; unique sequences are white (top). (B) *IGHV* SHM base pair counts of *IGHM* (left), *IGHG* (right) genes in expanded (Exp) and non-expanded (Non-Exp) PfCSP memory B cells in immunized volunteers. (C) Frequency of clonally expanded cells per volunteer at indicated time point (III+14, III+35 and III+63) in PfCSP memory B cells. Bar graphs show the mean and standard deviation, the circles mark individual volunteers as indicated in different colours. Clusters of representative B cells overlapping between memory B cells (light coral; CD27+CD38-) and plasmablasts (Teal; CD27+CD38+) in all immunized volunteers. Data shown in (A), (B) and (D) are from pooled time points. Data shown in (B) are from pooled volunteers and time points Horizontal red lines in (B) indicate mean SHMs. * $P < 0.05$, ** $P < 0.01$, Wilcoxon test (C).

4.4.4 Strong enrichment of *IGH3-33* and *IGHV3-21* gene segments in PfCSP-reactive memory B cells

To assess the gene usage following *Pf* RAS immunization, I analyzed the variable heavy (*IGHV*) gene usage in PfCSP-reactive MBCs and compared to plasmablasts or previously published total memory B cells from healthy volunteers ². *IGHV3* gene family was strongly enriched in PfCSP-reactive MBCs compared to plasmablasts or memory B cells from healthy volunteers (Figure 14A). Gene segments analyses revealed that *IGHV3* gene enrichment in PfCSP-reactive MBCs was predominantly driven by *IGHV3-33* and *IGHV3-21* gene segments in most volunteers (Figure 14B; supplementary Figure 3A). *IGHV3-33* gene segments were mostly paired with *IGKV1-5*, a gene combination that is strongly associated with the central NANP repeat reactivity ^{4,8,108,182}. In contrast, *IGHV3-21* gene segments were mainly paired with the *IGLV3-1* or *IGLV3-21* (Figure 14C; Supplementary Figure 3B), a gene combination not strongly associated with PfCSP reactivity. The vast majority of *IGHV3-33* and *IGHV3-21* gene segments originated from the non-expanded B cells (Figure 14D). Remarkably, while the *IGHV3-33*-encoded PfCSP memory B cell Ig genes were dominated by B cells expressing *IGHM* genes, *IGHV3-21*-encoded Ig genes were dominated by B cells expressing *IGHG* genes and carried higher mutation counts (Figure 14E and 14F), suggesting the active participation of VH3-21 antibodies in the germinal center response for affinity maturation. Collectively, these results show that repeated exposure to *Pf* RAS induced PfCSP-reactive MBC response that is associated with strong enrichment of *IGHV3-33* and *IGHV3-21* gene segments.

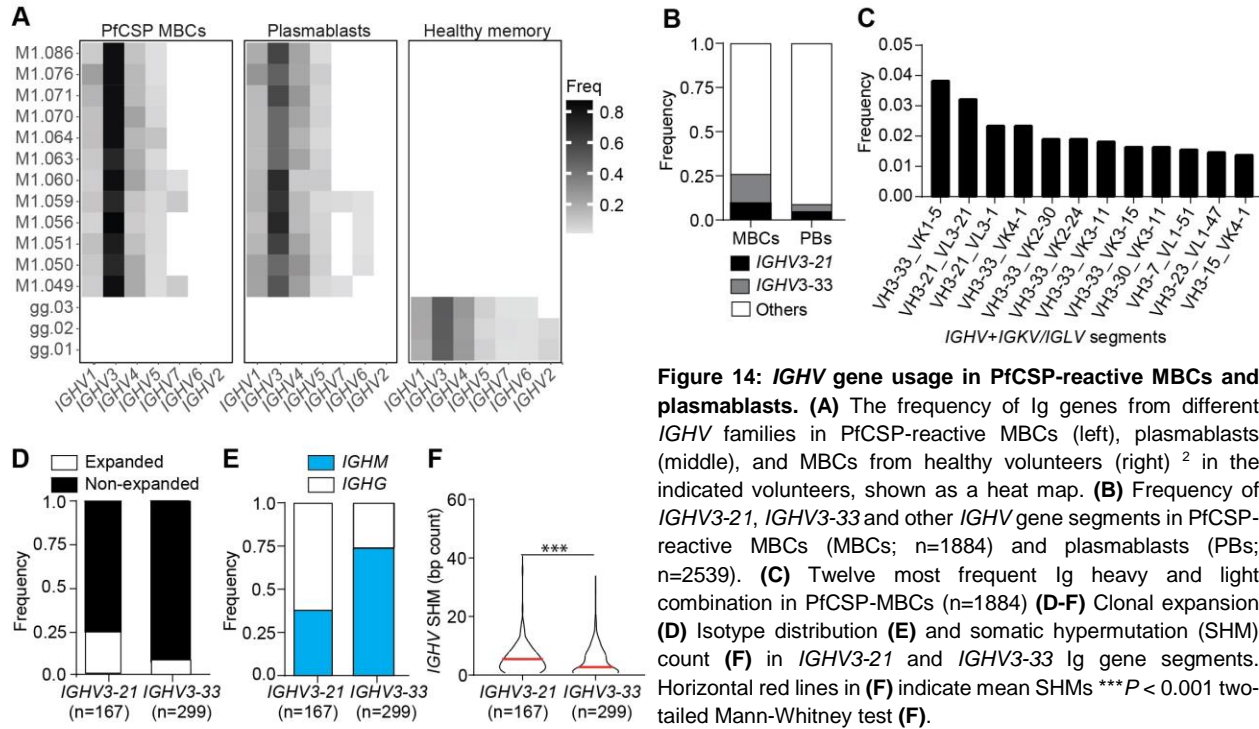


Figure 14: IGHV gene usage in PfCSP-reactive MBCs and plasmablasts. (A) The frequency of Ig genes from different IGHV families in PfCSP-reactive MBCs (left), plasmablasts (middle), and MBCs from healthy volunteers (right) ² in the indicated volunteers, shown as a heat map. (B) Frequency of IGHV3-21, IGHV3-33 and other IGHV gene segments in PfCSP-reactive MBCs (MBCs; n=1884) and plasmablasts (PBs; n=2539). (C) Twelve most frequent Ig heavy and light combination in PfCSP-MBCs (n=1884) (D-F) Clonal expansion (D) Isotype distribution (E) and somatic hypermutation (SHM) count (F) in IGHV3-21 and IGHV3-33 Ig gene segments. Horizontal red lines in (F) indicate mean SHMs ***P < 0.001 two-tailed Mann-Whitney test (F).

4.5 Reactivity, epitope specificity and functional characterization of PfCSP reactive MBCs monoclonal antibodies (mAbs)

To evaluate the antigen binding profiles of PfCSP mAbs, I cloned and recombinantly expressed a total of 267 mAbs from PfCSP MBCs of all volunteers corresponding to III+14 and III+35 time points (supplementary Table 1 and 2). The selected mAbs covered the entire repertoire diversity, including 42 VH3-21 and 47 VH3-33 mAbs with similar isotype distribution (Supplementary Figure 4A). Regardless of their original isotype, all mAbs were expressed as IgG1 for fair comparison. Binding of mAbs to FL-CSP and PfCSP-derived peptides, and their affinities, were evaluated by ELISA and surface plasmon resonance (SPR), respectively. Based on their binding profiles and Ig gene characteristics, a subset of the mAbs was tested *in vitro* and *in vivo* for their ability to inhibit sporozoites traversal and mediate protection.

4.5.1 PfCSP-reactive mAbs target N-Junc, NANP and C-CSP epitopes

The reactivity of expressed mAbs to FL-CSP was assessed by ELISA (Figure 15A; Supplementary Figure 4B). In this assay, a chimeric version of a PfCSP-reactive mAb 2A10^{1,85}, and a non-PfCSP-reactive mAb mGO53³, were used as positive and negative controls, respectively. Serial dilutions with a starting concentration of 4 µg/ml were performed for each antibody and the AUC was calculated as a measure for the binding quality. An AUC cut-off value of three was chosen to distinguish between reactive (AUC ≥ 3) and non-reactive (AUC < 3) mAbs. Of the panel of expressed mAbs, 177 (66%) were reactive to FL-CSP and showed no reactivity against irrelevant antigens (Figure 15A), demonstrating their specificity for the PfCSP antigen. Most of the high-binding FL-CSP-reactive mAbs had relatively few mutations in their heavy chains regardless of their isotype (Figure 15B).

To determine the epitope specificity and cross-reactivity profile of the PfCSP-reactive mAbs, I measured binding to N-CSP, N-Junc, NANP₅, NANP₁₀ (a longer representative of the central repeat), and C-CSP domain. While no N-CSP specific mAb was identified, 23 mAbs were specific for the N-Junc, 19 recognized NANP₅, 72 showed specificity for C-CSP and 25 mAbs recognized more than one epitope and were therefore referred as cross-reactive mAbs (Figure 15C). With the exception of mAb 1961, that showed cross-reactivity to the N-Junc, NANP₅ and C-CSP, all cross-reactive mAbs showed dual specificity for the N-Junc and NANP repeat alone. The remaining mAbs (38/178) showed reactivity to the longer NANP₁₀ peptide, likely due to their weak affinity for the short (NANP₅) peptide (Figure 15D). N-Junc, NANP and C-CSP reactive mAbs were identified in most volunteers (Figure 15E), demonstrating the parallel targeting of the three epitopes at monoclonal level in response to *Pf* RAS immunization. Only volunteer M1.070, from whom only 2 mAbs were successfully cloned, lacked N-Junc or C-CSP specific mAbs. Taken together, these results show that *Pf* RAS immunization induced cross-reactive and epitope specific antibodies against the N-Junc, NANP repeat, and C-CSP domains.

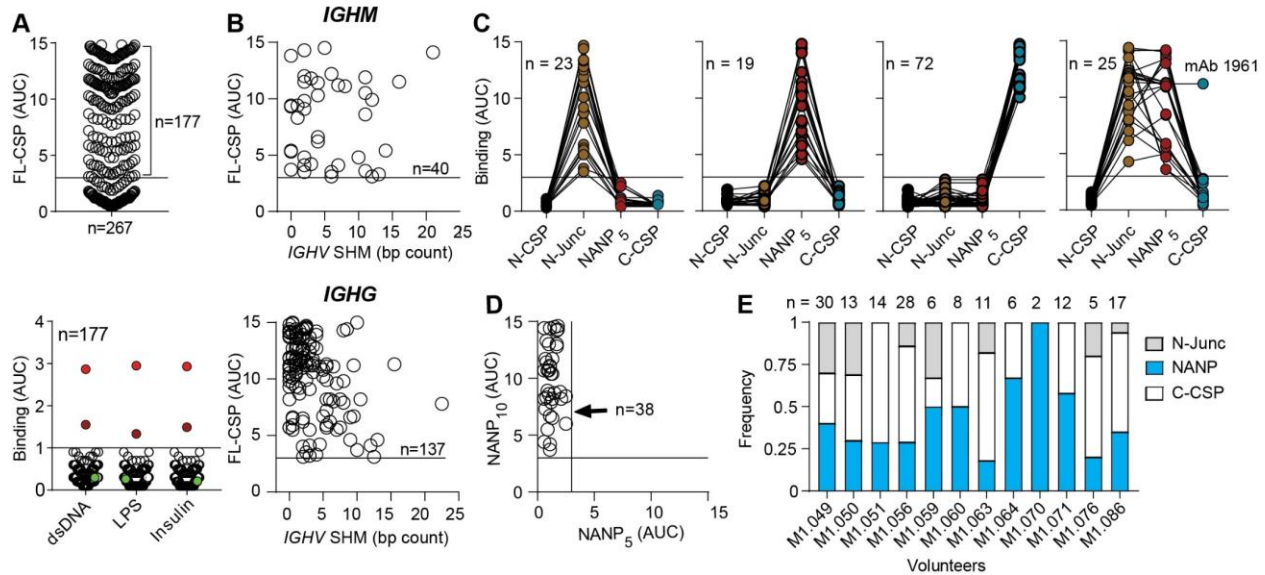


Figure 15: ELISA binding profiles of PfCSP-reactive MBCs mAbs. (A) Corresponding ELISA AUC values of Pf-CSP-reactive memory B cell mAbs (n=267; top) reactivity to FL-CSP, and of FL-CSP reactive mAbs to irrelevant antigens (n=177; bottom). mAbs polyreactivity were compared to the highly polyreactive mAb ED38¹¹ (bright red), the mildly polyreactive mAb JB40¹¹ (dark red), and the non-polyreactive mAb mGO53³ (green). (B) ELISA FL-CSP binding versus *IGHV* SHM counts in *IGHM* (top) and *IGHG* (bottom) encoded FL-CSP reactive mAbs. (C) ELISA reactivity of FL-CSP reactive mAbs with the PfCSP-derived N-CSP, N-Junc, NANP₅ and C-CSP antigens. (D) ELISA binding strength of NANP₁₀ reactive mAbs to NANP₅ versus NANP₁₀ peptide. (E) Frequency of N-Junc, NANP and C-CSP specific mAbs in indicated volunteers. Black horizontal lines in A-D indicate the threshold for binding. The data shown in A-D are average of three independent experiments.

4.5.2 Determination of the relative affinity of epitope-specific and cross-reactive mAbs

To further characterize the N-Junc, NANP and C-CSP specific mAbs, I determined their binding affinities by surface resonance plasmon (SPR) and compared to affinities of cross-reactive mAbs. The affinity range for N-Junc or NANP₅ specific mAbs was between 10⁻³ and 10⁻⁸ M (Figures 16A and 16B). In contrast, C-CSP-specific mAbs recognized the epitope with affinity between 10⁻⁵ to 10⁻¹⁰ M, demonstrating their strong affinity for the domain (Figure 16C). Similar to previous study⁴, majority of the cross-reactive mAbs showed higher affinity for the NANP₅ (Figures 16A to 16C), suggesting that their affinity to NANP₅, but not N-Junc or C-CSP, mediates cross-reactivity. Although most high affinity N-Junc, NANP₅, and C-CSP specific mAbs were class-switched and carried somatic mutations as signs of affinity maturation, several germline mAbs with high affinity for these epitopes were also identified (Figure 16D). This indicates that naïve human B cell repertoire contains numerous N-Junc, NANP, and C-CSP specific progenitor B cells. Taken together, these data provide evidence of efficient affinity maturation of N-Junc, NANP and C-CSP specific mAbs.

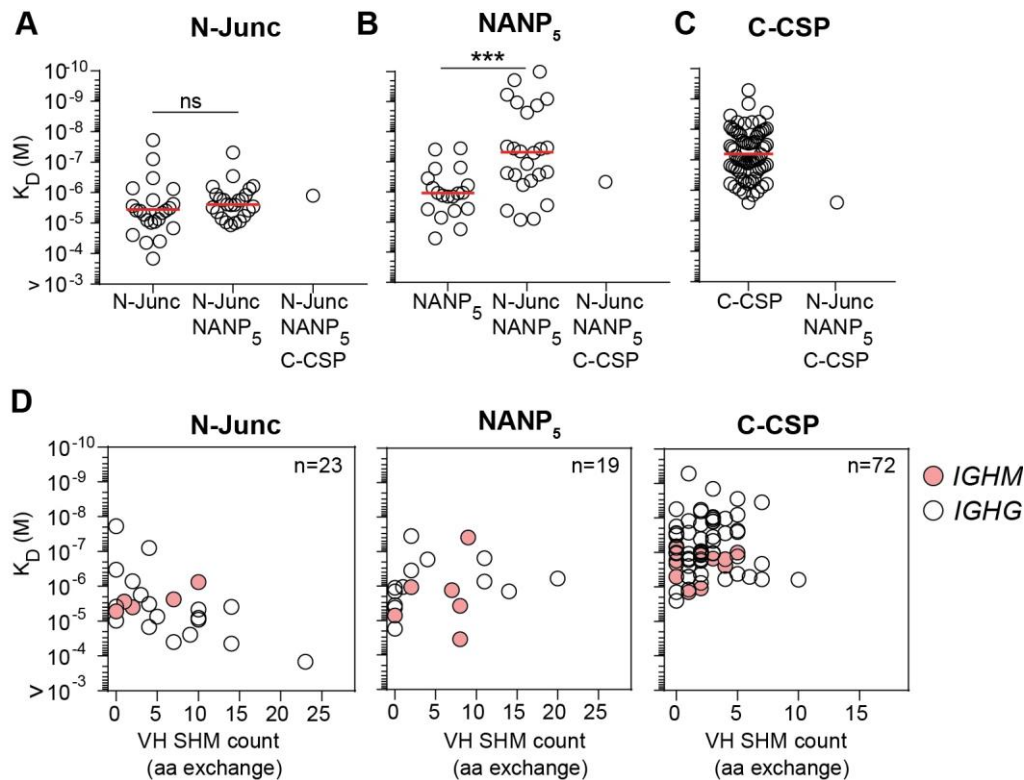


Figure 16: SPR affinity profiles of PfCSP reactive mAbs. (A) N-Junc affinity of N-Junc-specific mAbs (n= 23), N-Junc binders with cross-reactivity with NANP₅ (n= 25) and of the N-Junc binder with cross-reactivity with NANP₅ and C-CSP (mAb 1961). (B) NANP₅ affinity of NANP₅ specific mAbs (n=19), N-Junc binders with cross-reactivity with NANP₅ (n= 25) and of the N-Junc binder with cross-reactivity with NANP₅ and C-CSP (mAb 1961). (C) C-CSP affinity of C-CSP specific mAbs (n=72) and of the N-Junc binder with cross-reactivity with NANP₅ and C-CSP (mAb 1961). (D) N-Junc (left), NANP₅ (middle) and C-CSP (right) affinities versus VH mutation counts (aa exchange) of N-Junc (left; n=23), NANP₅ (middle; n=19) and C-CSP (right; n=72) specific mAbs. The red horizontal lines in A to C indicate mean values. *** $P < 0.001$, two-tailed Mann-Whitney test (A). The data are representative of two independent experiments.

4.5.3 N-Junc, and C-CSP specific mAbs are frequently encoded by *IGLV1-47* and *IGHV3-21* gene segments, respectively.

mAbs encoded by *IGHV3-33*, frequently in tandem with *IGKV1-5*, has been linked to NANP binding^{108,120}; Supplementary Figure 5). To understand and identify the molecular gene features associated with N-Junc and C-CSP specific mAbs, I analysed the *IGHV* and *IGKV/IGLV* genes encoded by the N-Junc and C-CSP specific mAbs. Over half of the C-CSP-specific mAbs were encoded by *IGHV3-21*, most of which paired with *IGLV3-1* or *IGLV3-21* gene segments (Figure 17A), while *IGLV1-47* gene segment often with *IGHV3-23* was highly enriched among N-Junc-specific mAbs (Figure 17B). Sequence analysis of all expressed mAbs revealed that almost all V_L1-47 and V_H3-21 mAbs with FL-CSP reactivity were specific for N-Junc and C-CSP, respectively (Figures 17C and 17D). Remarkably, the remaining C-CSP-specific mAbs were encoded by diverse gene segments but had similar isotype distribution, somatic mutations, and

affinity as the VH3-21 mAbs (Figures 17E–17G), suggesting efficient affinity maturation of C-CSP-specific mAbs independent of their gene usage. In summary, these data show a strong association of V λ 1-47 mAbs with N-Junc binding and VH3-21 mAbs with C-CSP binding.

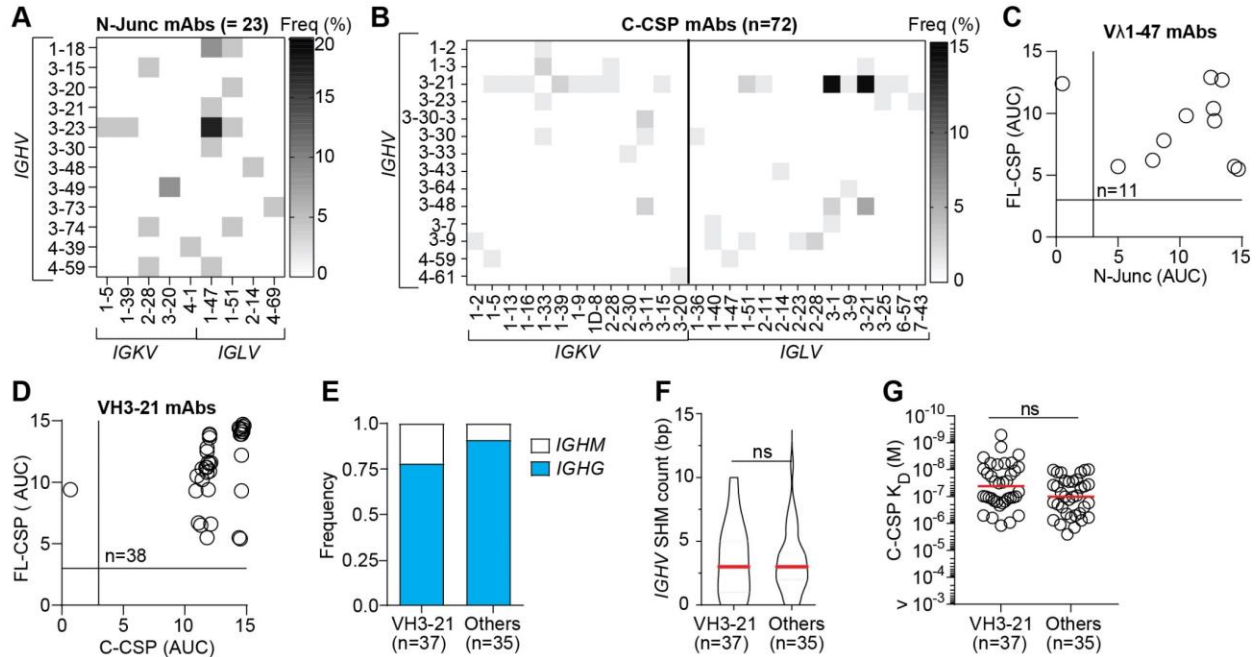


Figure 17: Gene segments associated with N-Junc and C-CSP specificity. (A and B) Paired *IGHV*+*IGKV*/*IGLV* frequency in N-Junc specific (A) and C-CSP specific mAbs (B). (C and D) ELISA AUC of FL-CSP reactive V λ 1-47 mAbs (n=11) binding to N-Junc peptide (C), and VH3-21 mAbs (n=38) binding to C-CSP (D). (E-G) Isotype distribution (E), SHM count (F) and affinity of VH3-21 versus non-VH3-21 C-CSP specific mAbs (G). The red horizontal lines in F and G indicate mean values. Black horizontal lines in C and D indicate the binding threshold. ns (not significant), two-tailed Mann-Whitney test (G). The data shown in C, D and G are representative of two independent experiments.

4.6 Affinity maturation, sub-epitope and strain specificity of C-CSP specific mAbs

4.6.1 Affinity maturation of VH3-21 mAbs is aided by threonine selection in the HCDR1.

The high affinity of VH3-33 mAbs to NANP motifs has been strongly linked to the replacement mutation and selection of asparagine at position 31 of the heavy complementarity determining region 1 (HCDR1); H.S31N) and isoleucine at position 50 of HCDR2 (H.V50I)¹⁸²; Supplementary Figure 6A). To assess the impact of mutations on affinity maturation of VH3-21 C-CSP specific mAbs, Anna Obratsova performed sequence alignments on all *IGHV3-21* encoded Ig genes in the whole repertoire (Figures 17B and 17D). All antibodies encoded by

IGHV3-21 gene showed enrichment of replacement mutations in the CDRs over the framework regions (FWRs) (Figure 18A). The HCDR1 of almost half of the antibodies were found to have a high frequency of replacement mutations at two positions (H.31 and H.33), with a strong enrichment of threonine over the germline-encoded serine residue at position H.33 compared to the neutral mutation model^{6,7} (Figures 18A and 18B; Supplementary Figures 6B and 6C). Interestingly, VH3-21 mAbs carrying replacement mutation from serine to threonine at position 33 (H.S33T) had, on average, higher C-CSP affinities than those carrying the germline-encoded serine residue (H.33) or unselected mutations (Figure 18C). Taken together, these data provide direct evidence of H.S33T mutation role in the affinity maturation process of VH3-21 C-CSP specific mAbs, similar to the H.S31N and H.V50I contribution to the affinity maturation process of VH3-33 anti-NANP mAbs¹⁸².

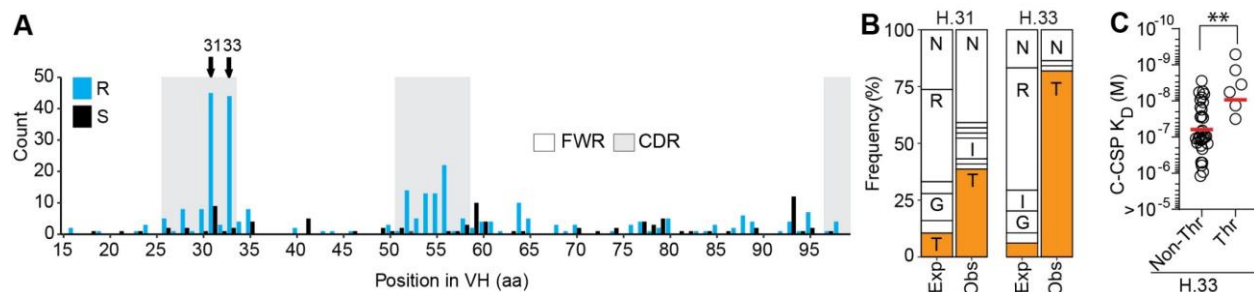


Figure 18: Threonine selection at position 33 of the HCDR1 in VH3-21 mAbs enhances affinity maturation. (A) Amino acid (aa) replacement (light blue bars) and silent (black) mutations in *IGHV3-21* encoded Ig genes ($n=299$). Replacement (R), silent (S), framework region (FWR), and complementarity-determining region (CDR) are indicated. **(B)** Selected replacement mutations (aa; Obs) at positions H.31 (left) and H.33 (right) in VH3-21 antibodies, as compared to the predicted neutral mutation model (Exp)^{6,7}. Single-letters indicate aa residues: G, Glycine; I, Isoleucine; N, Asparagine, R, Arginine; T, Threonine. **(C)** VH3-21 mAbs with and without a threonine mutation at H.33 and their C-CSP SPR affinities. Horizontal red lines in **(C)** indicate mean values. $**P < 0.01$, two-tailed Mann-Whitney test **(C)**. Analyses shown in **A** and **B** were performed by Anna Obratsova.

4.6.2 C-CSP specific mAbs preferentially target distinct epitopes in the α -TSR sub-domain of C-CSP

The C-CSP domain is conformational in structure and comprises a linker subdomain (C-linker) with a unique NANA motif followed by an α -thrombospondin type-1 repeat (α -TSR) subdomain. Within the α -TSR subdomain are the polymorphic Th2R/Th3R epitopes, and the conserved RII+ epitope^{5,88,93}. To determine the fine-epitope specificity of C-CSP specific mAbs and the cross-reactive mAb 1961 (Figure 15C), I measured binding of the mAbs by ELISA to the C-linker covering amino acids 273-310, and to the α -TSR region covering amino acids 311-384 (Supplementary Figure 7A; Supplementary Table 9). With the exception of mAbs 1961 and 3764, that showed specificity for the C-linker, all mAbs demonstrated binding to the α -TSR subdomain

in this assay (Figure 19A). Epitope mapping with 14 overlapping peptides (P1–14) covering the C-linker and α -TSR regions revealed that while mAb 1961 recognized peptide 3 covering amino acids 289-302 (PNRNVDENANANSA) with the unique NANA motif that has been linked to mediate antibody cross-reactivity to the C-CSP⁴, mAb 3764 specifically recognized peptide 2 covering amino acids 281-294 (QGHNMPNDPNRNVD) in the C-linker subdomain (Figure 19B; Supplementary Figure 7B). In contrast, none of the α -TSR-reactive mAbs except mAb 1061 showed detectable binding to the linear peptides, suggesting that they recognized conformational epitopes as previously described⁵. Notably, mAb 1061 preferentially bound peptides 10 and 11, which span amino acids 345–358 (RIKPGSANKPKDEL) and 353–366 (KPKDEL DYANDIEK) in the Th3R region (Figure 19B, Supplementary Figure 7B). These peptides have six common amino acid motifs (KPKDEL), suggesting that the binding of mAb 1061 to these peptides was mediated by the overlapping amino acids.

Many of the α -TSR-reactive mAbs were encoded by the *IGHV3-21* gene segment, suggesting that they may recognize the same or overlapping epitopes as mAb 1710, a VH3-21 anti- α -TSR mAb with specificity for the polymorphic Th2R/Th3R epitopes⁵. To address this question, I selected 38 representatives of α -TSR-reactive mAbs, comprising 21 VH3-21 and 17 non-VH3-21 C-CSP-specific mAbs with similar or higher C-CSP affinity compared to mAb 1710 ($< 10^{-7}$ M; Supplementary Table 3), and tested their ability to block mAb 1710 binding to C-CSP in ELISA (Figure 19C; Supplementary Figure 7C). In this assay, mAb 1710 (self-block) and a non-VH3-21, RTS,S-induced mAb 1512⁹ with specificity for the conserved RII+ region of the α -TSR subdomain, were used as experimental controls. All VH3-21 mAbs and majority of the non-VH3-21 mAbs blocked mAb 1710 binding to C-CSP, demonstrating that the vast majority of anti-C-CSP mAbs target the same or overlapping epitopes as mAb 1710. Only five mAbs encoded by diverse gene segments failed to block mAb 1710 binding. However, these mAbs blocked the binding of mAb 1512 to C-CSP (Figure 19D), demonstrating their specificity for the RII+ region. Overall, the vast majority of C-CSP specific antibodies showed specificity for the polymorphic Th2R/Th3R epitopes in the α -TSR subdomain, and binding to these epitopes was strongly associated with antibodies encoded by *IGHV3-21* gene segment, whereas antibodies specific for the C-linker or the conserved RII+ region were rare and used diverse gene segments.

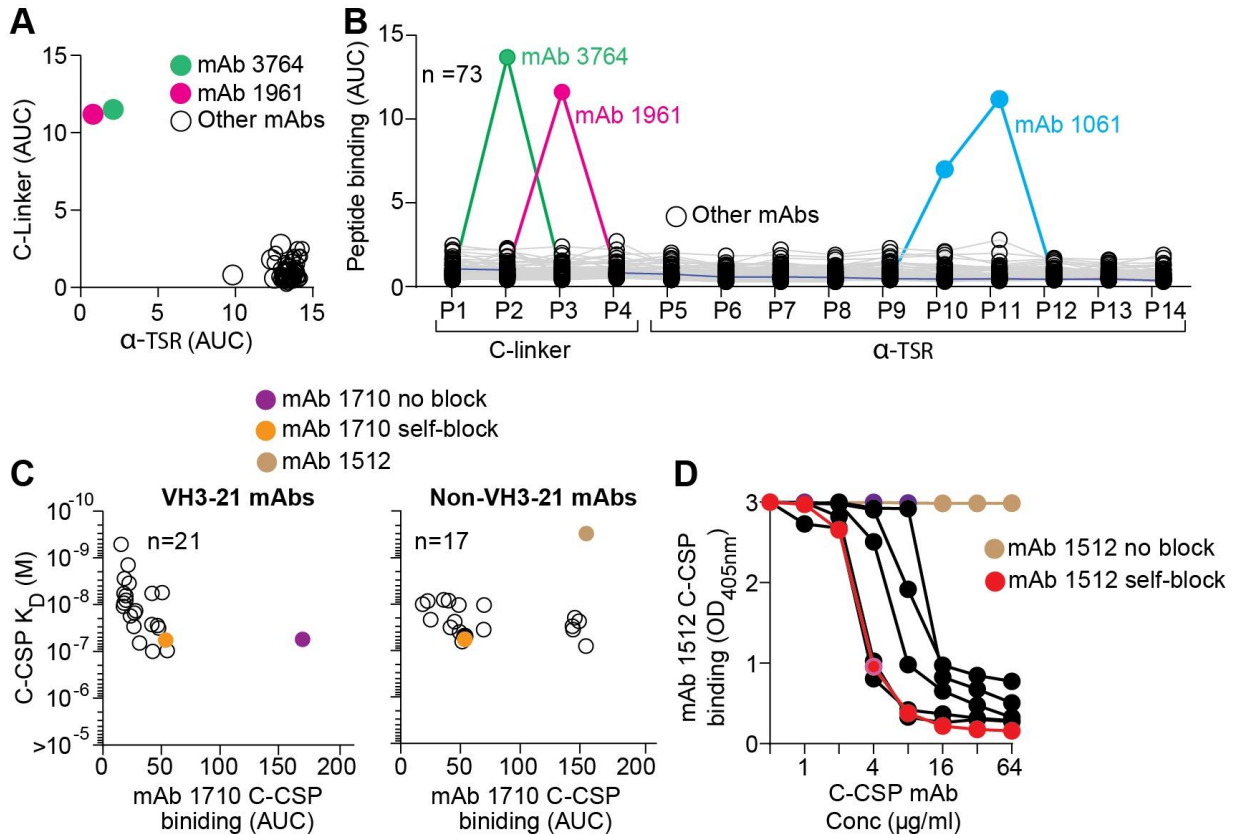
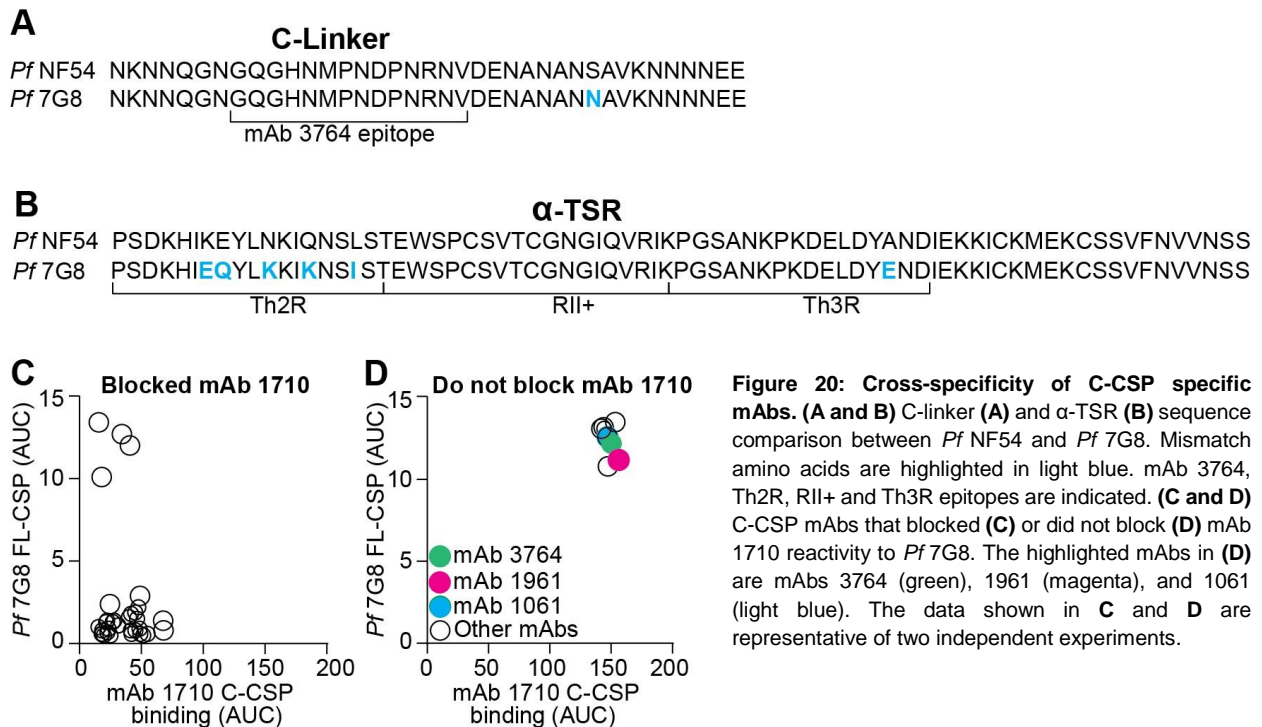


Figure 19: Epitope fine-specificity of C-CSP specific mAbs. (A and B) ELISA reactivity of C-CSP specific mAbs and C-CSP cross-reactive mAb 1961 against the C-linker and the α -TSR (A), and overlapping peptides (P1-P14) covering the C-linker and α -TSR (B). The C-linker specific mAb 3764 (green line), C-CSP cross-reactive mAb 1961 (magenta line) and linear Th3R binding mAb 1061 (light blue line), are indicated. (C) ELISA binding of Th2R/Th3 specific mAb 1710⁵ to C-CSP in a blocking assay with VH3-21 (n=21; left) and non-VH3-21 (n=17; right) C-CSP specific mAbs with indicated SPR affinities. The blocking capacity of mAb 1512⁹ (golden), and binding (red-violet) and self-blocking (orange) capacities of mAb 1710 are shown for comparison. (D) ELISA binding of RII+ specific mAb 1512⁹ to C-CSP in a blocking assay with C-CSP specific mAbs that did not block mAb 1710 binding. The binding (golden) and self-blocking (red) capacities of mAb 1512 are shown for comparison. The data shown in A-D are representative of two independent experiments.

4.6.3 C-CSP specific mAbs exhibit limited cross-reactivity

Given the sequence diversity in natural *Plasmodium falciparum* strains, I investigated whether C-CSP-specific mAbs, including the cross-reactive mAb 1961, are able to accommodate the polymorphisms in the C-linker and α -TSR subdomains, by assessing their ability to cross-bind to Pf7G8, a Pf strain with over 90% C-CSP sequence similarities as PfNF54, but differing by one amino acid (aa) in the C-linker region and six amino acids in the Th2R/Th3R regions of the α -TSR subdomain (Figures 20A and 20B). With the exception of four mAbs, all mAbs that blocked mAb 1710 did not bind Pf7G8 (Figure 20C), presumably because of the high level of polymorphism in the Th2R/Th3R regions. In contrast, mAb 3764, which recognized the C-linker region covering

amino acid sequence 281-294, mAb 1061, which targeted overlapping peptides 10 and 11 (aa 345-366) with one amino acid mismatch, and the C-CSP cross-reactive mAb 1961, bound *Pf* 7G8 (Figure 20D). Similarly, the five mAbs that did not block the binding of mAb 1710 also showed cross-reactivity with *Pf* 7G8, confirming that the mAbs recognized conserved RII+ region in the α -TSR subdomain. Overall, limited cross-reactivity was observed among the C-CSP-specific mAbs, and was not associated with any particular gene segment.



4.7 Protective capacity of N-Junc, C-CSP and cross-reactive mAbs

4.7.1 N-Junc and C-CSP specific mAbs showed poor parasite inhibitory capacity

The ability of antibodies to inhibit parasites and mediate protection may be associated with variations in epitope specificity. To functionally characterize the parasite inhibitory capacity of N-Junc and C-CSP specific mAbs, 5 representatives of N-Junc specific mAbs, 15 representatives of C-CSP specific mAbs and 5 representatives of NANP₅ and N-Junc cross-reactive mAbs, were selected and assessed for inhibition of *Plasmodium falciparum* parasites in an *in vitro* hepatocyte traversal assay as previously described⁴. A wide range of criteria, including gene usage, isotype, somatic hypermutation count, affinity and epitope-specificity, were considered in the selection of these mAbs (Supplementary Table 4). In this assay, mAb 2A10¹ and mAb mGO53³ were used as positive and negative experimental controls, respectively. The parasite inhibitory capacities of

the mAbs were compared to the N-Junc and C-CSP cross-reactive mAb 1961 or already published anti-NANP cross-reactive mAb 317¹⁸³. The experiments were performed by Dr. Giulia Costa in the laboratory of Professor Elena A. Levashina at the Max Planck Institute for Infection Biology in Berlin, Germany.

Compared to N-Junc mAbs with cross-reactive to NANP₅, or C-CSP cross-reactive mAb 1961, which inhibited *Plasmodium falciparum* sporozoite hepatocyte traversal by 42% to 67% at 1 µg/ml, N-Junc-specific mAbs only inhibited sporozoite hepatocyte traversal by 5% to 25% at the same concentration (Figure 21A). In contrast, none of the C-CSP specific mAbs inhibited sporozoite hepatocyte traversal, even at high concentration of 100 µg/ml (Figure 21B; Supplementary Figure 8A). In agreement with their inability to inhibit *Plasmodium falciparum* sporozoites, none of the C-CSP specific mAbs targeting the α-TSR subdomain recognized live sporozoites in flow cytometry (Figure 21C; Supplementary Figure 8B), suggesting that the α-TSR subdomain is not accessible for mAbs binding on the surface of sporozoites. Only the C-CSP cross-reactive mAb 1961 showed high binding to sporozoites, similar to the anti-NANP repeat mAb 2A10, whereas weak binding was observed with mAb 3764, the C-linker-specific mAb, at 100 µg/ml but not at 1 µg/ml (Figures 21D and 21E; Supplementary Figure 8C).

Although C-CSP cross-reactive mAb 1961 inhibited sporozoite traversal in a manner similar to anti-NANP repeat mAb 317⁸ and other anti-NANP and N-Junc cross-reactive mAbs (Figures 21A and 21B), it was less effective than mAb 317, and not significantly better than C-CSP specific mAb 1710⁵ in preventing the development of parasitemia in passively immunized mice (Figure 21F; Supplementary Figure 8D). Taken together, the N-Junc-specific mAbs have a weak inhibitory capacity on *Plasmodium falciparum* parasites, whereas the C-CSP-specific mAbs have no measurable inhibitory capacity *in vitro* and do not mediate protection *in vivo*.

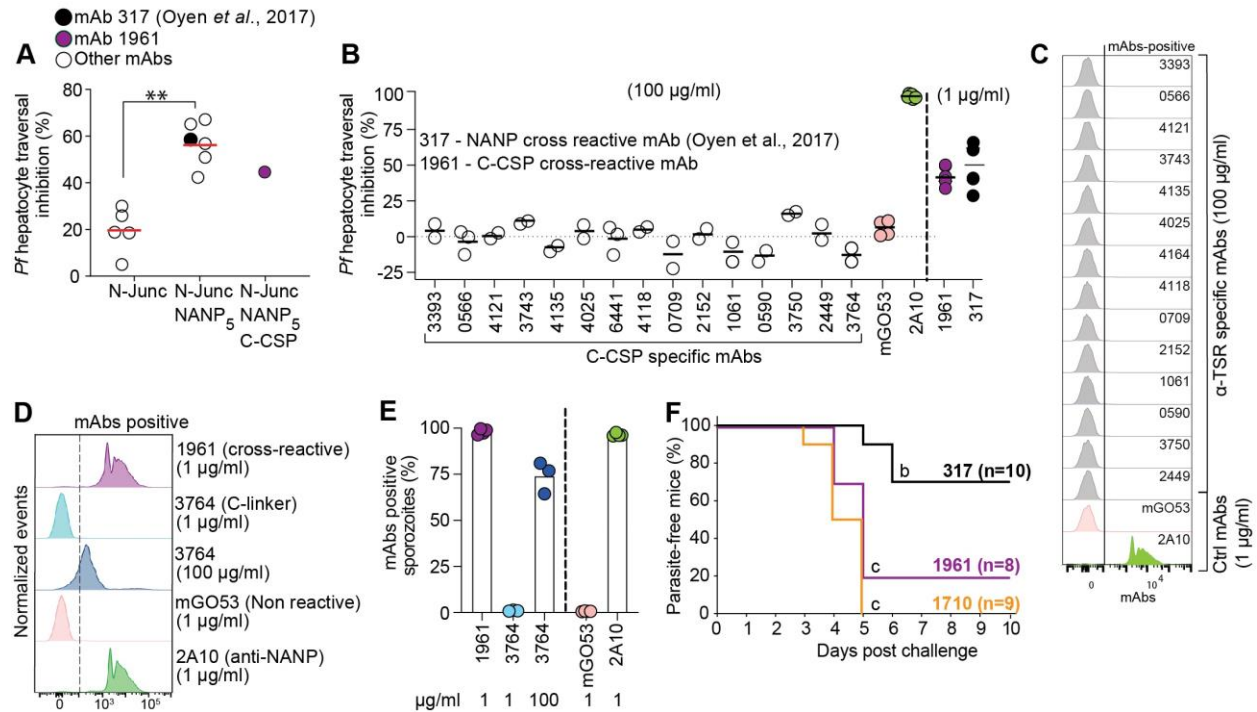


Figure 21: Protective capacities of N-Junc specific, C-CSP specific, and cross-reactive mAbs. (A) *Plasmodium falciparum* sporozoites hepatocyte traversal inhibitory capacity of N-Junc specific mAbs and N-Junc mAbs with cross-reactivity to NANP₅ and C-CSP cross-reactive mAb 1961 (purple). Each circle represents one mAb. Experiment was performed as previously described⁴ (B) *Plasmodium falciparum* sporozoites hepatocyte inhibitory capacity of indicated C-CSP specific mAbs and control mAbs at indicated concentrations. Each circle per indicated mAbs represents one experiment. mAb 317⁸ (Closed black circle, a published NANP cross-reactive mAbs, is shown for comparison in (A) and (B). (C) Live *Plasmodium berghei* (*Pb-PfCSP*) sporozoites binding of indicated C-CSP specific mAbs tested at 100 µg/ml and the positive control anti-NANP repeat mAb 2A10¹, and negative control mAb mGO53³ tested at 1 µg/ml. (D and E) Flow cytometric profiles (D) percent of mAb-positive live *Pb-PfCSP* sporozoites (E) of C-linker specific mAb 3764 tested at 1 µg/ml or 100 µg/ml, and cross-reactive mAb 1961 and control mAbs 2A10 and mGO53, tested at 1 µg/ml. Each circle in (E) represents one experiment. (F) Protective efficacy of the indicated mAbs (100 µg/ml) against parasitemia in mice following passive transfer in comparison to the C-CSP-specific mAb 1710⁵. Passive immunization experiment was performed as previously described⁴. The data shown in (A) are average of at least two independent experiments. The data shown in (F) represent the percentage of parasite-free mice in two separate experiments. The groups denoted by the same letter in (F) do not differ statistically (Mantel-Cox log-rank test). All experiments shown were performed by Dr. Giulia Costa in the laboratory of Professor Elena A. Levashina at the Max Planck Institute for Infection Biology in Berlin, Germany

5.0 DISCUSSION

The use of whole sporozoites heavily coated with PfCSP as a vaccine strategy has shown promising results in malaria-naïve volunteers by eliciting a protective humoral and cellular immune response against PfCSP^{10,24,107,110,115,120,184}. While the molecular features of mAbs targeting the central NANP repeat domains with or without cross-reactivity to the junction or C-CSP have been widely studied due to their high parasite inhibitory ability^{86,107,122,123}, the molecular properties, target breadth, frequency, and parasite inhibitory role of N-Junc and C-CSP-specific mAbs are less understood. The data presented in this PhD thesis combined an unbiased isolation strategy with high-throughput analysis of the single-cell immunoglobulin (Ig) gene repertoire and monoclonal antibody production to characterize the gene features, affinity range, fine-epitope specificity and parasite inhibitory capacity of human anti-N-Junc and anti-C-CSP mAbs elicited after three intravenous immunizations with radiation-attenuated sporozoites.

5.1 Serum antibodies and memory B-cells generated after *Pf* RAS immunization

Repeated antigen exposure is necessary for the development of strong humoral and cell-mediated immune responses^{120,185-191}. Serum antibody response against PfCSP epitopes was assessed in twelve malaria-naïve volunteers after exposure to three doses of *Pf* RAS immunization. The overall magnitude of the antibody response in this study was generated against a broader range of epitopes, including the N-Junc and the C-CSP epitopes. Although these results provide data for the development of new *Pf*-sporozoite-based vaccination strategies, the antibody response against the epitopes decreased over time. This observation is not surprising as PfCSP-specific serum IgM and IgG antibodies have been shown to be unstable and only persist in circulation for 25 and 21 days, respectively¹⁹²⁻¹⁹⁸. In addition, exposure to a low dose (3,200) live sporozoites during the controlled human malaria infection (CHMI) may have resulted in a low level of antigens accessible to the immune system. Therefore, to maintain an elevated level of anti-PfCSP serum antibodies over a longer period of time, constant and continuous boosting with a high dose of malaria vaccine may be necessary.

The fact that all vaccine recipients developed serum antibodies against the N-Junc, NANP₅, and C-CSP, but not against N-CSP, demonstrates the poor immunogenicity of N-CSP domain. This observation may be attributed to the proteolytic cleavage of the RI region of N-terminus during hepatocyte invasion of sporozoites in the liver, thus limiting humoral and cell-mediated responses against the epitope^{103,199}. Another likely explanation for this observation

could be that other epitopes are more immunodominant than the N-CSP, thereby limiting antibody response against the N-CSP. This hypothesis is supported by the fact that anti-N-CSP antibodies were induced more in mice immunized with N-terminal antigen than in mice immunized with full length PfCSP antigen²⁰⁰. The strapping induction of anti-NANP repeat antibodies confirms the immunodominant nature of this epitope^{1,8,85,107,182}, which may be attributed to its repetitive nature^{120,201}. Despite this, most vaccine recipients elicited high levels of serum IgG antibodies against the N-Junc and C-CSP, demonstrating the cross-reactivity of antibodies against the N-Junc, NANP repeats and the C-CSP epitopes in response to *Pf RAS* immunization. These findings are in agreement with previous reports that separately showed strong anti-NANP and anti-C-CSP serum IgG responses in volunteers immunized with RTS,S/AS01 vaccine or recombinant PfCSP^{26,28,202-204}. The strong induction of anti-N-Junc serum antibodies is possibly due to the presence of two NANP motifs that are interspersed in the N-Junc sequence (GKQPADGNPDP**NANP**NVDP**NANP**), or the altered response in NANP affinity maturation, in which antibodies specific for NANP motifs are formed, but also react with junctional epitopes that share amino acid sequence similarities with NANP⁴. However, it is important to note that although quantification of the polyclonal antibody response can provide information on the overall magnitude of anti-PfCSP response, it does not provide information on whether the antibodies formed are cross-reactive or specific for either of the epitopes.

5.2 Signs of germinal center selection in PfCSP-reactive memory B cells

Successful immune responses are characterized by their ability to create and maintain a strong immunological memory. Antigen-induced activation leads to isotype class switching, Ig gene diversification through somatic hypermutation, and clonal expansion of a pool of B cell progenitors, resulting in a cluster of B cell clones²⁰⁵. Although the majority of the *Pf RAS*-induced PfCSP-reactive memory B cells were IgM cells, IgG class-switched and mutated cells were also identified. This allows conclusions about the selection and participation of the PfCSP-reactive memory B cells in germinal center for affinity maturation. The high frequency of IgM cells, including many non-mutated memory B cells, suggests a continuous recruitment of germline-expressing IgM memory cells in response to *Pf RAS* immunization, similar to the naturally exposed volunteers or volunteers immunized with live sporozoites^{1,120}. The average mutation count of PfCSP reactive memory cells increased over time after the last immunization, suggesting that the cells continued to undergo affinity maturation. This increase may be due to the repeated exposure to the high dose (900,000) of radiation-attenuated sporozoites used in the clinical trial,

which may have triggered the active selection and participation of PfCSP-reactive memory B cells in the germinal center ¹²⁰.

Surprisingly, some PfCSP-reactive memory B cells showed relatively high SHM counts (> 30), suggesting that the cells were pre-existing memory B cells recruited into the infection. These B cells could be memory B cells that had emerged from a response to a different antigen but were nevertheless recruited during *Plasmodium falciparum* sporozoites immunization, due to their ability to cross-bind to PfCSP ¹²⁰. This hypothesis is supported by recent studies that showed the participation of SARS-COV-2 memory B cell antibodies in other SARS-COV infections ²⁰⁶, and also in DENV1-specific memory B cells actively participating in ZIKA infection, ²⁰⁷, due to their sequence similarities .

5.3 Enrichment of affinity-mature *IGHV3-33* and *IGHV3-21* encoded Ig genes in PfCSP-reactive memory B cells

Antibodies elicited against a given antigen are likely to share structural similarities with that antigen, and this likely plays a role in determining the *IGHV* family that predominates in the antibodies. In this study, *IGHV3* family were found to be commonly used by the anti-PfCSP memory repertoire. This enrichment was mainly mediated by *IGHV3-33*, a gene segment that has been widely described to be associated with NANP repeat binding ^{108,120}, and *IGHV3-21*, a gene segment not strongly associated with PfCSP binding, but rather with chronic lymphocytic leukemia ²⁰⁸⁻²¹⁰. This finding suggests that antibodies encoded by these gene segments can readily be induced by *Plasmodium falciparum* sporozoites immunization, similar to previous study on the use of *IGH1-69* gene segment in response to influenza haemagglutinin ²¹¹⁻²¹³ or *IGHV5-51* encoded mAbs in celiac disease ²¹⁴. The relative abundance of IgG over IgM cells, and the higher somatic hypermutation counts in *IGHV3-21* over *IGHV3-33* encoded antibodies in all volunteers indicate clear signs of affinity maturation of VH3-21 antibodies. B-cell activation, differentiation, enrichment, and germinal center selection of VH3-21 antibodies may have been influenced by the high dose and nature of the antigen (irradiated sporozoites) used in the clinical trial. Alternatively, the nature of the epitope (structured C-CSP domain) being targeted by VH3-21 antibodies, as revealed at monoclonal level, may underlie these observations. Antibodies targeting disordered epitopes are predicted to have fewer mutations in their sequences relative to antibodies targeting structured epitopes, which impedes their affinity maturation in the germinal center, and preventing the development of an adequate immune response ^{215,216}. Further studies are needed to determine whether affinity-mature VH3-21 antibodies are also strongly enriched in

response to recombinant PfCSP based vaccines, and to define the underlying molecular and cellular mechanisms of B-cell activation in response to *Pf* RAS immunization.

5.4 PfCSP reactive mAbs preferentially target the C-CSP domain

The fact that the NANP repeats, and regions I and II, located at the N-terminus and C-terminus, respectively, are conserved in all *Plasmodium falciparum* strains^{88,113} makes them a useful target for the immune system. Antibodies directed against these regions have the potential to be effective against a wide range of *Plasmodium* species, whereas antibodies directed against other parts of the C-CSP would be species-specific due to the high degree of polymorphism between *Plasmodium falciparum* strains. Consistent with other studies and similar to the serum response, none of the PfCSP-reactive mAbs recognized the N-terminal domain. This result is not surprising, as it has been shown that the N-terminus is cleaved during sporozoite development in the mosquito midgut, therefore restricting its recognition by the human immune system^{103,106,199,217,218}.

Although a wide range of different mAbs binding patterns, including the N-Junc and NANP-specific mAbs, were identified, the vast majority of the mAbs identified in this study targeted the C-CSP domain specifically, despite its controversial description as a masked epitope that remains hidden from the immune system during parasite transmission until the time of hepatocyte invasion^{88,218}. A possible explanation for this surprising finding may be linked to the expansion of C-CSP specific antibody responses following subsequent malaria vaccination²¹⁹, or the apparent broadening of antibody responses to the C-CSP domain²⁰². Alternatively, immunization with *Pf* RAS may also have contributed to the exposure of the C-terminal domain to the immune system in immunized volunteers. Future studies need to determine whether the C-CSP domain is masked or exposed on the surface of *Pf* RAS. Interestingly, C-CSP-specific mAbs were identified in all but one volunteer, demonstrating the immunodominance and immunogenicity of the C-CSP domain, similar to the NANP repeat. Results from different malaria vaccine trials^{5,9,28,107,121} are strong evidence that the C-CSP is another immunodominant B-cell epitope. Similar to anti-NANP reactive mAbs that can be easily induced in response to malaria vaccination, this study also shows that the C-CSP specific mAbs belong to public lineage and can be readily induced by vaccination. However, it remains to be determined whether C-CSP specific mAbs can be induced in response to natural *Plasmodium falciparum* exposure.

5.5 Naïve human B cells contain numerous C-CSP-specific mAbs encoded by *IGHV3-21* gene segment.

The large panel of C-CSP specific mAbs identified in this study provides a strong rationale for further analysis of the molecular features, fine epitope specificity, and overall protective capacity of C-CSP specific mAbs. This is important not only for identifying gene features associated with C-CSP binding in the human B-cell repertoire, but also for deciding on the inclusion of C-CSP epitope in the development of the next generation subunit malaria vaccine. This study shows that C-CSP specific mAbs are encoded by diverse gene segments, including *IGHV3-33* (C-linker binding), a gene segment known to be associated with NANP binding^{4,108,120,182}. Despite the diversity in gene usage, the majority of C-CSP mAbs originated almost exclusively from B cells expressing *IGHV3-21* in association with *IgL3-1* or *IgL3-21*, similar to the known association between VH3-33/V κ 1-5 mAbs and NANP repeat binding^{1,4,8,107,220}, VH3-30 mAbs and Pneumovax®23 cell wall polysaccharide binding²²¹, VH3-23/V κ 1-5 mAbs in DENV1 and ZIKV envelope domain binding²⁰⁷ and VH1-2 and VH1-69 mAbs in HIV gp140 binding^{188,222}. It is important to note that the spectrum of VH3-21 mAbs in this study was not limited to those paired with V λ 3-1 or V λ 3-21 light chain alone, but encompassed diverse light chain V gene segments. While a few VH3-21 C-CSP specific mAbs have been reported^{5,9}, this study provides the first evidence of an association of this gene segment with C-CSP binding. Although, there was no significant difference in average affinity between VH3-21 and non-VH3-21 C-CSP specific mAbs, the higher affinity trend observed in VH3-21 mAbs (Figure 17G), suggests that the affinity maturation of VH3-21 C-CSP mAbs was effective in this context. However, more data are needed to validate this observation.

Numerous high affinity C-CSP specific germline mAbs or mAbs with moderate levels of somatic hypermutation were identified in this study, suggesting the selection of high affinity C-CSP specific mAbs from naïve precursor B cells. This result is not surprising as previous studies showed that somatic hypermutation is inefficient for affinity maturation in PfCSP-specific B cells^{108,120}. An independent mathematical model also predicted that the clonal selection of precursor B cells expressing germline mAbs with high affinity could be efficiently generated if higher antigen doses were used in the immunization scheme¹²⁰. Thus, the high sporozoite dosages (900,000) used in this clinical trial may have also provided an ideal environment for the selection of mAbs with high affinity from the extensively diverse naïve B cell pool.

The finding that most C-CSP-specific mAbs use the same *IGHV3-21* gene segment in different volunteers harken back to research on the role of specific *IGHV* genes such as the

IGHV3-33 and their allelic forms in the recognition of NANP repeat or *IGHV1-69* in response to influenza haemagglutinin. The possible reasons for the strong enrichment of *IGHV3-21* gene segment among the C-CSP specific mAbs may have been influenced by the abundance of VH3-21 germline-encoded antibodies in these volunteers or the structural complementarity of the mAbs with the C-CSP epitope. It is well established that the CDR regions of *IGHV* genes vary in length and conformationally flexible depending on the amino acid sequence and target preference of the *IGHV* genes^{223,224}. Interestingly, sequence alignment of VH3-21 C-CSP mAbs revealed that these mAbs belong to somatically mutated cells with strong selection of threonine replacement mutation in the HCDR1 (H.S33T), likely as a result of affinity maturation. Although these data, similar to the isoleucine mutation (H.V50I) in HCDR2 of VH3-33 mAbs¹⁸², provide evidence for the involvement of the selected threonine mutation in affinity maturation, germline reversions are required to understand the major role of this mutation in affinity maturation of VH3-21 antibodies.

5.6 C-CSP specific mAbs bind novel epitopes and exhibit limited cross-reactivity to other *Plasmodium falciparum* strains.

It is currently unclear whether targeting other subdomains of the C-CSP epitope mediates better protection than the known Th2R/Th3R and RII+ regions^{5,28}. Similar to previous reports^{5,9,121}, the vast majority of C-CSP specific mAbs in this study recognized the polymorphic Th2R/Th3R regions of the α -TSR subdomain, demonstrating not just the immunodominance, but also the immunogenicity nature of these epitopes. This convergent response has been described to be mediated by interaction of CDRs L1 and L2 with Th2R, the CDRs H1 and H2 recognition of Th3R, and the CDR H3 insertion in the conserved hydrophobic pocket in C-CSP⁹. Another possibility could be attributed to the presence of overlapping T cell epitopes encompassed in these regions⁸⁹. The efficient binding of the rare mAb 3764 to the C-linker region with specificity for the P2 peptide spanning aa 281-294 (QGHNMPNDPNRNVD) reveals the presence of a novel epitope in the C-linker region that is distinct from the NANA epitope known to be recognized by a few TCRs or C-CSP mAbs that cross-react with the NANP repeat^{4,89}. Given that mAb 3764 is the only C-linker-specific mAb identified to date suggests that C-linker-specific mAbs are generally rare and that the C-linker subdomain of the C-CSP is less immunogenic and has limited specificity, even though it may be easier to reach than the α -TSR subdomain. Although the DPN motif in the C-linker sequence (NKNNQGNGQGHNMPNDPNRNVDENANANSVKNNNNEE) share similarity with the N-terminal junction (GKQPADGNPDPNANPNVDPNANP) motif, it remains unclear why mAb 3764 showed specificity for the C-linker subdomain of the C-CSP and not for

the N-Junc. Antibody modelling or a crystal structure of mAb 3764 in complex with the C-linker peptide is necessary to understand the molecular basis for its specificity for the C-linker subdomain.

In contrast, mAb 1061 recognized linear epitope spanning aa 345-366 in the Th3R region of the α -TSR subdomain. This is the first direct evidence demonstrating the existence of a linear epitope in the α -TSR subdomain that may also be accessible to the immune system. Although these data revealed the existence of a linear epitope in the Th3R subregion, mAbs of this type are rare, and the exact mechanism for this binding is not yet clear. As expected, cross-reactivity to *Pf*7G8 strain was mainly associated with mAbs specific for the conserved amino acids covering aa 273-286, 281-294, 345-366 or the RII+ subdomain. The unexpected observation that the four mAbs with similar or overlapping epitopes as mAb 1710 showed cross-reactivity with *Pf* 7G8 suggests that these mAbs bind to shared amino acid sequences in the Th2/Th3 region. Alternatively, it could be speculated that the binding surface of these mAbs is large enough to accommodate amino acid differences in the *Pf*7G8 strain. Further studies are needed to understand the mechanism behind their binding promiscuity and to test their binding ability to other *Plasmodium falciparum* strains.

5.7 V λ 1-47/VH3-23 mAbs are highly reactive against the N-Junc

In addition to the VH3-33 and VH3-21 mAbs with NANP and C-CSP reactivity, respectively, all but one (10/11) of the V λ 1-47 mAbs with PfCSP reactivity were found to be specific for the N-Junc epitope in this study. Four of the mAbs paired with *IGHV3-23* heavy chain, while the rest paired with diverse heavy gene segments, including *IGHV3-21*, a gene segment that is strongly linked with C-CSP binding in this study. Interestingly, the only *IGHV3-21* encoded mAb that exhibited N-Junc specificity, paired with *IGLV1-47*, a light chain gene segment not used by any of the C-CSP mAbs, but unique for N-Junc binding. Based on these data, it can be speculated that the V λ 1-47 light chain plays a crucial role in antibody specificity for N-Junc binding. Although almost all FL-CSP reactive mAbs encoded by *IGLV1-47* gene segment bind to the N-Junc epitope, data from more N-Junc-specific mAbs are needed to confirm the strong association of this gene segment with N-Junc specificity. Future studies should also investigate the binding mode of N-Junc-specific mAbs in separate clinical trials.

5.8 Antibody cross-reactivity to the N-Junc is mediated by affinity to NANP repeat

Cross-reactive anti-PfCSP mAbs have been shown to have overall higher affinity than mAbs targeting the junction, repeat or the C-CSP specifically ⁴. Antibody cross-reactivity has been widely described as a feature of mAbs encoded by diverse Ig gene combinations with extensive mutations, including mAbs that have evolved in response to live sporozoites, radiation-attenuated sporozoites, or natural exposure ^{1,4,108}, indicating that these mAbs are also part of the public response that can be readily induced by vaccination. In addition to mAbs with exclusive specificity for the C-CSP or the N-Junc epitope, some of the PfCSP-reactive mAbs described in this study recognized the NANP repeat and showed cross-reactivity to the N-Junc or C-CSP domain. Intuitively, repeated antigen exposure would lead to an increase in cross-reactive mAbs due to the direct correlation between affinity and epitope cross-reactivity. Similar to previous study ⁴, the anti-PfCSP cross-reactive mAbs isolated in this study had, on average, a higher affinity for the NANP₅ peptide than for the N-Junc epitope regardless of the gene usage or cellular origin, suggesting that a higher affinity for NANP and not N-Junc was the driving force in the selection of cross-reactive mAbs during affinity maturation in humans. These findings are supported by the evidence of strong enrichment of class-switched and mutated cross-reactive mAbs encoded by *IGHV3-33* paired with *IGKV1-5*, which are involved in homotypic interaction that has been linked to be associated with affinity maturation of NANP mAbs ¹⁸².

5.9 Efficient parasite inhibition is limited to PfCSP mAbs with dual-specificity for NANP, N-Junc and/or C-CSP domain.

Several lines of evidence suggest that mAbs targeting the C-CSP domain of PfCSP are suboptimal in binding live sporozoites and lack parasite inhibitory activity in mice ^{5,121}. Yet, a few other studies have challenged this notion. For example, a recent report showed that C-CSP specific mAbs reduced parasite liver burden in mice, while other studies found a strong correlation between C-CSP antibodies and protection in RTS,S and recombinant PfCSP immunized individuals ^{9,28,202,203}. The data presented in this thesis reveal that C-CSP specific mAbs lack the ability to bind *Plasmodium falciparum* sporozoites and are poor parasite inhibitors regardless of their affinity, epitope specificity and gene usage. Minimum protection against the blood-stage parasitemia was limited to C-CSP reactive mAb 1961 that cross-reacted with NANP repeat and N-Junc. This corroborates the results of previous passive transfer studies, which showed that C-

CSP reactive mAbs mediate protection only by binding to the repeat and junction epitopes that are readily accessible on the surface of sporozoites ⁴. The molecular displacement of PfCSP on the sporozoites membrane may have limited the accessibility of antibodies targeting the C-terminus to their epitopes, thus reducing their binding and protective effects ⁵. Alternatively, the concealed location of the C-terminus of PfCSP on the surface of sporozoites may also hinder the generation of antibodies targeting the C-terminal domain. The C-terminal domain may become accessible to antibodies only after the N-terminal domain in region I is cleaved ^{84,225}. Consequently, the data reported in this study argue that the C-CSP correlates of protection observed after vaccination with RTS,S/AS01 ²⁰² or recombinant PfCSP ²⁸ may have been mediated exclusively by C-CSP antibodies cross-reacting with the N-terminal junction and/or the NANP repeat. It is however important to know that despite these results, the possibility still exists that C-CSP antibodies might be playing a role in parasite inhibition via Fc-mediated effector functions like opsonization, phagocytosis or complement activation ^{200,226,227}, as evidence by the predominance of cytophilic IgG1 subclasses in these mAbs (Supplementary Table 2). However, to mediate Fc function, C-CSP mAbs may require the presence of high-affinity anti-repeat mAbs for them to bind native PfCSP on sporozoites ¹²¹. In addition, Fc-mediated effector function mechanisms are not readily detectable in animal models with human mAbs, and will only be limited to *Plasmodium falciparum* strains with sequence similarity and antibodies against the conserved regions in natural infection.

In contrast to the C-CSP-specific mAbs, the N-Junc-specific mAbs showed a better parasite inhibitory ability, although still at a lower range than the cross-reactive mAbs. This observation could be due to their lower affinity against the N-Junc epitope compared to the N-Junc affinity of the cross-reactive mAbs. This finding agrees with recent study that independently showed in animal model that anti-PfCSP mAbs with dual specificity for NANP repeat and N-junction are more potent than mAbs that exclusive recognize NANP or peptides covering the N-junction epitope ⁴. It appears that high affinity cross-reactive mAbs, rather than N-Junc or NANP specific mAbs, are responsible for effective protective efficacy against blood-stage parasitemia. The data shown in this study demonstrate that the N-terminal junction and the central NANP motifs remain the most promising PfCSP epitopes to be prioritized in the design and development of next-generation PfCSP-based subunit vaccines against malaria. Future studies will need to determine whether efforts to design a second generation PfCSP vaccine might benefit from suppressing or even abrogating the humoral response against C-CSP, e.g. by boosting the anti-repeat and junction response. However, exclusion of the complete domain, especially the highly immunodominant α -TSR, would eliminate the main T helper cell epitopes with likely strong

negative effects on the quality and strength of the humoral response against the potent repeat and the junction epitopes. Inclusion of linear peptide epitopes rather than the complete C-CSP may be sufficient to provide efficient T cell help without inducing non-protective humoral responses⁸⁹. Alternatively, non-PfCSP T cell epitopes could substitute for the loss of T cell help and promote affinity maturation of the PfCSP-specific response. Taken together, these findings support the inclusion of the N-Junc rather than the C-CSP epitope in next-generation PfCSP-based subunit vaccines against malaria and underscore the need for further exploration of prime-boost strategies that will elicit cross-reactive antibodies.

6.0 OUTLOOK

This study demonstrated the strong enrichment of *IGHV3-21* and *IGHV3-33* gene segments, and highlighted the molecular features of mAbs against N-Junc and C-CSP, which were predominantly encoded by *IGLV1-47* and *IGHV3-21*, respectively, in the *Pf* RAS immunization trial. To draw profound conclusions about the Ig gene features, especially for the N-Junc-specific binders, evaluation of mAbs encoded by these gene segments should be extended to a larger set of PfCSP reactive memory B-cell mAbs and other malaria clinical trials that target the *Plasmodium falciparum* sporozoite stage. Structural studies involving a combination of molecular modeling, X-ray crystallography, and possibly cryogenic electron microscopic analysis (cryo EM) are also required to confirm this conjecture. This information could be used as a future predictive tool for Ig genes encoding N-Junc and C-CSP-specific antibodies in the memory B-cell pool after immunization with PfCSP-based vaccines such as the *Pf* RAS or recombinant PfCSP-based vaccines. Epitope specificity, efficient affinity maturation, and IgG class switching appear to be associated with differences in cell differentiation pathways or kinetics, as evidenced by the higher frequency of the selected affinity-increasing H.S33T mutation in VH3-21 C-CSP-specific mAbs. Reverting the mAbs to their germline versions will help to fully understand the role of the selected mutation in the affinity maturation of the mAbs.

In the same line, it is unknown whether the high-affinity C-linker, and the RII+ specific C-CSP mAbs can contribute directly or indirectly to Fc-mediated effector functions, such as complement fixation, phagocytosis and opsonization. Cloning the C-CSP specific mAbs in their native isotypes and subsequently testing them in an *in vitro* human complement activation assays²²⁷ in the presence or absence of anti-repeat mAbs could reveal the role of Fc receptors in human protection. Alternatively, incubating the sporozoites with anti-repeat mAbs to precipitate the surface of sporozoites before incubating with the high-affinity C-linker-specific mAb 3764 or the RII+ specific mAbs could help reveal the true binding capacity, potency and parasite inhibitory capacity of these mAbs. Sterile immunity and long-term protection are two of the most sought-after outcomes in this field, which is why the development of a vaccine candidate is a top priority. RTS,S, the leading PfCSP-based malaria vaccine candidate, provides protection, but it is weak and short-lived¹⁹⁸. Compared to PfCSP-based recombinant or viral vaccine candidates, nanoparticle approaches have shown greater efficacy in inducing long-lasting protective antibody and CD8+ T cell responses against PfCSP in mouse models^{228,229}. Since the N-junction epitope is missing in the currently available nanoparticle vaccines, the insertion of this epitope is likely to improve the efficacy of these vaccines and induce a long-lasting humoral and cell-mediate immune responses against PfCSP in mice and humans.

7.0 REFERENCES

1. Triller, G., *et al.* Natural Parasite Exposure Induces Protective Human Anti-Malarial Antibodies. *Immunity* **47**, 1197-1209 e1110 (2017).
2. DeKosky, B.J., *et al.* Large-scale sequence and structural comparisons of human naive and antigen-experienced antibody repertoires. *Proc Natl Acad Sci U S A* **113**, E2636-2645 (2016).
3. Wardemann, H., *et al.* Predominant autoantibody production by early human B cell precursors. *Science* **301**, 1374-1377 (2003).
4. Murugan, R., *et al.* Evolution of protective human antibodies against Plasmodium falciparum circumsporozoite protein repeat motifs. *Nat Med* **26**, 1135-1145 (2020).
5. Scally, S.W., *et al.* Rare PfCSP C-terminal antibodies induced by live sporozoite vaccination are ineffective against malaria infection. *J Exp Med* **215**, 63-75 (2018).
6. Gupta, N.T., *et al.* Change-O: a toolkit for analyzing large-scale B cell immunoglobulin repertoire sequencing data. *Bioinformatics* **31**, 3356-3358 (2015).
7. Yaari, G., *et al.* Models of somatic hypermutation targeting and substitution based on synonymous mutations from high-throughput immunoglobulin sequencing data. *Front Immunol* **4**, 358 (2013).
8. Oyen, D., *et al.* Structural basis for antibody recognition of the NANP repeats in Plasmodium falciparum circumsporozoite protein. *Proc Natl Acad Sci U S A* **114**, E10438-E10445 (2017).
9. Beutler, N., *et al.* A novel CSP C-terminal epitope targeted by an antibody with protective activity against Plasmodium falciparum. *PLoS Pathog* **18**, e1010409 (2022).
10. Mordmuller, B., *et al.* A PfSPZ vaccine immunization regimen equally protective against homologous and heterologous controlled human malaria infection. *NPJ Vaccines* **7**, 100 (2022).
11. Meffre, E., *et al.* Surrogate light chain expressing human peripheral B cells produce self-reactive antibodies. *J Exp Med* **199**, 145-150 (2004).
12. Dayananda, K.K., Achur, R.N. & Gowda, D.C. Epidemiology, drug resistance, and pathophysiology of Plasmodium vivax malaria. *J Vector Borne Dis* **55**, 1-8 (2018).
13. White, N.J. Plasmodium knowlesi: the fifth human malaria parasite. *Clin Infect Dis* **46**, 172-173 (2008).
14. Dzeing-Ella, A., *et al.* Severe falciparum malaria in Gabonese children: clinical and laboratory features. *Malar J* **4**, 1 (2005).
15. Mishra, S.K., Panigrahi, P., Mishra, R. & Mohanty, S. Prediction of outcome in adults with severe falciparum malaria: a new scoring system. *Malar J* **6**, 24 (2007).
16. Robinson, T., Mosha, F., Grainge, M. & Madeley, R. Indicators of mortality in African adults with malaria. *Trans R Soc Trop Med Hyg* **100**, 719-724 (2006).
17. White, N.J., *et al.* Malaria. *Lancet* **383**, 723-735 (2014).
18. Monroe, A., Williams, N.A., Ogoma, S., Karema, C. & Okumu, F. Reflections on the 2021 World Malaria Report and the future of malaria control. *Malar J* **21**, 154 (2022).
19. WHO. *World malaria report 2021*. Geneva: World Health Organization; 2021, (2021).
20. WHO. *World malaria report 2020* (2020).
21. WHO. WHO recommends groundbreaking malaria vaccine for children at risk. (2021).
22. Dattoo, M.S., *et al.* Efficacy of a low-dose candidate malaria vaccine, R21 in adjuvant Matrix-M, with seasonal administration to children in Burkina Faso: a randomised controlled trial. *Lancet* **397**, 1809-1818 (2021).
23. Dattoo, *et al.* Efficacy and immunogenicity of R21/Matrix-M vaccine against clinical malaria after 2 years' follow-up in children in Burkina Faso: a phase 1/2b randomised controlled trial. (2022).
24. Mordmuller, B., *et al.* Sterile protection against human malaria by chemoattenuated PfSPZ vaccine. *Nature* **542**, 445-449 (2017).

25. Sulyok, Z., *et al.* Heterologous protection against malaria by a simple chemoattenuated PfSPZ vaccine regimen in a randomized trial. *Nat Commun* **12**, 2518 (2021).
26. Cawlfeld, A., *et al.* Safety, toxicity and immunogenicity of a malaria vaccine based on the circumsporozoite protein (FMP013) with the adjuvant army liposome formulation containing QS21 (ALFQ). *Vaccine* **37**, 3793-3803 (2019).
27. Genito, C.J., *et al.* Liposomes containing monophosphoryl lipid A and QS-21 serve as an effective adjuvant for soluble circumsporozoite protein malaria vaccine FMP013. *Vaccine* **35**, 3865-3874 (2017).
28. Hutter, J.N., *et al.* First-in-human assessment of safety and immunogenicity of low and high doses of Plasmodium falciparum malaria protein 013 (FMP013) administered intramuscularly with ALFQ adjuvant in healthy malaria-naive adults. *Vaccine* **40**, 5781-5790 (2022).
29. Baum, J., *et al.* Reticulocyte-binding protein homologue 5 - an essential adhesin involved in invasion of human erythrocytes by Plasmodium falciparum. *Int J Parasitol* **39**, 371-380 (2009).
30. Alanine, D.G.W., *et al.* Human Antibodies that Slow Erythrocyte Invasion Potentiate Malaria-Neutralizing Antibodies. *Cell* **178**, 216-228 e221 (2019).
31. Rts, S.C.T.P. Efficacy and safety of RTS,S/AS01 malaria vaccine with or without a booster dose in infants and children in Africa: final results of a phase 3, individually randomised, controlled trial. *Lancet* **386**, 31-45 (2015).
32. Rts, S.C.T.P., *et al.* First results of phase 3 trial of RTS,S/AS01 malaria vaccine in African children. *N Engl J Med* **365**, 1863-1875 (2011).
33. White, M.T., *et al.* Immunogenicity of the RTS,S/AS01 malaria vaccine and implications for duration of vaccine efficacy: secondary analysis of data from a phase 3 randomised controlled trial. *Lancet Infect Dis* **15**, 1450-1458 (2015).
34. Bojang, K.A., *et al.* Efficacy of RTS,S/AS02 malaria vaccine against Plasmodium falciparum infection in semi-immune adult men in The Gambia: a randomised trial. *Lancet* **358**, 1927-1934 (2001).
35. Polhemus, M.E., *et al.* Evaluation of RTS,S/AS02A and RTS,S/AS01B in adults in a high malaria transmission area. *PLoS One* **4**, e6465 (2009).
36. Nilsson, S.K., Childs, L.M., Buckee, C. & Marti, M. Targeting Human Transmission Biology for Malaria Elimination. *PLoS Pathog* **11**, e1004871 (2015).
37. Amino, R., *et al.* Quantitative imaging of Plasmodium transmission from mosquito to mammal. *Nat Med* **12**, 220-224 (2006).
38. Tavares, J., *et al.* Role of host cell traversal by the malaria sporozoite during liver infection. *J Exp Med* **210**, 905-915 (2013).
39. Mota, M.M., *et al.* Migration of Plasmodium sporozoites through cells before infection. *Science* **291**, 141-144 (2001).
40. Sturm, A., *et al.* Manipulation of host hepatocytes by the malaria parasite for delivery into liver sinusoids. *Science* **313**, 1287-1290 (2006).
41. Venugopal, K., Hentzschel, F., Valkiunas, G. & Marti, M. Plasmodium asexual growth and sexual development in the haematopoietic niche of the host. *Nat Rev Microbiol* **18**, 177-189 (2020).
42. Beeson, J.G., *et al.* Challenges and strategies for developing efficacious and long-lasting malaria vaccines. *Sci Transl Med* **11**(2019).
43. Sologub, L., *et al.* Malaria proteases mediate inside-out egress of gametocytes from red blood cells following parasite transmission to the mosquito. *Cell Microbiol* **13**, 897-912 (2011).
44. Cowman, A.F., Healer, J., Marapana, D. & Marsh, K. Malaria: Biology and Disease. *Cell* **167**, 610-624 (2016).
45. Wahl, I. & Wardemann, H. How to induce protective humoral immunity against Plasmodium falciparum circumsporozoite protein. *J Exp Med* **219**(2022).

46. Pombo, D.J., *et al.* Immunity to malaria after administration of ultra-low doses of red cells infected with *Plasmodium falciparum*. *Lancet* **360**, 610-617 (2002).
47. Genton, B., *et al.* A recombinant blood-stage malaria vaccine reduces *Plasmodium falciparum* density and exerts selective pressure on parasite populations in a phase 1-2b trial in Papua New Guinea. *J Infect Dis* **185**, 820-827 (2002).
48. Ogutu, B.R., *et al.* Blood stage malaria vaccine eliciting high antigen-specific antibody concentrations confers no protection to young children in Western Kenya. *PLoS One* **4**, e4708 (2009).
49. Payne, R.O., *et al.* Demonstration of the Blood-Stage *Plasmodium falciparum* Controlled Human Malaria Infection Model to Assess Efficacy of the P. *falciparum* Apical Membrane Antigen 1 Vaccine, FMP2.1/AS01. *J Infect Dis* **213**, 1743-1751 (2016).
50. Sagara, I., *et al.* A randomized controlled phase 2 trial of the blood stage AMA1-C1/Alhydrogel malaria vaccine in children in Mali. *Vaccine* **27**, 3090-3098 (2009).
51. Sheehy, S.H., *et al.* Phase Ia clinical evaluation of the safety and immunogenicity of the *Plasmodium falciparum* blood-stage antigen AMA1 in ChAd63 and MVA vaccine vectors. *PLoS One* **7**, e31208 (2012).
52. Thera, M.A., *et al.* A field trial to assess a blood-stage malaria vaccine. *N Engl J Med* **365**, 1004-1013 (2011).
53. Payne, R.O., *et al.* Human vaccination against RH5 induces neutralizing antimalarial antibodies that inhibit RH5 invasion complex interactions. *JCI Insight* **2**(2017).
54. Fowkes, F.J., Richards, J.S., Simpson, J.A. & Beeson, J.G. The relationship between anti-merozoite antibodies and incidence of *Plasmodium falciparum* malaria: A systematic review and meta-analysis. *PLoS Med* **7**, e1000218 (2010).
55. Marsh, K. & Howard, R.J. Antigens induced on erythrocytes by P. *falciparum*: expression of diverse and conserved determinants. *Science* **231**, 150-153 (1986).
56. Bull, P.C., *et al.* Parasite antigens on the infected red cell surface are targets for naturally acquired immunity to malaria. *Nat Med* **4**, 358-360 (1998).
57. Leech, J.H., Barnwell, J.W., Aikawa, M., Miller, L.H. & Howard, R.J. *Plasmodium falciparum* malaria: association of knobs on the surface of infected erythrocytes with a histidine-rich protein and the erythrocyte skeleton. *J Cell Biol* **98**, 1256-1264 (1984).
58. Tan, J., Piccoli, L. & Lanzavecchia, A. The Antibody Response to *Plasmodium falciparum*: Cues for Vaccine Design and the Discovery of Receptor-Based Antibodies. *Annu Rev Immunol* **37**, 225-246 (2019).
59. Frischknecht, F. & Matuschewski, K. *Plasmodium* Sporozoite Biology. *Cold Spring Harb Perspect Med* **7**(2017).
60. White, M.T., *et al.* The relationship between RTS,S vaccine-induced antibodies, CD4(+) T cell responses and protection against *Plasmodium falciparum* infection. *PLoS One* **8**, e61395 (2013).
61. Nussenzweig, R.S., Vanderberg, J.P., Most, H. & Orton, C. Specificity of protective immunity produced by x-irradiated *Plasmodium berghei* sporozoites. *Nature* **222**, 488-489 (1969).
62. Itsara, L.S., *et al.* The Development of Whole Sporozoite Vaccines for *Plasmodium falciparum* Malaria. *Front Immunol* **9**, 2748 (2018).
63. Julien, J.P. & Wardemann, H. Antibodies against *Plasmodium falciparum* malaria at the molecular level. *Nat Rev Immunol* **19**, 761-775 (2019).
64. Aliprandini, E., *et al.* Cytotoxic anti-circumsporozoite antibodies target malaria sporozoites in the host skin. *Nat Microbiol* **3**, 1224-1233 (2018).
65. Hollingdale, M.R., Nardin, E.H., Tharavanij, S., Schwartz, A.L. & Nussenzweig, R.S. Inhibition of entry of *Plasmodium falciparum* and P. *vivax* sporozoites into cultured cells; an in vitro assay of protective antibodies. *J Immunol* **132**, 909-913 (1984).

66. Hollingdale, M.R., Zavala, F., Nussenzweig, R.S. & Nussenzweig, V. Antibodies to the protective antigen of *Plasmodium berghei* sporozoites prevent entry into cultured cells. *J Immunol* **128**, 1929-1930 (1982).
67. Potocnjak, P., Yoshida, N., Nussenzweig, R.S. & Nussenzweig, V. Monovalent fragments (Fab) of monoclonal antibodies to a sporozoite surface antigen (Pb44) protect mice against malarial infection. *J Exp Med* **151**, 1504-1513 (1980).
68. Yoshida, N., Nussenzweig, R.S., Potocnjak, P., Nussenzweig, V. & Aikawa, M. Hybridoma produces protective antibodies directed against the sporozoite stage of malaria parasite. *Science* **207**, 71-73 (1980).
69. Langhorne, J., Ndungu, F.M., Sponaas, A.M. & Marsh, K. Immunity to malaria: more questions than answers. *Nat Immunol* **9**, 725-732 (2008).
70. Doolan, D.L., Dobano, C. & Baird, J.K. Acquired immunity to malaria. *Clin Microbiol Rev* **22**, 13-36, Table of Contents (2009).
71. Stanisic, D.I., Mueller, I., Betuela, I., Siba, P. & Schofield, L. Robert Koch redux: malaria immunology in Papua New Guinea. *Parasite Immunol* **32**, 623-632 (2010).
72. Wipasa, J., *et al.* Long-lived antibody and B Cell memory responses to the human malaria parasites, *Plasmodium falciparum* and *Plasmodium vivax*. *PLoS Pathog* **6**, e1000770 (2010).
73. Tran, T.M., *et al.* An intensive longitudinal cohort study of Malian children and adults reveals no evidence of acquired immunity to *Plasmodium falciparum* infection. *Clin Infect Dis* **57**, 40-47 (2013).
74. Brown, K. Protective immunity to malaria provides a model for the survival of cells in an immunologically hostile environment. *Nature* **1971;230:163-167**(1971).
75. Tran, T.M., *et al.* Naturally acquired antibodies specific for *Plasmodium falciparum* reticulocyte-binding protein homologue 5 inhibit parasite growth and predict protection from malaria. *J Infect Dis* **209**, 789-798 (2014).
76. Day, K.P. & Marsh, K. Naturally acquired immunity to *Plasmodium falciparum*. *Immunol Today* **12**, A68-71 (1991).
77. Kyes, S.A., Kraemer, S.M. & Smith, J.D. Antigenic variation in *Plasmodium falciparum*: gene organization and regulation of the var multigene family. *Eukaryot Cell* **6**, 1511-1520 (2007).
78. Drew, D.R., *et al.* Defining the antigenic diversity of *Plasmodium falciparum* apical membrane antigen 1 and the requirements for a multi-allele vaccine against malaria. *PLoS One* **7**, e51023 (2012).
79. Fandeur, T. & Chalvet, W. Variant- and strain-specific immunity in Saimiri infected with *Plasmodium falciparum*. *Am J Trop Med Hyg* **58**, 225-231 (1998).
80. King, C.L., *et al.* Biosignatures of Exposure/Transmission and Immunity. *Am J Trop Med Hyg* **93**, 16-27 (2015).
81. Kobayashi, T., *et al.* Distinct Antibody Signatures Associated with Different Malaria Transmission Intensities in Zambia and Zimbabwe. *mSphere* **4**(2019).
82. McCallum, F.J., *et al.* Differing rates of antibody acquisition to merozoite antigens in malaria: implications for immunity and surveillance. *J Leukoc Biol* **101**, 913-925 (2017).
83. Liu, E.W., *et al.* Protein-Specific Features Associated with Variability in Human Antibody Responses to *Plasmodium falciparum* Malaria Antigens. *Am J Trop Med Hyg* **98**, 57-66 (2018).
84. Zhao, J., Bhanot, P., Hu, J. & Wang, Q. A Comprehensive Analysis of *Plasmodium* Circumsporozoite Protein Binding to Hepatocytes. *PLoS One* **11**, e0161607 (2016).
85. Zavala, F., Cochrane, A.H., Nardin, E.H., Nussenzweig, R.S. & Nussenzweig, V. Circumsporozoite proteins of malaria parasites contain a single immunodominant region with two or more identical epitopes. *J Exp Med* **157**, 1947-1957 (1983).

86. Wang, L.T., *et al.* A Potent Anti-Malarial Human Monoclonal Antibody Targets Circumsporozoite Protein Minor Repeats and Neutralizes Sporozoites in the Liver. *Immunity* **53**, 733-744 e738 (2020).
87. Foquet, L., *et al.* Vaccine-induced monoclonal antibodies targeting circumsporozoite protein prevent Plasmodium falciparum infection. *J Clin Invest* **124**, 140-144 (2014).
88. Doud, M.B., *et al.* Unexpected fold in the circumsporozoite protein target of malaria vaccines. *Proc Natl Acad Sci U S A* **109**, 7817-7822 (2012).
89. Wahl, I., *et al.* Clonal evolution and TCR specificity of the human TFH cell response to Plasmodium falciparum CSP. *Sci Immunol* **7**, eabm9644 (2022).
90. Dame, J.B., *et al.* Structure of the gene encoding the immunodominant surface antigen on the sporozoite of the human malaria parasite Plasmodium falciparum. *Science* **225**, 593-599 (1984).
91. Enea, V., *et al.* DNA cloning of Plasmodium falciparum circumsporozoite gene: amino acid sequence of repetitive epitope. *Science* **225**, 628-630 (1984).
92. Bowman, S., *et al.* The complete nucleotide sequence of chromosome 3 of Plasmodium falciparum. *Nature* **400**, 532-538 (1999).
93. McCutchan, F.E., *et al.* Diversity of the envelope glycoprotein among human immunodeficiency virus type 1 isolates of clade E from Asia and Africa. *J Virol* **70**, 3331-3338 (1996).
94. Wang, Q., Fujioka, H. & Nussenzweig, V. Mutational analysis of the GPI-anchor addition sequence from the circumsporozoite protein of Plasmodium. *Cell Microbiol* **7**, 1616-1626 (2005).
95. Kusi, K.A., *et al.* Identification of Plasmodium falciparum circumsporozoite protein-specific CD8+ T cell epitopes in a malaria exposed population. *PLoS One* **15**, e0228177 (2020).
96. Guttinger, M., *et al.* Human T cells recognize polymorphic and non-polymorphic regions of the Plasmodium falciparum circumsporozoite protein. *EMBO J* **7**, 2555-2558 (1988).
97. Good, M.F., *et al.* Human T-cell recognition of the circumsporozoite protein of Plasmodium falciparum: immunodominant T-cell domains map to the polymorphic regions of the molecule. *Proc Natl Acad Sci U S A* **85**, 1199-1203 (1988).
98. Kappe, S.H., Buscaglia, C.A., Bergman, L.W., Coppens, I. & Nussenzweig, V. Apicomplexan gliding motility and host cell invasion: overhauling the motor model. *Trends Parasitol* **20**, 13-16 (2004).
99. Aikawa, M., Yoshida, N., Nussenzweig, R.S. & Nussenzweig, V. The protective antigen of malarial sporozoites (Plasmodium berghei) is a differentiation antigen. *J Immunol* **126**, 2494-2495 (1981).
100. Cerami, C., *et al.* The basolateral domain of the hepatocyte plasma membrane bears receptors for the circumsporozoite protein of Plasmodium falciparum sporozoites. *Cell* **70**, 1021-1033 (1992).
101. Frevert, U., *et al.* Malaria circumsporozoite protein binds to heparan sulfate proteoglycans associated with the surface membrane of hepatocytes. *J Exp Med* **177**, 1287-1298 (1993).
102. Menard, R., *et al.* Circumsporozoite protein is required for development of malaria sporozoites in mosquitoes. *Nature* **385**, 336-340 (1997).
103. Coppi, A., Pinzon-Ortiz, C., Hutter, C. & Sinnis, P. The Plasmodium circumsporozoite protein is proteolytically processed during cell invasion. *J Exp Med* **201**, 27-33 (2005).
104. Stewart, M.J. & Vanderberg, J.P. Malaria sporozoites release circumsporozoite protein from their apical end and translocate it along their surface. *J Protozool* **38**, 411-421 (1991).
105. Vanderberg, J.P. Studies on the motility of Plasmodium sporozoites. *J Protozool* **21**, 527-537 (1974).
106. Coppi, A., *et al.* Heparan sulfate proteoglycans provide a signal to Plasmodium sporozoites to stop migrating and productively invade host cells. *Cell Host Microbe* **2**, 316-327 (2007).
107. Kisalu, N.K., *et al.* A human monoclonal antibody prevents malaria infection by targeting a new site of vulnerability on the parasite. *Nat Med* **24**, 408-416 (2018).
108. Tan, J., *et al.* A public antibody lineage that potently inhibits malaria infection through dual binding to the circumsporozoite protein. *Nat Med* **24**, 401-407 (2018).

109. Sissoko, M.S., *et al.* Safety and efficacy of a three-dose regimen of Plasmodium falciparum sporozoite vaccine in adults during an intense malaria transmission season in Mali: a randomised, controlled phase 1 trial. *Lancet Infect Dis* **22**, 377-389 (2022).
110. Hoffman, S.L., *et al.* Protection of humans against malaria by immunization with radiation-attenuated Plasmodium falciparum sporozoites. *J Infect Dis* **185**, 1155-1164 (2002).
111. Mwakingwe-Omari, A., *et al.* Two chemoattenuated PfSPZ malaria vaccines induce sterile hepatic immunity. *Nature* **595**, 289-294 (2021).
112. Spring, M., *et al.* First-in-human evaluation of genetically attenuated Plasmodium falciparum sporozoites administered by bite of Anopheles mosquitoes to adult volunteers. *Vaccine* **31**, 4975-4983 (2013).
113. Mohamed, N.S., *et al.* Assessment of genetic diversity of Plasmodium falciparum circumsporozoite protein in Sudan: the RTS,S leading malaria vaccine candidate. *Malar J* **20**, 436 (2021).
114. Nussenzweig, R.S., Vanderberg, J., Most, H. & Orton, C. Protective immunity produced by the injection of x-irradiated sporozoites of plasmodium berghei. *Nature* **216**, 160-162 (1967).
115. Epstein, J.E., *et al.* Protection against Plasmodium falciparum malaria by PfSPZ Vaccine. *JCI Insight* **2**, e89154 (2017).
116. Collins, K.A., Snaith, R., Cottingham, M.G., Gilbert, S.C. & Hill, A.V.S. Enhancing protective immunity to malaria with a highly immunogenic virus-like particle vaccine. *Sci Rep* **7**, 46621 (2017).
117. Olotu, A., *et al.* Seven-Year Efficacy of RTS,S/AS01 Malaria Vaccine among Young African Children. *N Engl J Med* **374**, 2519-2529 (2016).
118. Rts, S.C.T.P., *et al.* A phase 3 trial of RTS,S/AS01 malaria vaccine in African infants. *N Engl J Med* **367**, 2284-2295 (2012).
119. Roestenberg, M., *et al.* Protection against a malaria challenge by sporozoite inoculation. *N Engl J Med* **361**, 468-477 (2009).
120. Murugan, R., *et al.* Clonal selection drives protective memory B cell responses in controlled human malaria infection. *Sci Immunol* **3**(2018).
121. Wang, L.T., *et al.* Protective effects of combining monoclonal antibodies and vaccines against the Plasmodium falciparum circumsporozoite protein. *PLoS Pathog* **17**, e1010133 (2021).
122. Gaudinski, M.R., *et al.* A Monoclonal Antibody for Malaria Prevention. *N Engl J Med* **385**, 803-814 (2021).
123. Wu, R.L., *et al.* Low-Dose Subcutaneous or Intravenous Monoclonal Antibody to Prevent Malaria. *N Engl J Med* **387**, 397-407 (2022).
124. Soulas-Sprauel, P., *et al.* V(D)J and immunoglobulin class switch recombinations: a paradigm to study the regulation of DNA end-joining. *Oncogene* **26**, 7780-7791 (2007).
125. Dudley, D.D., Chaudhuri, J., Bassing, C.H. & Alt, F.W. Mechanism and control of V(D)J recombination versus class switch recombination: similarities and differences. *Adv Immunol* **86**, 43-112 (2005).
126. Hwang, J.K., Alt, F.W. & Yeap, L.S. Related Mechanisms of Antibody Somatic Hypermutation and Class Switch Recombination. *Microbiol Spectr* **3**, MDNA3-0037-2014 (2015).
127. Carmona, L.M. & Schatz, D.G. New insights into the evolutionary origins of the recombination-activating gene proteins and V(D)J recombination. *FEBS J* **284**, 1590-1605 (2017).
128. Chi, X., Li, Y. & Qiu, X. V(D)J recombination, somatic hypermutation and class switch recombination of immunoglobulins: mechanism and regulation. *Immunology* **160**, 233-247 (2020).
129. Schatz, D.G., Oettinger, M.A. & Baltimore, D. The V(D)J recombination activating gene, RAG-1. *Cell* **59**, 1035-1048 (1989).

130. Oettinger, M.A., Schatz, D.G., Gorka, C. & Baltimore, D. RAG-1 and RAG-2, adjacent genes that synergistically activate V(D)J recombination. *Science* **248**, 1517-1523 (1990).
131. Hozumi, N. & Tonegawa, S. Evidence for somatic rearrangement of immunoglobulin genes coding for variable and constant regions. *Proc Natl Acad Sci U S A* **73**, 3628-3632 (1976).
132. Roth, D.B. V(D)J Recombination: Mechanism, Errors, and Fidelity. *Microbiol Spectr* **2**(2014).
133. Toyama, H., *et al.* Memory B cells without somatic hypermutation are generated from Bcl6-deficient B cells. *Immunity* **17**, 329-339 (2002).
134. Berek, C., Berger, A. & Apel, M. Maturation of the immune response in germinal centers. *Cell* **67**, 1121-1129 (1991).
135. Jacob, J., Kelsoe, G., Rajewsky, K. & Weiss, U. Intraclonal generation of antibody mutants in germinal centres. *Nature* **354**, 389-392 (1991).
136. Bowers, P.M., Boyle, W.J. & Damoiseaux, R. The Use of Somatic Hypermutation for the Affinity Maturation of Therapeutic Antibodies. *Methods Mol Biol* **1827**, 479-489 (2018).
137. Odegard, V.H. & Schatz, D.G. Targeting of somatic hypermutation. *Nat Rev Immunol* **6**, 573-583 (2006).
138. Buerstedde, J.M., Alinikula, J., Arakawa, H., McDonald, J.J. & Schatz, D.G. Targeting of somatic hypermutation by immunoglobulin enhancer and enhancer-like sequences. *PLoS Biol* **12**, e1001831 (2014).
139. Janeway, C.A., Murphy, K., Travers, P., Walport, M. & Shlomchik, M. J. *Immunobiology: The Immune System in Health and Disease*, (Taylor & Francis, Inc. 5, 2001).
140. Farber, D.L., Netea, M.G., Radbruch, A., Rajewsky, K. & Zinkernagel, R.M. Immunological memory: lessons from the past and a look to the future. *Nat Rev Immunol* **16**, 124-128 (2016).
141. Ratajczak, W., Niedzwiedzka-Rystwej, P., Tokarz-Deptula, B. & Deptula, W. Immunological memory cells. *Cent Eur J Immunol* **43**, 194-203 (2018).
142. Kurosaki, T., Kometani, K. & Ise, W. Memory B cells. *Nat Rev Immunol* **15**, 149-159 (2015).
143. McHeyzer-Williams, M., Okitsu, S., Wang, N. & McHeyzer-Williams, L. Molecular programming of B cell memory. *Nat Rev Immunol* **12**, 24-34 (2011).
144. Jacob, J. & Kelsoe, G. In situ studies of the primary immune response to (4-hydroxy-3-nitrophenyl)acetyl. II. A common clonal origin for periarteriolar lymphoid sheath-associated foci and germinal centers. *J Exp Med* **176**, 679-687 (1992).
145. Berek, C. & Milstein, C. Mutation drift and repertoire shift in the maturation of the immune response. *Immunol Rev* **96**, 23-41 (1987).
146. Victora, G.D. & Nussenzweig, M.C. Germinal Centers. *Annu Rev Immunol* **40**, 413-442 (2022).
147. Tas, J.M., *et al.* Visualizing antibody affinity maturation in germinal centers. *Science* **351**, 1048-1054 (2016).
148. Kepler, T.B., *et al.* Reconstructing a B-Cell Clonal Lineage. II. Mutation, Selection, and Affinity Maturation. *Front Immunol* **5**, 170 (2014).
149. Qi, H. T follicular helper cells in space-time. *Nat Rev Immunol* **16**, 612-625 (2016).
150. Halliley, J.L., *et al.* Long-Lived Plasma Cells Are Contained within the CD19(-)CD38(hi)CD138(+) Subset in Human Bone Marrow. *Immunity* **43**, 132-145 (2015).
151. Dorner, T. & Radbruch, A. Antibodies and B cell memory in viral immunity. *Immunity* **27**, 384-392 (2007).
152. Klein, U., Rajewsky, K. & Kuppers, R. Human immunoglobulin (Ig)M+IgD+ peripheral blood B cells expressing the CD27 cell surface antigen carry somatically mutated variable region genes: CD27 as a general marker for somatically mutated (memory) B cells. *J Exp Med* **188**, 1679-1689 (1998).
153. Wu, Y.C., Kipling, D. & Dunn-Walters, D.K. The relationship between CD27 negative and positive B cell populations in human peripheral blood. *Front Immunol* **2**, 81 (2011).

154. Kurosaki, T., Aiba, Y., Kometani, K., Moriyama, S. & Takahashi, Y. Unique properties of memory B cells of different isotypes. *Immunol Rev* **237**, 104-116 (2010).
155. Neuberger, M.S. Novartis Medal Lecture. Antibodies: a paradigm for the evolution of molecular recognition. *Biochem Soc Trans* **30**, 341-350 (2002).
156. Sundberg, E.J. & Mariuzza, R.A. Molecular recognition in antibody-antigen complexes. *Adv Protein Chem* **61**, 119-160 (2002).
157. Rajewsky, K. Clonal selection and learning in the antibody system. *Nature* **381**, 751-758 (1996).
158. Padlan, E.A. Anatomy of the antibody molecule. *Mol Immunol* **31**, 169-217 (1994).
159. Harris, L.J., *et al.* The three-dimensional structure of an intact monoclonal antibody for canine lymphoma. *Nature* **360**, 369-372 (1992).
160. Wall, R. & Kuehl, M. Biosynthesis and regulation of immunoglobulins. *Annu Rev Immunol* **1**, 393-422 (1983).
161. Chiu, M.L., Goulet, D.R., Teplyakov, A. & Gilliland, G.L. Antibody Structure and Function: The Basis for Engineering Therapeutics. *Antibodies (Basel)* **8**(2019).
162. Schroeder, H.W., Jr. & Cavacini, L. Structure and function of immunoglobulins. *J Allergy Clin Immunol* **125**, S41-52 (2010).
163. Porter, R.R. The hydrolysis of rabbit γ -globulin and antibodies with crystalline papain. *Biochem J* **73**, 119-126 (1959).
164. Palmer, J.L., Nisonoff, A. & Vanholde, K.E. Dissociation of Rabbit Gamma Globulin into Subunits by Reduction and Acidification. *Proc Natl Acad Sci U S A* **50**, 314-321 (1963).
165. Dreyer, W.J. & Bennett, J.C. The molecular basis of antibody formation: a paradox. *Proc Natl Acad Sci U S A* **54**, 864-869 (1965).
166. Tiller, T., *et al.* Efficient generation of monoclonal antibodies from single human B cells by single cell RT-PCR and expression vector cloning. *J Immunol Methods* **329**, 112-124 (2008).
167. Murphy, K., and Weaver, C. . *Janeway Immunologie: The Immune System in Health and Disease*, (Springer Spektrum, Berlin, Heidelberg, 2018).
168. Reth, M. Antigen receptors on B lymphocytes. *Annu Rev Immunol* **10**, 97-121 (1992).
169. Maki, R., *et al.* The role of DNA rearrangement and alternative RNA processing in the expression of immunoglobulin delta genes. *Cell* **24**, 353-365 (1981).
170. Dunnick, W., Hertz, G.Z., Scappino, L. & Gritzmacher, C. DNA sequences at immunoglobulin switch region recombination sites. *Nucleic Acids Res* **21**, 365-372 (1993).
171. Della Corte, E. & Parkhouse, R.M. Biosynthesis of immunoglobulin A (IgA). Secretion and addition of carbohydrate to monomer and polymer forms of a mouse myeloma protein. *Biochem J* **136**, 589-596 (1973).
172. Davis, A.C. & Shulman, M.J. IgM--molecular requirements for its assembly and function. *Immunol Today* **10**, 118-122; 127-118 (1989).
173. Darlow, J.M. & Stott, D.I. Gene conversion in human rearranged immunoglobulin genes. *Immunogenetics* **58**, 511-522 (2006).
174. Zan, H. & Casali, P. Regulation of Aicda expression and AID activity. *Autoimmunity* **46**, 83-101 (2013).
175. Rees, A.R. Understanding the human antibody repertoire. *MAbs* **12**, 1729683 (2020).
176. Hong, B., *et al.* In-Depth Analysis of Human Neonatal and Adult IgM Antibody Repertoires. *Front Immunol* **9**, 128 (2018).
177. Murugan, R., Imkeller, K., Busse, C.E. & Wardemann, H. Direct high-throughput amplification and sequencing of immunoglobulin genes from single human B cells. *Eur J Immunol* **45**, 2698-2700 (2015).
178. Masella, A.P., Bartram, A.K., Truszkowski, J.M., Brown, D.G. & Neufeld, J.D. PANDAsseq: paired-end assembler for illumina sequences. *BMC Bioinformatics* **13**, 31 (2012).

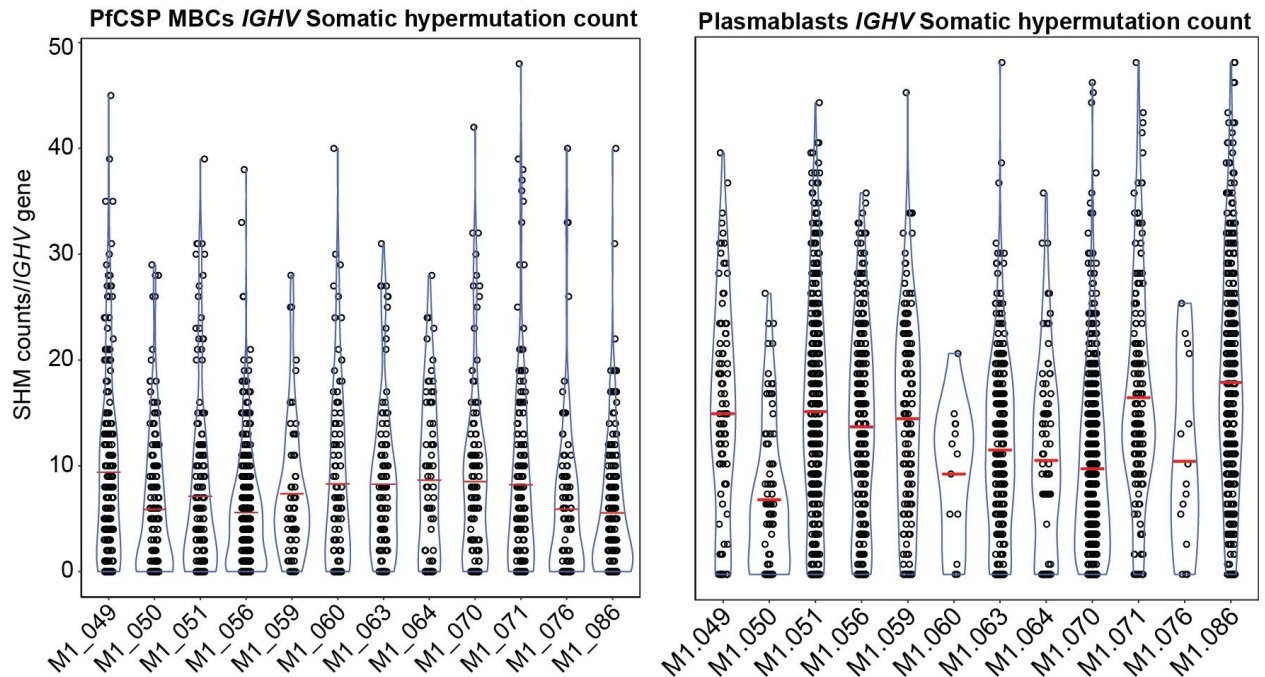
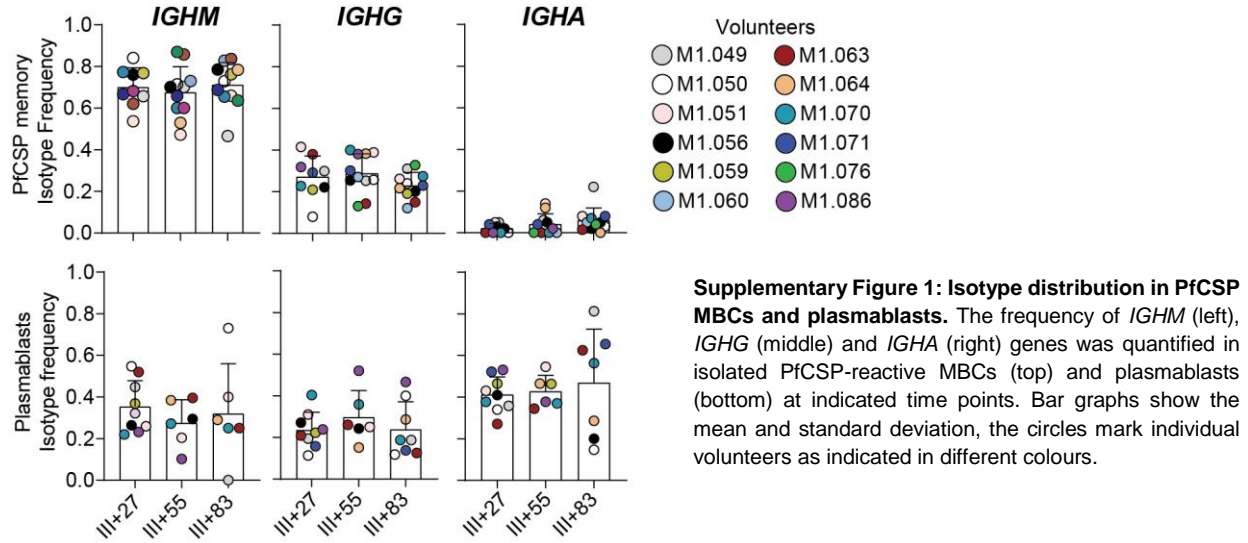
179. Ye, J., Ma, N., Madden, T.L. & Ostell, J.M. IgBLAST: an immunoglobulin variable domain sequence analysis tool. *Nucleic Acids Res* **41**, W34-40 (2013).
180. Team, R.C. R: A language and environment for statistical computing (R Foundation for Statistical, Computing, Vienna, Austria. , 2017).
181. H, W. *ggplot2: Elegant Graphics for Data Analysis*. (Springer-Verlag, New York, 2016).
182. Imkeller, K., *et al.* Antihomotypic affinity maturation improves human B cell responses against a repetitive epitope. *Science* **360**, 1358-1362 (2018).
183. Oyen, D., *et al.* Cryo-EM structure of *P. falciparum* circumsporozoite protein with a vaccine-elicited antibody is stabilized by somatically mutated inter-Fab contacts. *Sci Adv* **4**, eaau8529 (2018).
184. Bijker, E.M., *et al.* Novel approaches to whole sporozoite vaccination against malaria. *Vaccine* **33**, 7462-7468 (2015).
185. Del Giudice, G., *et al.* Detection of human antibodies against *Plasmodium falciparum* sporozoites using synthetic peptides. *J Clin Microbiol* **25**, 91-96 (1987).
186. Keitany, G.J., *et al.* Blood Stage Malaria Disrupts Humoral Immunity to the Pre-erythrocytic Stage Circumsporozoite Protein. *Cell Rep* **17**, 3193-3205 (2016).
187. De Angelis, M.L., *et al.* Repeated Exposure to Subinfectious Doses of SARS-CoV-2 May Promote T Cell Immunity and Protection against Severe COVID-19. *Viruses* **13**(2021).
188. Scheid, J.F., *et al.* Broad diversity of neutralizing antibodies isolated from memory B cells in HIV-infected individuals. *Nature* **458**, 636-640 (2009).
189. Breton, G., *et al.* Persistent cellular immunity to SARS-CoV-2 infection. *J Exp Med* **218**(2021).
190. Wang, Z., *et al.* Naturally enhanced neutralizing breadth against SARS-CoV-2 one year after infection. *Nature* **595**, 426-431 (2021).
191. Wang, Z., *et al.* Humoral immunity to SARS-CoV-2 elicited by combination COVID-19 vaccination regimens. *J Exp Med* **219**(2022).
192. Brown, A.E., *et al.* IgM antibody responses to the circumsporozoite protein in naturally acquired *falciparum* malaria. *J Clin Immunol* **8**, 342-348 (1988).
193. Collins, W.E., Skinner, J.C. & Jeffery, G.M. Studies on the persistence of malarial antibody response. *Am J Epidemiol* **87**, 592-598 (1968).
194. Kinyanjui, S.M., Conway, D.J., Lanar, D.E. & Marsh, K. IgG antibody responses to *Plasmodium falciparum* merozoite antigens in Kenyan children have a short half-life. *Malar J* **6**, 82 (2007).
195. Weiss, G.E., *et al.* The *Plasmodium falciparum*-specific human memory B cell compartment expands gradually with repeated malaria infections. *PLoS Pathog* **6**, e1000912 (2010).
196. Cavanagh, D.R., *et al.* A longitudinal study of type-specific antibody responses to *Plasmodium falciparum* merozoite surface protein-1 in an area of unstable malaria in Sudan. *J Immunol* **161**, 347-359 (1998).
197. Dorfman, J.R., *et al.* B cell memory to 3 *Plasmodium falciparum* blood-stage antigens in a malaria-endemic area. *J Infect Dis* **191**, 1623-1630 (2005).
198. Stoute, J.A., *et al.* Long-term efficacy and immune responses following immunization with the RTS,S malaria vaccine. *J Infect Dis* **178**, 1139-1144 (1998).
199. Espinosa, D.A., *et al.* Proteolytic Cleavage of the *Plasmodium falciparum* Circumsporozoite Protein Is a Target of Protective Antibodies. *J Infect Dis* **212**, 1111-1119 (2015).
200. Kurtovic, L., Drew, D.R., Dent, A.E., Kazura, J.W. & Beeson, J.G. Antibody Targets and Properties for Complement-Fixation Against the Circumsporozoite Protein in Malaria Immunity. *Front Immunol* **12**, 775659 (2021).
201. Plassmeyer, M.L., *et al.* Structure of the *Plasmodium falciparum* circumsporozoite protein, a leading malaria vaccine candidate. *J Biol Chem* **284**, 26951-26963 (2009).

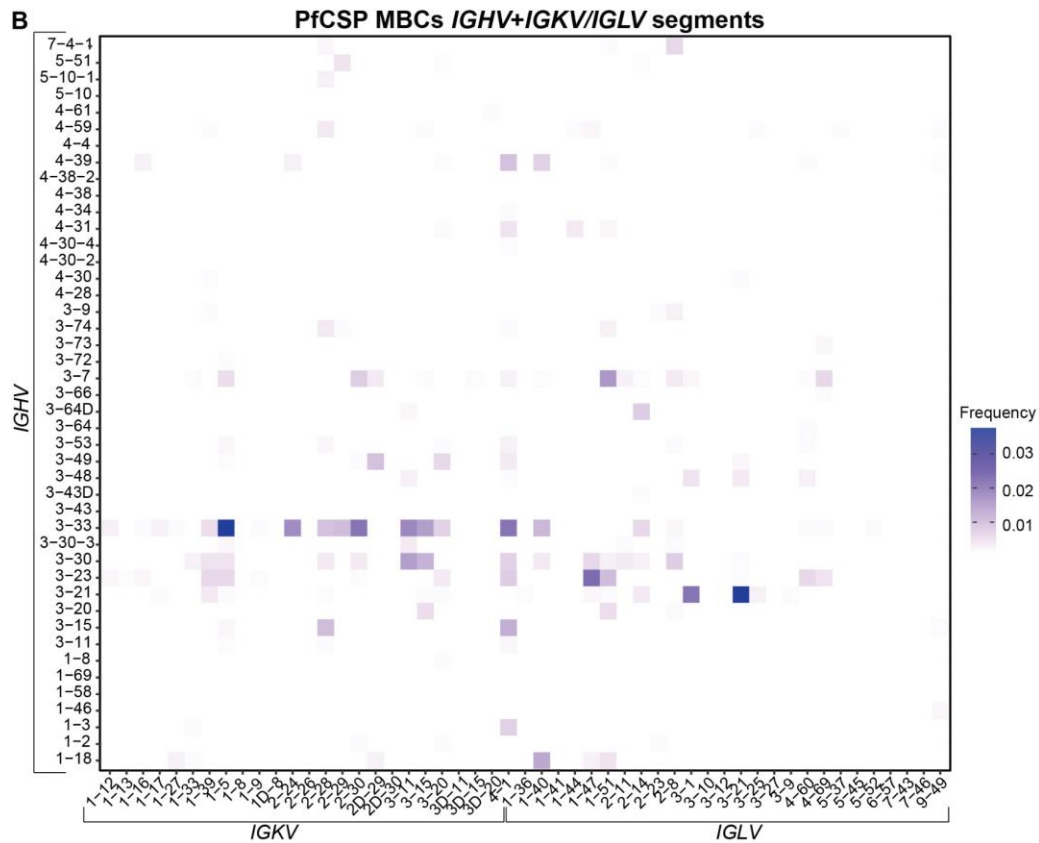
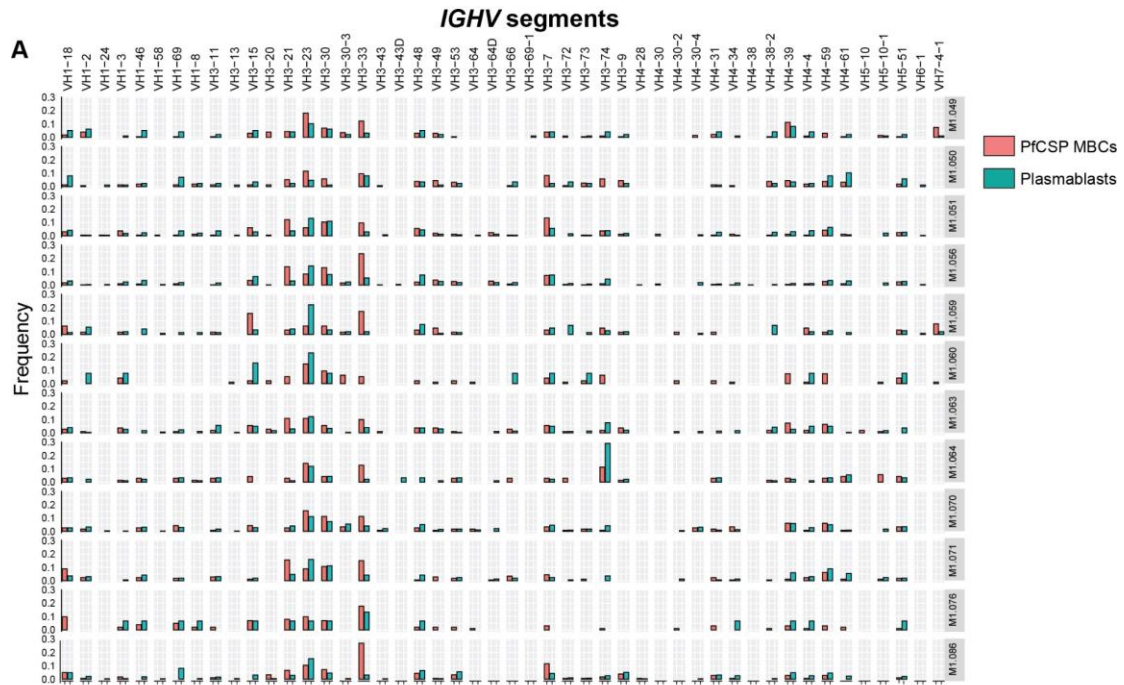
202. Chaudhury, S., *et al.* Breadth of humoral immune responses to the C-terminus of the circumsporozoite protein is associated with protective efficacy induced by the RTS,S malaria vaccine. *Vaccine* **39**, 968-975 (2021).
203. Chaudhury, S., *et al.* The biological function of antibodies induced by the RTS,S/AS01 malaria vaccine candidate is determined by their fine specificity. *Malar J* **15**, 301 (2016).
204. Dobano, C., *et al.* Concentration and avidity of antibodies to different circumsporozoite epitopes correlate with RTS,S/AS01E malaria vaccine efficacy. *Nat Commun* **10**, 2174 (2019).
205. Hershberg, U. & Luning Prak, E.T. The analysis of clonal expansions in normal and autoimmune B cell repertoires. *Philos Trans R Soc Lond B Biol Sci* **370**(2015).
206. Lv, H., *et al.* Cross-reactive antibody response between SARS-CoV-2 and SARS-CoV infections. *bioRxiv* (2020).
207. Robbiani, D.F., *et al.* Recurrent Potent Human Neutralizing Antibodies to Zika Virus in Brazil and Mexico. *Cell* **169**, 597-609 e511 (2017).
208. Ghia, E.M., *et al.* Use of IGHV3-21 in chronic lymphocytic leukemia is associated with high-risk disease and reflects antigen-driven, post-germinal center leukemogenic selection. *Blood* **111**, 5101-5108 (2008).
209. Tobin, G., *et al.* Somatically mutated Ig V(H)3-21 genes characterize a new subset of chronic lymphocytic leukemia. *Blood* **99**, 2262-2264 (2002).
210. Tobin, G., *et al.* Chronic lymphocytic leukemias utilizing the VH3-21 gene display highly restricted Vlambda2-14 gene use and homologous CDR3s: implicating recognition of a common antigen epitope. *Blood* **101**, 4952-4957 (2003).
211. Sharova, I. [Life forms and significance of convergence and parallelism in their classification]. *Zh Obshch Biol* **34**, 563-570 (1973).
212. Jackson, K.J., *et al.* Human responses to influenza vaccination show seroconversion signatures and convergent antibody rearrangements. *Cell Host Microbe* **16**, 105-114 (2014).
213. Vollmers, C., Sit, R.V., Weinstein, J.A., Dekker, C.L. & Quake, S.R. Genetic measurement of memory B-cell recall using antibody repertoire sequencing. *Proc Natl Acad Sci U S A* **110**, 13463-13468 (2013).
214. Roy, B., *et al.* High-Throughput Single-Cell Analysis of B Cell Receptor Usage among Autoantigen-Specific Plasma Cells in Celiac Disease. *J Immunol* **199**, 782-791 (2017).
215. MacRaid, C.A., Seow, J., Das, S.C. & Norton, R.S. Disordered epitopes as peptide vaccines. *Pept Sci (Hoboken)* **110**, e24067 (2018).
216. MacRaid, C.A., *et al.* Conformational dynamics and antigenicity in the disordered malaria antigen merozoite surface protein 2. *PLoS One* **10**, e0119899 (2015).
217. Tan, J., *et al.* A LAIR1 insertion generates broadly reactive antibodies against malaria variant antigens. *Nature* **529**, 105-109 (2016).
218. Herrera, R., *et al.* Reversible Conformational Change in the Plasmodium falciparum Circumsporozoite Protein Masks Its Adhesion Domains. *Infect Immun* **83**, 3771-3780 (2015).
219. McNamara, H.A., *et al.* Antibody Feedback Limits the Expansion of B Cell Responses to Malaria Vaccination but Drives Diversification of the Humoral Response. *Cell Host Microbe* **28**, 572-585 e577 (2020).
220. Imkeller, K., Arndt, P.F., Wardemann, H. & Busse, C.E. sciReptor: analysis of single-cell level immunoglobulin repertoires. *BMC Bioinformatics* **17**, 67 (2016).
221. Smith, K., *et al.* Fully human monoclonal antibodies from antibody secreting cells after vaccination with Pneumovax(R)23 are serotype specific and facilitate opsonophagocytosis. *Immunobiology* **218**, 745-754 (2013).
222. Kwong, P.D. & Wilson, I.A. HIV-1 and influenza antibodies: seeing antigens in new ways. *Nat Immunol* **10**, 573-578 (2009).

223. North, B., Lehmann, A. & Dunbrack, R.L., Jr. A new clustering of antibody CDR loop conformations. *J Mol Biol* **406**, 228-256 (2011).
224. Collis, A.V., Brouwer, A.P. & Martin, A.C. Analysis of the antigen combining site: correlations between length and sequence composition of the hypervariable loops and the nature of the antigen. *J Mol Biol* **325**, 337-354 (2003).
225. Coppi, A., *et al.* The malaria circumsporozoite protein has two functional domains, each with distinct roles as sporozoites journey from mosquito to mammalian host. *J Exp Med* **208**, 341-356 (2011).
226. Kurtovic, L., *et al.* Human antibodies activate complement against Plasmodium falciparum sporozoites, and are associated with protection against malaria in children. *BMC Med* **16**, 61 (2018).
227. Boyle, M.J., *et al.* Human antibodies fix complement to inhibit Plasmodium falciparum invasion of erythrocytes and are associated with protection against malaria. *Immunity* **42**, 580-590 (2015).
228. Kaba, S.A., *et al.* Protective antibody and CD8+ T-cell responses to the Plasmodium falciparum circumsporozoite protein induced by a nanoparticle vaccine. *PLoS One* **7**, e48304 (2012).
229. Seth, L., *et al.* Development of a self-assembling protein nanoparticle vaccine targeting Plasmodium falciparum Circumsporozoite Protein delivered in three Army Liposome Formulation adjuvants. *Vaccine* **35**, 5448-5454 (2017).
230. Wardemann, H. & Busse, C.E. Expression Cloning of Antibodies from Single Human B Cells. *Methods Mol Biol* **1956**, 105-125 (2019).

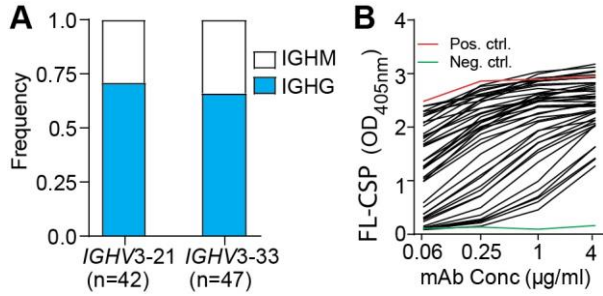
8.0 SUPPLEMENTARY DATA

8.1 Supplementary Figures

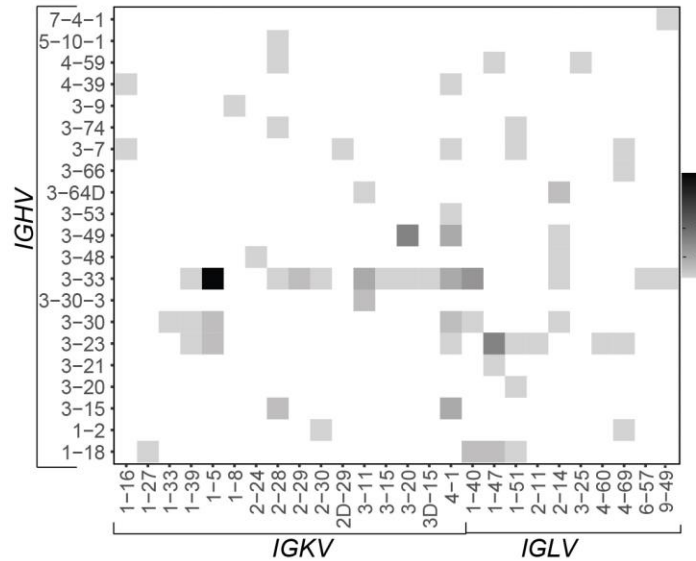




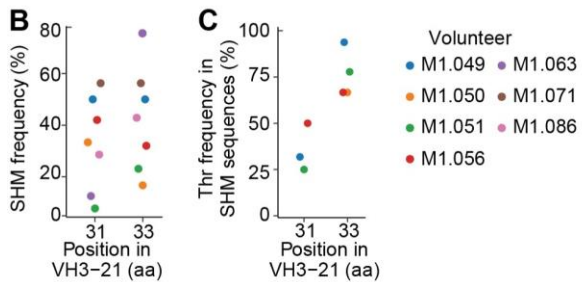
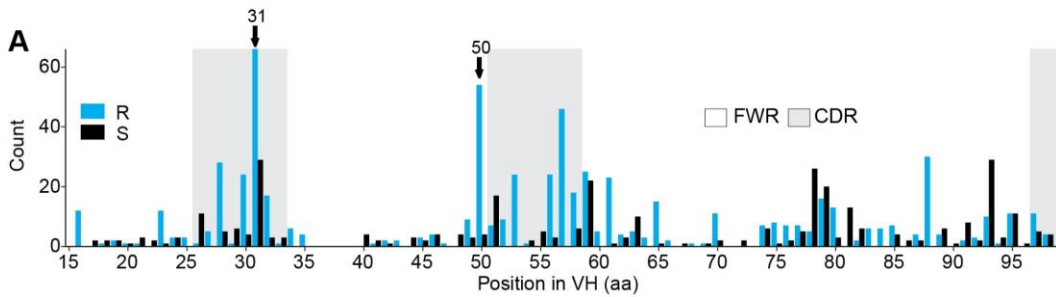
Supplementary Figure 3: Ig gene segments usage. (A) Frequency of *IGHV* segments in PfcSP MBCs (Salmon) and plasmablasts (green) in indicated volunteers. **(B)** Frequency of paired heavy (*IGHV*) and light chain (*IGKV/IGLV*) Ig gene usage in PfcSP MBCs (A; n=1884).



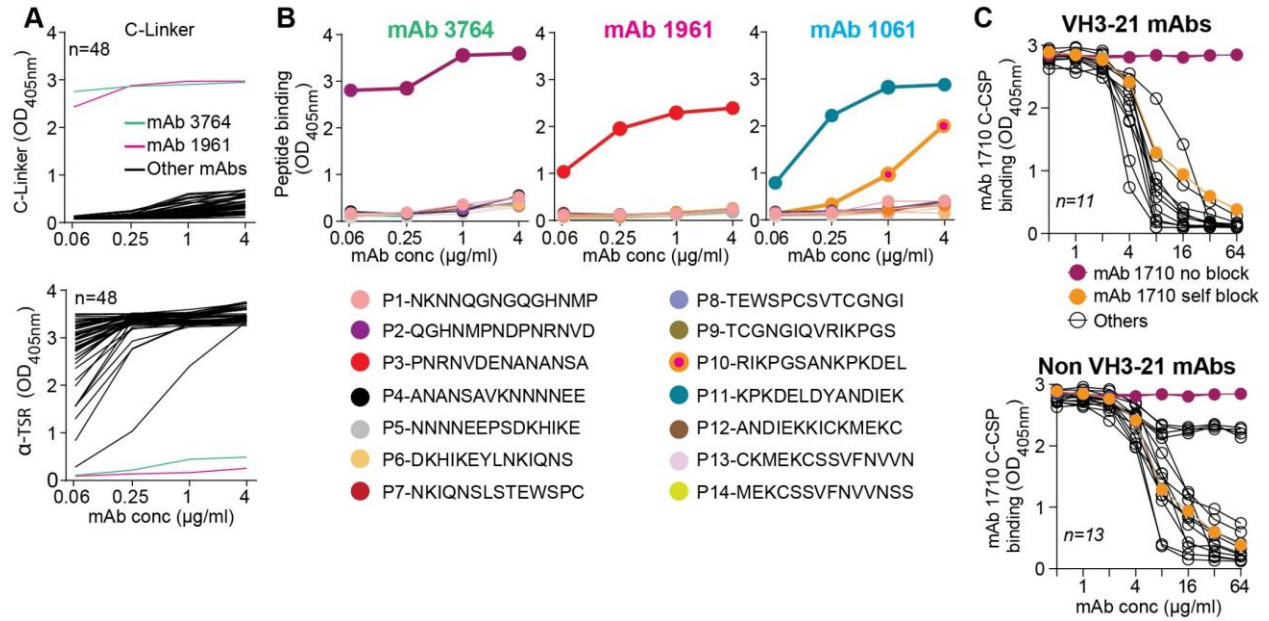
Supplementary Figure 4: Anti-PfCSP reactivity of memory B cell mAbs. (A) Isotype distribution of *IGHV3-21* and *IGHV3-33* encoded mAbs selected for cloning. (B) Representative ELISA curves showing the binding of PfCSP-reactive memory B-cell mAbs, or positive control mAb 2A10¹, or negative control mAb mGO53³, to full-length PfCSP (FL-CSP).



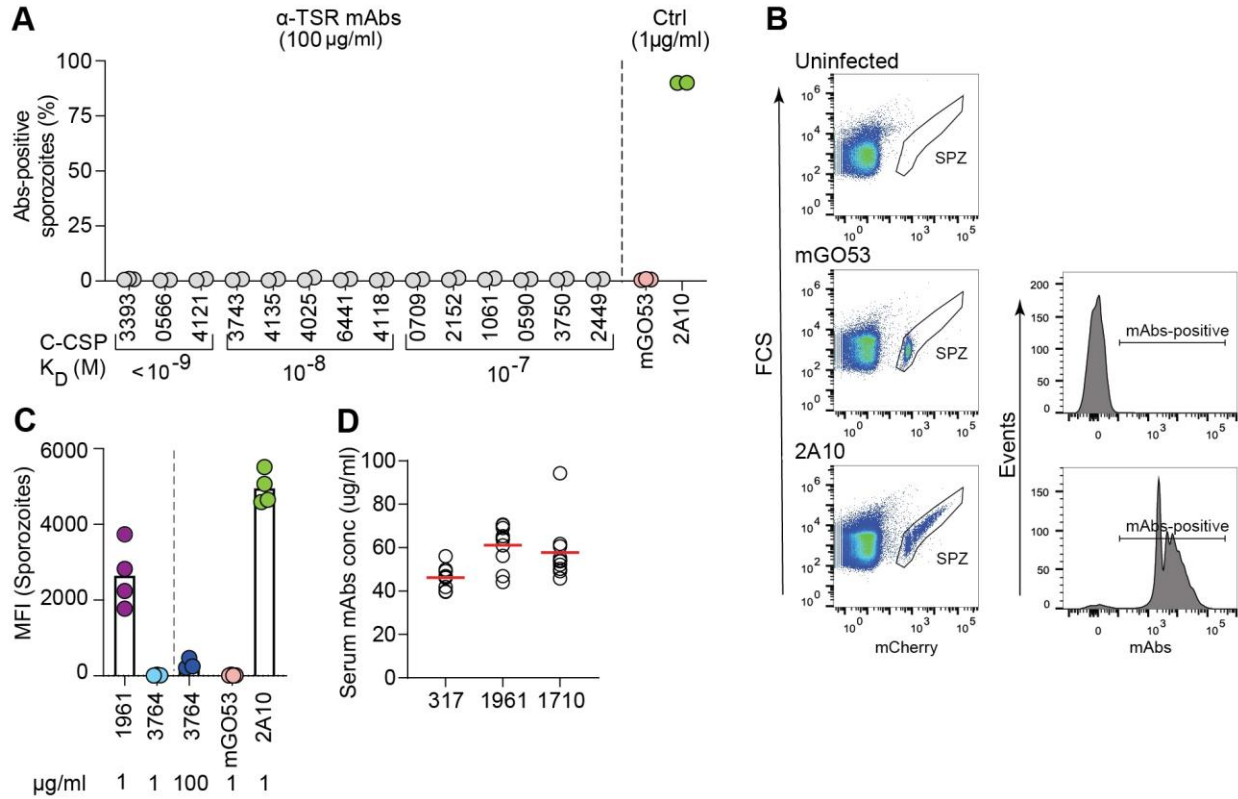
Supplementary Figure 5: Strong enrichment of *IGHV3-33* paired with *IGKV1-5* in NANP reactive mAbs. Frequency of paired heavy (*IGHV*) and light chain (*IGKV/IGLV*) Ig gene usage in NANP reactive mAbs with or without cross-reactivity to the N-Junc (n=102).



Supplementary Figure 6: Replacement mutation in VH3-33 and VH3-21 mAbs. (A) Amino acid (aa) VH replacement (light blue bars) and silent (black bars) mutations in VH3-33 mAbs (n=299). R, Replacement mutation; S, Silent mutation; FWR, framework region; CDR, complementarity-determining region. (B and C) Frequency of aa replacement mutation (B) and frequency of selected threonine at position H.31 and H.33 (C) in VH3-21 mAbs in indicate volunteers. Only volunteers with at least 5 VH3-21 sequences and volunteers with ≥ 4 mutated sequences at position H.33 are shown. These analyses were performed by Anna Obratsova.



Supplementary Figure 7: C-CSP-specific mAbs target epitopes in the C-linker and the α -TSR subdomains. (A) Representative ELISA curves showing the binding capacity of C-CSP specific mAbs to the C-linker (top) and α -TSR (bottom) subdomains. The C-linker specific mAb 3764 (green line), C-CSP cross-reactive mAb 1961 (magenta line) and Th3R binding mAb 1061 (light blue line) are indicated. **(B)** Representative ELISA curves showing binding of C-linker specific mAb 3764 (left), cross-reactive mAb 1961 (middle) and Th3R binding mAb 1061 (right) to peptides (P1-P14) covering the complete C-CSP. Amino acids of each peptide are indicated in different colours. **(C)** Representative ELISA curves illustrating the ability of VH3-21 (top) and non-VH3-21 (bottom) C-CSP-specific mAbs (black lines) to block mAb 1710⁵ binding to C-CSP. mAb 1710 self-block (orange line) and no block (red-violet line) are shown for comparison and experimental control.



Supplementary Figure 8: C-CSP specific mAbs lack protective capacity. (A) Percentage of live *Plasmodium berghei* sporozoites (*Pb-PfCSP*) stained by α -TSR-specific C-CSP mAbs (100 $\mu\text{g/ml}$) as determined by flow cytometry. The anti-NANP mAb 2A10¹ and irrelevant mAb mGO53³, both tested at 1 $\mu\text{g/ml}$, are shown for comparison (n=2-3). (B) Gate set for flow cytometric analysis of mAb-positive *Pb-PfCSP* transgenic live sporozoites expressing mCherry (*PbPfCSP*(mCherry)). Gating was performed on *PbPfCSP*(mCherry) live sporozoites (SPZ). Salivary gland extracts from uninfected mosquitoes were used as a control for the sporozoite gating. To facilitate comparison, the sporozoite binding profiles of the negative control mAb mGO53³ and the positive control anti-NANP mAb 2A10¹ are highlighted. (C) Mean fluorescence intensity (MFI) of mAb-positive live *Pb-PfCSP* sporozoites of C-linker specific mAb 3764 tested at 1 $\mu\text{g/ml}$ or 100 $\mu\text{g/ml}$, and cross-reactive mAb 1961 and control mAbs 2A10 and mGO53, tested at 1 $\mu\text{g/ml}$. Each circle in (C) represents one experiment. (D) Concentrations of monoclonal mAbs in the serum of mice after passive immunization with the indicated mAbs. Each open circle represents one mouse (n=10 for mAb 317⁸; n=8 for mAb 1961 and n=9 for mAb 1710⁵). Data shown in A to C were carried out by Dr. Giulia Costa in the laboratory of Professor Elena A. Levashina at the Max Planck Institute for Infection Biology in Berlin, Germany.

8.2 Supplementary Tables

Supplementary Table 1: Number of PfCSP reactive memory B cells and plasmablasts sequenced and cloned from indicated volunteers at indicated time points.

PfCSP Memory B cells						
	Sequenced antibodies			Cloned antibodies		
Donor	III+14	III+35	III+63	III+14	III+35	III+63
M1.049	67	107	58	24	23	-
M1.050	25	35	96	4	13	-
M1.051	41	36	88	13	12	-
M1.056	213	134	65	26	26	-
M1.059	43	NA	21	10	-	-
M1.060	-	37	58	-	12	-
M1.063	29	14	67	11	5	-
M1.064	NA	34	37	-	9	-
M1.070	22	10	84	5	1	-
M1.071	24	73	83	9	15	-
M1.076	NA	46	55	-	8	-
M1.086	132	50	-	29	12	-
Plasmablasts						
	Sequenced antibodies					
Donor	III+14	III+35	III+63			
M1.049	67	NA	32			
M1.050	53	NA	34			
M1.051	216	196	-			
M1.056	129	136	-			
M1.059	144	NA	5			
M1.060	NA	NA	13			
M1.063	177	119	8			
M1.064	NA	86	7			
M1.070	342	184	16			
M1.071	140	NA	29			
M1.076	NA	NA	15			
M1.086	147	244	-			

**NA: Sample not available

Supplementary Table 2: Gene features and reactivity of mAbs cloned from PfCSP memory B cells (n=267).

mAbs			IGH			IGK/IGL	Cluster size	ELISA (AUC)											Binding affinity K _D (M)		
ID	volunteer	time_point	IGHV	IGHC	SHM (bp)	IGKV/IGLV		FL-CSP	N-Junc	NANP ₅	NANP ₁₀	C-CSP	C-linker	α-TSR	dsDNA	LPS	Insulin	N-Junc	NANP ₅	C-CSP	
L2649x2947	M1.049	III+35	3-30	IGHG1	3	IGKV3-11	2	13.6	0.7	0.7	0.4	13.7	0.6	13.8	0.3	0.2	0.2			7.59E-09	
L2649x2920	M1.049	III+35	3-33	IGHG2	0	IGKV3-11	1	0.7	0.6	0.8	0.4	0.7			0.2	0.1	0.1				
L2649x2912	M1.049	III+35	3-48	IGHG1	5	IGKV3-11	1	0.5	0.4	0.6	0.2	0.6			0.2	0.1	0.1				
L2649x2910	M1.049	III+35	1-2	IGHG1	20	IGKV2-30	1	0.9	1.6	1.8	1.8	1.7			0.3	0.2	0.2				
L2649x2893	M1.049	III+35	3-15	IGHM	10	IGKV1-5	1	0.5	0.6	0.7	0.3	0.7			0.2	0.1	0.1				
L2649x2889	M1.049	III+35	3-21	IGHG1	5	IGLV3-21	1	14.4	0.6	1	0.8	14.4	0.7	13.6	0.1	0.1	0.1			9.73E-10	
L2649x2887	M1.049	III+35	3-33	IGHG1	3	IGKV4-1	1	11.7	0.8	1.1	14.4	0.9			0.2	0.1	0.1				
L2649x2885	M1.049	III+35	3-48	IGHG1	4	IGLV3-1	1	13.6	0.4	0.4	0.1	13.9	0.4	13.2	0.1	0.1	0.1			3.21E-10	
L2649x2871	M1.049	III+35	4-39	IGHG1	8	IGKV4-1	1	3.1	5.9	1	11.4	0.6			0.2	0.1	0.1	3.98E-05	9.71E-04		
L2649x2866	M1.049	III+35	7-4-1	IGHG1	21	IGLV2-8	11	1.2	0.6	0.5	1.8	0.4			0.2	0.1	0.1				
L2649x2852	M1.049	III+35	3-49	IGHM	3	IGKV4-1	1	4.2	1.6	1.3	8.2	1.5			0.3	0.2	0.2				
L2649x2842	M1.049	III+35	3-23	IGHG1	0	IGLV1-47	2	5.7	5	0.4	5.3	0.4			0.3	0.1	0.1	3.81E-06	5.58E-05		
L2649x2826	M1.049	III+35	5-10-1	IGHM	2	IGKV2-28	3	4.1	0.7	1.1	11	0.7			0.1	0.1	0.1				
L2649x2819	M1.049	III+35	3-23	IGHG1	6	IGLV4-60	1	3.2	0.4	0.8	13.3	0.5			0.1	0.1	0.1				
L2649x2817	M1.049	III+14	4-39	IGHG2	24	IGKV1-16	3	4.1	1.9	1	10.7	0.6			0.2	0.1	0.1				
L2649x2813	M1.049	III+35	1-2	IGHG2	18	IGLV4-69	1	6.6	1	0.9	8.9	1.1			0.2	0.1	0.1				
L2649x2801	M1.049	III+35	3-21	IGHG1	8	IGKV1-5	1	13.9	0.4	0.6	0.5	14.5	0.4	13.7	0.2	0.1	0.1			7.34E-09	
L2649x2788	M1.049	III+35	3-49	IGHA1	8	IGLV3-21	3	1.6	0.5	0.5	1	0.4			0.1	0.1	0.1				
L2649x2745	M1.049	III+35	7-4-1	IGHG1	29	IGLV2-8	11	1.6	0.6	0.7	1.9	0.4			0.2	0.1	0.1				
L2649x2740	M1.049	III+35	3-30	IGHG1	4	IGLV1-47	1	12.7	13.4	0.4	1.8	0.4			0.2	0.1	0.1	3.22E-06	2.93E-04		
L2649x2739	M1.049	III+35	3-9	IGHG1	6	IGKV1-8	1	4.1	1.5	1.3	6.5	0.9			0.1	0.1	0.1				
L2649x2729	M1.049	III+35	3-23	IGHG1	26	IGLV1-51	4	4.6	5.4	0.5	5.3	0.5			0.2	0.1	0.1	4.41E-05	1.29E-04		
L2649x2726	M1.049	III+35	1-2	IGHG1	3	IGKV1-33	1	12.8	0.6	0.6	0.1	13.7	0.4	13.6	0.2	0.1	0.1			7.42E-09	
L2649x2719	M1.049	III+35	4-39	IGHM	14	IGLV1-40	9	0.8	0.8	0.8	0.2	0.9			0.2	0.1	0.1				
L2649x1857	M1.049	III+14	4-59	IGHG1	11	IGLV3-25	3	5.9	1.7	0.8	8.3	0.9			0.2	0.1	0.1				
L2649x1833	M1.049	III+14	1-18	IGHG1	14	IGLV1-47	2	5.5	14.7	1.1	6.7	0.6			0.1	0.1	0.1	2.43E-05	3.54E-06		
L2649x1810	M1.049	III+14	3-20	IGHG1	0	IGLV1-51	2	11.9	14.5	0.8	7.9	0.5			0.1	0.1	0.1	9.59E-06	2.32E-04		
L2649x1805	M1.049	III+14	3-21	IGHG1	5	IGLV3-1	1	14.6	0.4	0.5	0.6	14.8	0.4	13.4	0.1	0.1	0.1			1.66E-09	

L2649x1790	M1.049	III+14	3-23	IGHM	17	IGLV1-51	12	1.2	1.9	0.6	0.9	0.6			0.1	0.1	0.1			
L2649x1789	M1.049	III+14	3-48	IGHG1	4	IGLV2-14	1	14.4	10.1	2.2	14.2	0.5			0.2	0.1	0.1	1.46E-05	7.20E-06	
L2649x1767	M1.049	III+14	3-33	IGHM	8	IGLV2-8	3	1.6	0.8	0.7	1.7	0.6			0.1	0.1	0.1			
L2649x1766	M1.049	III+14	1-2	IGHG3	14	IGKV2-30	1	9.6	0.5	0.6	14.4	0.6			0.2	0.1	0.1			
L2649x1745	M1.049	III+14	3-7	IGHM	21	IGKV4-1	2	14.1	14.1	3.6	14	1.4			0.1	0.1	0.1	1.72E-06	4.23E-07	
L2649x1739	M1.049	III+14	3-15	IGHM	7	IGKV4-1	2	1.2	0.7	0.5	1.7	0.5			0.1	0.1	0.1			
L2649x1726	M1.049	III+14	1-18	IGHG1	15	IGLV1-47	2	5.7	14.4	1.1	4.7	0.6			0.2	0.1	0.1	8.97E-06	3.93E-06	
L2649x1719	M1.049	III+14	3-33	IGHG1	0	IGKV4-1	2	13.7	1.8	7.8	14.2	0.6			0.2	0.1	0.1	1.32E-04	1.11E-06	
L2649x1704	M1.049	III+14	3-21	IGHG1	6	IGLV3-1	1	5.5	0.5	0.6	0.6	14.4	0.6	13.3	0.1	0.1	0.1			7.72E-08
L2649x1648	M1.049	III+14	4-59	IGHG3	45	IGLV1-47	1	7.8	8.7	0.7	10.2	0.8			0.2	0.2	0.2	1.45E-04	9.40E-04	
L2649x1647	M1.049	III+14	3-30-3	IGHG1	4	IGKV3-11	1	12.5	1.1	1.8	14.6	0.8			0.1	0.1	0.1			
L2649x1643	M1.049	III+14	4-39	IGHG1	15	IGKV1-16	1	0.6	0.6	0.9	1.4	0.8			0.2	0.1	0.1			
L2649x1608	M1.049	III+14	3-49	IGHM	15	IGKV2-30	2	0.7	1.5	0.8	1.1	0.9			0.2	0.2	0.2			
L2649x1594	M1.049	III+14	3-7	IGHM	13	IGKV1-5	5	0.7	0.6	0.7	1.4	0.7			0.2	0.1	0.1			
L2649x1593	M1.049	III+14	3-21	IGHG1	5	IGLV3-1	1	14.5	0.5	0.6	0.6	14.7	0.6	13.8	0.1	0.1	0.1			8.31E-09
L2649x1588	M1.049	III+14	3-21	IGHM	0	IGLV3-1	1	5.4	0.4	0.5	0.5	14.5	0.8	13	0.2	0.1	0.1			1.47E-07
L2649x1583	M1.049	III+14	1-2	IGHG1	31	IGKV3-20	1	0.6	0.9	0.8	0.9	0.7			0.2	0.2	0.2			
L2649x1565	M1.049	III+14	3-33	IGHG1	0	IGKV3-20	1	5.7	0.6	0.9	10.7	0.7			0.2	0.1	0.1			
L2649x1548	M1.049	III+14	3-33	IGHM	9	IGLV2-8	3	0.9	0.4	0.5	3.1	0.6			0.1	0.1	0.1			
L2650x3051	M1.050	III+35	3-49	IGHM	2	IGKV4-1	1	4.8	1.4	1.7	13	0.6			0.2	0.1	0.1			
L2650x3038	M1.050	III+35	3-7	IGHM	7	IGKV2D-29	5	4.1	0.8	1	13	0.7			0.2	0.1	0.1			
L2650x3033	M1.050	III+35	3-21	IGHG1	5	IGLV1-51	1	14.4	0.9	0.9	0.7	14.4	0.5	13.7	0.1	0.1	0.1			1.11E-08
L2650x3022	M1.050	III+35	3-21	IGHM	1	IGLV1-47	1	9.4	12.8	0.6	5.4	0.7			0.1	0.1	0.1	2.74E-06	1.63E-05	
L2650x3016	M1.050	III+35	3-53	IGHM	3	IGLV2-8	2	1.2	0.5	0.5	2	0.4			0.1	0.1	0.1			
L2650x3013	M1.050	III+35	3-9	IGHG3	4	IGLV2-8	1	12.7	0.5	0.4	0.1	13.4	0.4	12.5	0.1	0.1	0.1			5.13E-08
L2650x3009	M1.050	III+35	3-21	IGHM	0	IGLV2-11	1	9.3	1.1	1	0.7	14.6	1.7	13.7	0.1	0.1	0.1			8.31E-07
L2650x3008	M1.050	III+35	3-9	IGHG3	4	IGLV2-8	1	12.7	0.5	0.4	0.1	13.9	0.6	13.5	0.1	0.1	0.1			1.07E-07
L2650x2988	M1.050	III+35	3-33	IGHG1	1	IGKV3D-15	1	9.6	1.2	1.5	14.5	0.6			0.2	0.1	0.1			
L2650x2982	M1.050	III+35	3-74	IGHM	0	IGLV1-51	4	3.7	11.9	0.5	5.5	0.4			0.1	0.1	0.1	5.18E-06	4.56E-04	
L2650x2970	M1.050	III+35	3-33	IGHG3	6	IGKV3-11	1	13.1	14.1	14.2	14.8	1.1			0.3	0.2	0.2	2.42E-06	1.33E-09	
L2650x2959	M1.050	III+35	3-48	IGHG1	1	IGLV3-1	1	12.7	0.4	0.4	0.1	14.2	0.4	13.5	0.1	0.1	0.1			1.28E-08
L2650x2956	M1.050	III+35	3-23	IGHG3	7	IGLV1-47	1	12.9	12.5	2.2	14.5	0.4			0.1	0.1	0.1	7.35E-06	3.81E-06	

L2650x2113	M1.050	III+14	3-73	IGHM	13	IGLV4-69	3	3.3	9.2	0.6	1	0.7			0.2	0.1	0.1	7.56E-07	9.21E-04	
L2650x2036	M1.050	III+14	3-21	IGHG1	5	IGKV1-5	1	0.5	0.4	0.6	0.5	0.7			0.3	0.1	0.1			
L2650x1954	M1.050	III+14	1-3	IGHM	8	IGLV1-47	1	1.2	2.1	0.7	0.6	0.7			0.3	0.1	0.1			
L2650x1949	M1.050	III+14	3-23	IGHG1	11	IGLV2-11	1	5.7	1.4	1.1	11.1	0.9			0.4	0.1	0.1			
L2351x3667	M1.051	III+14	3-21	IGHG1	2	IGKV1-39	1	12.8	0.9	0.7	1.2	11.8	0.6	13.2	0.2	0.2	0.2			3.49E-09
L2351x3584	M1.051	III+14	3-21	IGHG3	10	IGKV1D-8	1	6.7	2.1	1.2	1.2	11.1	1.9	13.7	0.6	0.6	0.6			1.19E-06
L2351x3567	M1.051	III+14	3-33	IGHG1	11	IGKV1-5	2	8.2	1.2	2	8.8	0.7			0.3	0.3	0.3			
L2351x3550	M1.051	III+14	3-49	IGHA1	0	IGLV1-47	1	1.1	0.2	0.6	0.2	0.5			0.5	0.3	0.3			
L2351x3547	M1.051	III+14	3-21	IGHM	0	IGLV3-1	1	9.4	0.7	0.5	0.6	11.9	1.8	12.5	0.3	0.3	0.3			2.12E-07
L2351x3515	M1.051	III+14	3-64D	IGHG1	3	IGKV3-11	3	1.8	0.2	0.9	0.2	0.8			0.4	0.4	0.4			
L2351x3483	M1.051	III+14	1-3	IGHM	0	IGLV2-14	1	1.2	0.3	1	0.3	0.8			0.2	0.2	0.2			
L2351x3260	M1.051	III+35	1-3	IGHM	4	IGKV4-1	1	0.6	0.1	0.6	0.5	0.6			0.2	0.2	0.2			
L2351x3216	M1.051	III+35	3-23	IGHM	2	IGLV1-47	1	9.8	10.5	5.7	10.2	1.3			0.2	0.1	0.1	2.54E-06	5.85E-07	
L2351x3210	M1.051	III+35	3-33	IGHG1	13	IGKV1-5	1	11.1	11.8	11.1	12.4	1.2			0.5	0.4	0.4	1.16E-06	1.01E-10	
L2351x3186	M1.051	III+35	3-33	IGHG1	15	IGLV9-49	1	8.2	2.6	1.5	8.7	1.6			0.5	0.5	0.5			
L2251x3205	M1.051	III+14	3-74	IGHG1	0	IGLV1-47	1	1.9	1.2	0.5	1.2	1.6			0.1	0.1	0.1			
L2251x3195	M1.051	III+14	3-33	IGHG1	1	IGLV1-40	1	11.9	0.6	11	12.3	0.7			0.2	0.1	0.1	7.06E-04	1.42E-06	
L2251x3177	M1.051	III+14	3-30	IGHM	2	IGLV1-40	5	12	1.2	9.3	12.5	0.9			0.1	0.2	0.2	4.48E-06	1.07E-06	
L2251x3133	M1.051	III+14	3-33	IGHG1	9	IGKV1-5	1	11.1	8.7	11.1	12.6	1.4			0.6	0.6	0.6	3.06E-06	4.98E-08	
L2251x3128	M1.051	III+14	3-21	IGHG1	2	IGLV3-1	1	13.6	0.4	0.4	0.9	12	0.9	13.6	0.2	0.2	0.2			2.91E-08
L2251x3112	M1.051	III+14	3-15	IGHG2	22	IGKV4-1	1	1.2	1	1	1	0.8			0.4	0.4	0.4			
L2251x0762	M1.051	III+35	3-48	IGHG1	2	IGLV3-21	1	9.3	0.7	0.7	0.3	11.4	2	13.8	0.2	0.2	0.2			3.70E-08
L2251x0709	M1.051	III+35	3-48	IGHG1	6	IGKV3-11	1	13.7	0.5	0.5	1.1	12	1	13.9	0.4	0.2	0.2			4.11E-08
L2251x0621	M1.051	III+35	3-23	IGHG1	3	IGLV3-25	1	8.7	0.6	0.6	1.1	11.4	2	14.2	0.5	0.5	0.5			1.02E-07
L2251x0592	M1.051	III+35	3-30	IGHG1	4	IGKV1-33	1	6.2	0.5	0.8	0.4	10.1	0.8	10	0.2	0.2	0.2			7.55E-07
L2251x0590	M1.051	III+35	1-3	IGHM	4	IGLV3-21	1	10.3	1.2	1.1	1.4	11.9	0.5	13.6	0.4	0.2	0.2			2.45E-07
L2251x0566	M1.051	III+35	3-21	IGHG1	10	IGLV3-21	1	10.2	0.5	0.5	1.3	11.4	0.7	14	0.2	0.2	0.2			5.70E-09
L2251x0555	M1.051	III+35	3-23	IGHG1	12	IGKV1-5	1	8.2	6.2	8.4	10.5	2			0.9	0.9	0.9	6.98E-06	7.74E-06	
L2251x0529	M1.056	III+35	3-64D	IGHM	11	IGKV3-11	3	10.5	0.5	10.5	12.6	0.7			0.3	0.3	0.3	1.37E-05	3.86E-08	
L2656x3503	M1.056	III+35	3-33	IGHM	2	IGLV1-40	1	3.5	0.9	0.7	7.3	0.6			0.2	0.1	0.1			
L2656x3487	M1.056	III+35	3-33	IGHM	12	IGLV2-14	2	3.1	0.9	0.6	4.4	0.6			0.2	0.1	0.1			
L2656x3467	M1.056	III+35	1-3	IGHM	6	IGKV4-1	2	0.8	0.9	0.9	2.6	0.7			0.2	0.1	0.1			

L2656x3466	M1.056	III+35	3-33	IGHM	11	IGKV2-29	6	3.6	0.6	0.8	11.4	0.6			0.1	0.1	0.1			
L2656x3465	M1.056	III+35	3-33	IGHG1	2	IGKV4-1	1	13.1	7	4.7	14.1	0.8			0.2	0.1	0.1	5.78E-06	2.64E-07	
L2356x4192	M1.056	III+14	3-21	IGHG1	0	IGLV3-21	1	11.1	0.5	0.5	0.8	11.4	0.7	14.1	0.2	0.2	0.2			2.77E-09
L2356x4150	M1.056	III+14	3-33	IGHG1	1	IGKV2-29	1	10.1	0.7	6.1	10.2	0.5			0.3	0.3	0.3	1.70E-06	1.05E-06	
L2356x4118	M1.056	III+14	3-23	IGHG1	8	IGLV7-43	1	12.7	1.1	0.9	1.1	11.8	0.5	13.3	0.2	0.1	0.1			2.74E-08
L2356x4109	M1.056	III+14	4-34	IGHM	15	IGKV4-1	1	1.4	1.2	1.1	1.2	1.6			0.6	0.5	0.5			
L2356x4025	M1.056	III+14	4-61	IGHG1	2	IGKV3-20	1	13.9	0.5	0.5	0.8	12	1.1	13.3	0.4	0.5	0.5			2.31E-08
L2356x3988	M1.056	III+14	3-15	IGHG1	0	IGKV2-28	4	13.8	12.7	0.6	8.2	0.6			0.1	0.1	0.1	1.87E-08	3.78E-05	
L2356x3976	M1.056	III+14	3-21	IGHG1	0	IGLV3-25	1	10.5	0.6	0.6	0.8	11	1	13.9	0.5	0.3	0.3			1.73E-07
L2356x3969	M1.056	III+14	3-49	IGHM	5	IGKV3-20	1	0.9	0.9	0.6	0.7	0.6			0.4	0.4	0.4			
L2356x3962	M1.056	III+14	3-23	IGHM	16	IGLV4-69	2	1.4	1.1	0.6	1.2	0.5			0.2	0.2	0.2			
L2356x3960	M1.056	III+14	4-59	IGHG1	4	IGKV2-28	1	13.6	12.6	0.5	5.7	0.5			0.2	0.2	0.2	7.85E-08	6.24E-06	
L2356x3782	M1.056	III+14	3-23	IGHG3	2	IGLV1-47	1	10.4	12.7	1.1	5.4	0.7			0.1	0.1	0.1	7.17E-07	4.57E-05	
L2356x3774	M1.056	III+14	4-30-4	IGHG2	11	IGLV3-21	1	2.2	1.2	1.3	1.4	1.2			0.3	0.3	0.3			
L2356x3764	M1.056	III+14	3-33	IGHG1	7	IGKV2-30	1	10.6	0.6	1.2	0.6	11.7	11.5	1.7	0.5	0.4	0.4			1.72E-07
L2356x3750	M1.056	III+14	1-3	IGHG1	5	IGKV1-33	2	9.9	0.6	0.5	0.4	12.1	0.6	13.3	0.2	0.2	0.2			4.17E-07
L2356x3451	M1.056	III+35	3-30-3	IGHG1	2	IGKV3-11	1	10.6	0.6	0.6	0.9	13.9	0.5	12.9	0.1	0.1	0.1			1.26E-08
L2356x3394	M1.056	III+35	3-21	IGHM	0	IGLV4-60	1	0.7	0.9	0.6	1	0.7			0.2	0.2	0.2			
L2356x3393	M1.056	III+35	3-21	IGHG1	7	IGLV3-1	4	11.2	0.7	0.7	0.9	11.7	1.3	13.9	0.3	0.3	0.3			5.11E-10
L2356x3364	M1.056	III+35	3-30	IGHG2	11	IGKV4-1	2	11.3	8	13.6	12.3	0.5			0.6	0.5	0.5	1.16E-05	2.16E-07	
L2356x3323	M1.056	III+35	3-48	IGHG1	11	IGKV3-11	1	9.9	1.6	1.5	1.5	11.3	2	14.1	0.6	0.7	0.7			1.29E-07
L2356x3307	M1.056	III+35	3-11	IGHA1	4	IGLV3-21	1	0.9	0.9	0.8	0.8	0.8			0.2	0.2	0.2			
L2356x3297	M1.056	III+35	3-49	IGHM	0	IGLV3-21	1	1	1	0.9	1	0.9			0.2	0.2	0.2			
L2356x3290	M1.056	III+35	3-33	IGHG1	7	IGKV1-5	1	11.4	11.3	11.2	12.5	0.7			0.3	0.3	0.3	1.80E-06	1.05E-09	
L2256x1891	M1.056	III+14	3-48	IGHG1	2	IGLV3-21	1	11.7	0.7	1.9	1.9	11.8	0.5	13	0.3	0.2	0.2			1.25E-08
L2256x1850	M1.056	III+14	1-3	IGHM	8	IGKV4-1	1	1.2	1	1.2	1	0.8			0.5	0.5	0.5			
L2256x1823	M1.056	III+14	3-21	IGHM	10	IGLV2-14	1	0.9	1.3	0.6	0.6	0.6			0.6	0.3	0.3			
L2256x1809	M1.056	III+14	3-33	IGHG1	3	IGKV1-39	1	9.2	0.7	2.1	8.2	0.5			0.2	0.2	0.2			
L2256x1798	M1.056	III+14	1-46	IGHM	26	IGLV2-14	1	1.4	1.2	0.7	1.2	0.8			0.6	0.8	0.8			
L2256x1779	M1.056	III+14	3-7	IGHG3	0	IGLV1-40	1	10.2	0.5	0.5	0.4	11.4	0.7	13.7	0.3	0.3	0.3			2.47E-07
L2256x1752	M1.056	III+14	3-21	IGHG1	0	IGLV3-1	1	9.3	0.7	0.4	0.5	10.9	0.9	13.8	0.9	0.2	0.2			1.43E-07
L2256x1726	M1.056	III+14	4-39	IGHM	20	IGKV2-24	1	0.7	0.6	0.6	0.6	0.6			0.2	0.2	0.2			

L2256x1716	M1.056	III+14	3-21	IGHG1	2	IGKV3-15	1	10.9	1.2	1.1	1.2	12	0.7	12.8	0.6	0.6	0.6			9.21E-07
L2256x1715	M1.056	III+14	3-30	IGHM	17	IGLV2-8	1	1.2	1.2	0.9	1.2	0.9			0.4	0.4	0.4			
L2256x1711	M1.056	III+14	3-7	IGHM	15	IGLV2-8	3	1.1	1	0.7	1	1			0.3	0.3	0.3			
L2256x1644	M1.056	III+14	3-43D	IGHM	9	IGLV2-14	2	1.7	1.2	1.1	1.2	0.8			0.2	0.2	0.2			
L2256x1122	M1.056	III+35	4-59	IGHG1	0	IGLV1-44	1	1.1	1	1	1	1			0.9	0.6	0.6			
L2256x1118	M1.056	III+35	3-33	IGHM	7	IGLV2-14	1	0.7	0.7	0.6	0.7	0.4			0.2	0.3	0.3			
L2256x1100	M1.056	III+35	3-20	IGHM	12	IGLV2-14	1	2.6	1.2	0.7	1.2	0.5			0.1	0.1	0.1			
L2256x1061	M1.056	III+35	4-59	IGHG3	6	IGLV1-47	1	12.4	0.5	0.5	1	12.1	1.5	13.3	0.3	0.3	0.3			1.93E-07
L2256x1059	M1.056	III+35	3-23	IGHM	11	IGKV1-39	3	8.6	3.8	2.5	10.2	0.5			0.3	0.2	0.2	2.34E-06	2.92E-06	
L2256x1032	M1.056	III+35	1-3	IGHM	4	IGKV1-33	2	6.2	0.5	0.4	0.4	10.8	0.6	13.3	0.2	0.1	0.1			1.10E-06
L2256x1010	M1.056	III+35	3-64D	IGHM	14	IGLV2-14	10	5.4	1	4.9	8.6	0.7			0.3	0.3	0.3	2.09E-05	3.70E-06	
L2256x0994	M1.056	III+35	3-64D	IGHG1	16	IGLV2-14	10	7.7	0.8	2.5	8.4	1.1			0.2	0.2	0.2	9.02E-05	6.71E-06	
L2256x0952	M1.056	III+35	3-7	IGHM	12	IGKV3-15	1	0.5	0.5	0.5	0.8	0.5			0.3	0.2	0.2			
L2256x0948	M1.056	III+35	3-33	IGHM	10	IGKV2-29	5	0.9	0.7	0.7	0.4	0.8			0.2	0.2	0.2			
L2256x0937	M1.056	III+35	3-21	IGHG1	5	IGLV3-21	1	11.5	1.2	0.6	1.1	12	0.8	13.1	0.3	0.3	0.3			1.34E-08
L2256x0786	M1.056	III+35	3-49	IGHG1	6	IGKV3-20	1	11.2	12.4	10.9	12.4	1			0.4	0.4	0.4	4.77E-08	3.08E-08	
L2256x0772	M1.056	III+35	4-31	IGHG2	33	IGLV1-51	1	0.7	0.9	0.6	0.1	1.4			0.2	0.2	0.2			
L2659x2619	M1.059	III+14	3-15	IGHG1	3	IGKV4-1	1	13.6	8	5.9	14.3	0.8			0.2	0.2	0.2	3.82E-06	2.34E-07	
L2659x2586	M1.059	III+14	3-23	IGHG1	5	IGKV1-5	2	3.5	13	1	5.3	0.6			0.2	0.1	0.1	1.75E-06	6.56E-04	
L2659x2572	M1.059	III+14	3-15	IGHM	6	IGKV4-1	1	3.5	1	1.2	7.9	0.8			0.2	0.1	0.1			
L2659x2509	M1.059	III+14	3-49	IGHG1	25	IGKV3-20	1	3.1	3.5	0.8	4.2	0.7			0.1	0.1	0.1	3.86E-06	1.05E-05	
L2659x2461	M1.059	III+14	1-3	IGHM	5	IGLV2-11	1	1.7	2.2	1.1	2	0.8			0.8	0.3	0.3			
L2659x2446	M1.059	III+14	3-21	IGHG1	5	IGLV3-9	1	14.7	0.4	0.5	0.5	14.7	0.6	13.7	0.1	0.1	0.1			3.21E-08
L2659x2440	M1.059	III+14	3-7	IGHM	11	IGLV2-14	2	0.7	0.6	0.5	0.1	0.4			0.2	0.1	0.1			
L2659x2400	M1.059	III+14	7-4-1	IGHG1	16	IGLV9-49	1	14.3	1	1.8	14.3	0.7			0.3	0.1	0.1			
L2659x2390	M1.059	III+14	3-33	IGHG1	1	IGLV1-40	1	15	9.3	13	14.4	0.6			0.2	0.1	0.1	8.72E-06	1.16E-07	
L2659x2338	M1.059	III+14	3-30	IGHG1	20	IGKV1-33	1	3.7	0.6	1.7	12.8	0.7			0.1	0.1	0.1			
L2660x3210	M1.060	III+35	7-4-1	IGHG1	10	IGLV1-47	3	1	0.8	0.5	0.1	0.5			0.1	0.1	0.1			
L2660x3182	M1.060	III+35	3-49	IGHM	10	IGKV3-20	1	4.8	2.3	0.9	5.5	1.6			0.2	0.2	0.2			
L2660x3151	M1.060	III+35	3-21	IGHG1	0	IGLV3-21	1	14.1	0.4	0.5	0.5	14.6	0.6	14.2	0.1	0.1	0.1			1.03E-07
L2660x3133	M1.060	III+35	3-64	IGHG1	2	IGLV3-9	1	13.6	0.6	0.5	0.1	14.1	0.5	14.1	0.1	0.1	0.1			1.23E-08
L2660x3131	M1.060	III+35	3-53	IGHG1	0	IGKV4-1	1	14.4	14.2	14.1	14.3	0.8			0.3	0.1	0.1	2.47E-06	4.15E-06	

L2660x3116	M1.060	III+35	3-21	IGHG1	3	IGLV3-1	1	14.3	0.5	0.6	0.6	14.5	1	14	0.2	0.1	0.1			1.95E-08
L2660x3101	M1.060	III+35	3-33	IGHG3	0	IGKV1-5	1	14.2	1.1	8	14.6	0.6			0.2	0.1	0.1	4.13E-05	3.57E-06	
L2660x3100	M1.060	III+35	3-30	IGHG1	2	IGKV1-5	1	14.4	1.3	14.8	14.6	0.9			0.4	0.1	0.1	1.04E-06	3.52E-07	
L2660x3097	M1.060	III+35	3-21	IGHM	6	IGKV2-28	1	12.2	0.4	0.5	0.4	14.6	0.8	13.8	0.1	0.1	0.1			7.17E-08
L2660x3090	M1.060	III+35	4-39	IGHG1	11	IGKV4-1	1	1.4	2.1	1	1.2	0.7			0.3	0.1	0.1			
L2660x3077	M1.060	III+35	4-39	IGHG1	29	IGLV1-51	1	0.5	0.5	0.4	0.1	0.4			0.2	0.1	0.1			
L2660x3074	M1.060	III+35	3-30-3	IGHM	2	IGKV3-11	3	9.1	1.7	1.7	14.2	0.6			0.2	0.1	0.1			
L2263x3743	M1.063	III+14	3-9	IGHG1	0	IGLV2-23	1	11.8	0.7	0.7	1.2	12	2.8	13.1	0.7	0.5	0.5			1.04E-08
L2263x3725	M1.063	III+14	3-49	IGHG1	14	IGKV4-1	1	2.8	2.1	0.7	1.5	0.7			0.3	0.2	0.2			
L2263x3715	M1.063	III+14	3-33	IGHM	8	IGKV1-5	1	11.1	10.3	11	11.9	0.7			0.3	0.3	0.3	2.83E-06	1.91E-10	
L2263x3714	M1.063	III+14	3-49	IGHM	2	IGKV3-20	1	11.5	11.4	0.5	10.9	0.5			0.3	0.3	0.3	3.96E-06	1.17E-07	
L2263x3666	M1.063	III+14	3-21	IGHG1	3	IGLV3-21	1	11.6	1.3	0.6	1.2	11.9	0.8	13.1	0.2	0.2	0.2			5.50E-09
L2263x3638	M1.063	III+14	3-30-3	IGHG1	6	IGKV3-11	1	9.1	1.8	2.8	1.2	13.7	1.6	12.5	0.8	0.5	0.5			1.03E-07
L2263x3616	M1.063	III+14	3-48	IGHG1	2	IGLV3-21	1	11.2	1.3	1.4	1.6	11.9	0.7	13	0.2	0.2	0.2			4.63E-08
L2263x3586	M1.063	III+14	3-11	IGHM	9	IGKV4-1	2	0.5	0.4	0.4	0.2	0.3			0.1	0.1	0.1			
L2263x3571	M1.063	III+14	3-21	IGHG1	1	IGLV3-1	1	6.5	0.6	0.5	1.1	11.3	1.1	13.4	0.5	0.5	0.5			1.10E-07
L2263x3550	M1.063	III+14	3-49	IGHM	4	IGKV4-1	1	11.4	1.2	0.6	10.7	0.5			0.3	0.2	0.2			
L2263x3529	M1.063	III+14	1-3	IGHM	9	IGKV4-1	1	1.3	1	0.9	1	1.6			0.4	0.4	0.4			
L2263x0335	M1.063	III+35	3-43	IGHG1	2	IGLV2-14	1	12.6	0.9	0.9	1.2	11.8	0.6	13.2	0.2	0.2	0.2			7.34E-08
L2263x0294	M1.063	III+35	3-33	IGHG1	9	IGLV6-57	1	4.2	1.2	1.1	5.2	0.6			0.3	0.3	0.3			
L2263x0266	M1.063	III+35	3-11	IGHM	5	IGKV3D-20	2	0.9	0.7	0.7	0.9	1.1			0.2	0.2	0.2			
L2263x0234	M1.063	III+35	3-20	IGHM	8	IGLV1-51	1	1	1.2	0.7	0.5	0.9			0.2	0.2	0.2			
L2263x0156	M1.063	III+35	3-21	IGHM	4	IGLV3-21	1	6.6	1.2	1.1	1.2	12.1	1.2	12.9	0.6	0.6	0.6			1.50E-07
L2664x3839	M1.063	III+35	3-74	IGHG1	1	IGKV2-28	6	6.6	5.6	1.1	12.1	0.6			0.3	0.1	0.1	3.30E-07	2.59E-05	
L2664x3797	M1.064	III+35	3-33	IGHG1	0	IGKV1-5	2	14.8	0.9	4.6	14.3	0.6			0.2	0.1	0.1	3.15E-06	4.20E-06	
L2664x3785	M1.064	III+35	3-33	IGHG3	20	IGKV3-15	1	15	14.4	14	14.3	0.6			0.2	0.1	0.1	7.55E-07	5.82E-10	
L2664x3768	M1.064	III+35	3-74	IGHA2	14	IGLV2-14	4	0.5	0.9	0.5	0.1	0.5			0.2	0.1	0.1			
L2664x3713	M1.064	III+35	3-21	IGHG1	2	IGLV3-1	1	14.1	0.5	0.7	0.6	14.6	0.4	13.6	0.2	0.1	0.1			9.61E-08
L2664x3694	M1.064	III+35	4-59	IGHG1	1	IGKV1-5	1	14.9	0.6	0.5	0.4	14.6	0.6	13.8	0.2	0.1	0.1			8.49E-08
L2664x3689	M1.064	III+35	3-7	IGHG2	11	IGKV1-16	2	7.2	1	1.2	10.4	0.7			0.3	0.1	0.1			
L2664x3673	M1.064	III+35	3-33	IGHG1	0	IGKV1-5	2	14.1	0.7	10.2	14.6	0.7			0.2	0.1	0.1	1.03E-05	1.72E-05	
L2664x3626	M1.064	III+35	3-33	IGHG3	17	IGKV2-28	2	14.4	2	12.3	14.3	1.2			0.3	0.1	0.1	2.08E-05	1.54E-07	

L2370x2709	M1.070	III+14	3-23	IGHG1	19	IGLV4-69	1	11.2	0.6	11.4	12.4	0.6			0.1	0.1	0.1	2.36E-05	1.41E-06	
L2270x2816	M1.070	III+35	3-33	IGHM	7	IGKV4-1	1	1	1.2	0.9	0.8	0.9			0.2	0.1	0.1			
L2270x1519	M1.070	III+14	4-34	IGHM	10	IGKV3-11	1	1.1	0.3	1	0.5	1.3			0.2	0.1	0.1			
L2270x1418	M1.070	III+14	3-7	IGHM	12	IGLV1-51	1	9.9	0.5	5.8	10.4	1.4			0.3	0.1	0.1	9.01E-05	3.45E-05	
L2270x1281	M1.070	III+14	3-64	IGHM	26	IGLV4-60	2	0.5	0.7	0.4	0.6	0.3			0.1	0.2	0.2			
L2270x1190	M1.070	III+14	3-30	IGHG1	20	IGLV1-47	1	1.2	0.6	0.9	0.8	0.5			0.1	0.1	0.1			
L2271x4595	M1.071	III+14	3-21	IGHG1	10	IGLV1-51	1	10.8	1.2	0.9	1.5	11.8	2.5	14.3	0.9	0.9	0.9			6.40E-09
L2271x4585	M1.071	III+14	3-33	IGHM	6	IGKV3-20	1	1.2	1.2	0.7	1	1.5			0.2	0.2	0.2			
L2271x4518	M1.071	III+14	1-18	IGHG1	16	IGLV1-40	4	9.8	0.5	1.3	10.4	0.5			0.3	0.3	0.3			
L2271x4426	M1.071	III+14	3-30	IGHG3	21	IGKV1-39	1	8.2	1.3	7.1	12.4	0.9			0.8	0.5	0.5	1.28E-05	7.37E-07	
L2271x4401	M1.071	III+14	4-61	IGHM	9	IGKV3-15	5	0.9	1	0.4	1	0.5			0.2	0.2	0.2			
L2271x4382	M1.071	III+14	3-33	IGHG3	1	IGKV1-5	1	12	7.9	13.9	11.6	0.4			0.3	0.4	0.4	9.90E-06	3.58E-08	
L2271x4342	M1.071	III+14	3-30	IGHG1	4	IGKV1-5	1	11.9	0.8	1.3	11.7	0.9			0.4	0.3	0.3			
L2271x4301	M1.071	III+14	3-33	IGHM	8	IGKV2-30	1	2.4	1.5	0.8	1.2	0.6			0.4	0.3	0.3			
L2271x4232	M1.071	III+14	1-69	IGHG1	8	IGLV2-14	1	1.2	1	1	0.9	1			0.3	0.2	0.2			
L2271x4188	M1.071	III+35	3-23	IGHM	11	IGKV4-1	4	1.6	1.2	0.9	1.2	1.1			0.4	0.4	0.4			
L2271x4164	M1.071	III+35	3-7	IGHG1	0	IGLV3-1	1	9.8	0.5	0.4	0.9	11.5	0.6	13.8	0.2	0.2	0.2			2.54E-08
L2271x4152	M1.071	III+35	3-49	IGHG3	0	IGLV2-14	1	8.2	0.7	1.1	5.7	0.9			0.4	0.4	0.4			
L2271x4135	M1.071	III+35	3-21	IGHG1	5	IGLV6-57	1	11.6	0.6	0.7	0.8	12.1	0.7	13	0.2	0.2	0.2			3.15E-08
L2271x4121	M1.071	III+35	3-30	IGHG1	7	IGLV1-36	1	11.7	1.4	0.6	0.7	12.1	1.1	13.2	0.3	0.2	0.2			9.81E-09
L2271x4097	M1.071	III+35	3-30	IGHM	19	IGKV3-15	4	1.7	1.2	1	1	0.9			0.3	0.3	0.3			
L2271x4067	M1.071	III+35	4-31	IGHM	9	IGLV1-51	2	1	0.8	0.8	0.5	1			0.3	0.2	0.2			
L2271x4063	M1.071	III+35	3-21	IGHM	13	IGLV2-14	1	1.8	1	1.1	0.6	0.8			0.1	0.2	0.2			
L2271x4052	M1.071	III+35	3-30	IGHM	16	IGLV2-14	1	11.5	0.6	1	8.6	0.5			0.2	0.2	0.2			
L2271x4034	M1.071	III+35	3-33	IGHM	5	IGLV4-69	1	2.7	1	1	0.9	0.7			0.3	0.2	0.2			
L2271x4022	M1.071	III+35	3-49	IGHM	4	IGKV3-20	1	1.6	1	1.3	1	1.2			0.2	0.2	0.2			
L2271x3984	M1.071	III+35	3-21	IGHG1	4	IGKV1-39	1	12.5	1.2	1	1.4	11.8	0.8	13	0.3	0.3	0.3			5.12E-07
L2271x3949	M1.071	III+35	1-18	IGHG1	16	IGKV1-27	5	7.9	0.6	1.1	6.7	0.7			0.4	0.3	0.3			
L2271x3941	M1.071	III+35	3-23	IGHG1	1	IGKV4-1	4	5.9	8.7	5.6	5.6	1			0.3	0.4	0.4	9.36E-06	8.32E-06	
L2271x3866	M1.071	III+35	3-66	IGHM	11	IGLV4-69	2	11.9	0.4	14	13.2	0.7			0.2	0.1	0.1	9.24E-05	1.31E-06	
L2676x3323	M1.076	III+35	3-15	IGHM	5	IGKV2-28	1	14.5	14.1	8.5	14.5	1.2			0.3	0.2	0.2	1.18E-06	2.70E-07	
L2676x3315	M1.076	III+35	1-18	IGHG1	8	IGLV1-51	5	1.3	2.8	0.6	0.1	0.6			0.2	0.1	0.1			

L2676x3314	M1.076	III+35	3-21	IGHG1	1	IGLV3-21	1	14.1	0.6	0.8	0.6	14.7	0.2	13.3	0.2	0.1	0.1			1.34E-07
L2676x3302	M1.076	III+35	1-18	IGHG1	18	IGLV1-51	1	4.6	13.3	0.8	5.2	0.5			0.3	0.1	0.1	4.58E-06	2.34E-05	
L2676x3268	M1.076	III+35	3-21	IGHG3	2	IGKV1-16	1	13.9	0.8	1.8	0.8	14.6	0.3	13.4	0.2	0.1	0.1			2.63E-08
L2676x3243	M1.076	III+35	3-15	IGHG1	8	IGKV4-1	1	3.3	13.5	3.6	5.8	0.7			0.2	0.1	0.1	6.09E-07	2.72E-06	
L2676x3221	M1.076	III+35	1-18	IGHM	6	IGLV1-40	4	3.1	0.6	0.7	11.7	0.5			0.1	0.1	0.1			
L2676x3217	M1.076	III+35	3-21	IGHM	2	IGLV3-21	1	14.3	0.5	0.7	0.6	14.7	1.6	13.2	0.2	0.1	0.1			9.76E-09
L2386x2620	M1.086	III+14	3-33	IGHG1	5	IGKV1-5	1	11.2	12	11.1	12.7	0.9			0.3	0.3	0.3	4.29E-06	2.29E-09	
L2386x2611	M1.086	III+14	3-7	IGHG1	19	IGLV4-69	3	0.9	1	0.7	0.2	0.6			0.2	0.1	0.1			
L2386x2600	M1.086	III+14	3-23	IGHM	17	IGKV3-20	1	0.6	0.2	0.6	0.7	0.6			0.3	0.3	0.3			
L2386x2581	M1.086	III+14	3-48	IGHM	0	IGKV2-24	1	5.3	2.2	5	10.2	1.6			0.6	0.6	0.6	3.21E-05	7.08E-06	
L2386x2563	M1.086	III+14	3-33	IGHG1	5	IGKV1-5	1	11.2	12.1	11.3	12.6	1.6			0.5	0.5	0.5	6.44E-07	8.06E-10	
L2386x2513	M1.086	III+14	4-39	IGHM	11	IGLV9-49	1	1.9	0.4	0.6	1	1			0.2	0.3	0.3			
L2386x2428	M1.086	III+14	3-33	IGHG1	8	IGKV1-5	1	14.2	1.9	14.4	14.6	0.8			0.1	0.1	0.1	6.29E-06	1.68E-07	
L2386x2417	M1.086	III+14	1-2	IGHM	19	IGKV3-20	1	0.9	1.5	0.5	0.5	0.5			0.2	0.2	0.2			
L2386x2378	M1.086	III+14	4-39	IGHM	11	IGKV3-20	2	0.9	0.6	0.8	1	1			0.3	0.3	0.3			
L2386x2192	M1.086	III+35	3-21	IGHM	7	IGKV1-9	1	11.2	0.6	0.5	0.6	11.8	1.5	14	0.5	0.8	0.8			1.00E-07
L2386x1594	M1.086	III+35	4-31	IGHG1	17	IGLV1-44	5	2.2	1.4	0.5	0.6	0.5			0.3	0.3	0.3			
L2386x1587	M1.086	III+35	3-23	IGHG1	12	IGLV1-47	4	6.2	7.8	1.2	5.2	1.2			0.4	0.4	0.4	7.98E-06	4.67E-05	
L2386x1582	M1.086	III+35	1-18	IGHG1	14	IGKV2-28	1	1.6	1	1.2	1	1.8			0.5	0.5	0.5			
L2386x1572	M1.086	III+35	3-33	IGHM	11	IGLV2-11	1	1.2	1	0.5	0.5	0.4			0.1	0.1	0.1			
L2286x2608	M1.086	III+14	4-28	IGHG1	6	IGKV1-5	1	2.6	1.4	0.5	0.7	0.5			0.4	0.4	0.4			
L2286x2599	M1.086	III+14	3-21	IGHM	0	IGKV1-13	1	13.8	0.5	0.5	0.6	12	1.1	13.3	0.7	0.5	0.5			6.61E-08
L2286x2573	M1.086	III+14	3-30	IGHG1	31	IGKV4-1	1	11.3	1.5	6.7	12.3	1.8			0.5	0.5	0.5	1.22E-04	6.01E-07	
L2286x2554	M1.086	III+14	3-33	IGHG3	2	IGLV1-40	1	11.4	12.4	11.3	12.6	0.5			0.6	0.7	0.7	1.64E-06	3.71E-08	
L2286x2542	M1.086	III+14	3-33	IGHM	12	IGKV3-20	1	1.1	1	0.8	0.8	0.8			0.3	0.2	0.2			
L2286x2495	M1.086	III+14	3-30	IGHG1	16	IGLV2-8	2	2.1	1.2	1.1	0.9	0.5			0.2	0.2	0.2			
L2286x2490	M1.086	III+14	3-33	IGHG3	0	IGKV2-30	8	11.2	12.2	13.4	12.6	1.4			0.9	0.3	0.3	2.86E-07	4.47E-08	
L2286x2473	M1.086	III+14	3-7	IGHG1	19	IGLV4-69	3	6.7	0.9	2.5	6	0.9			0.2	0.2	0.2			
L2286x2453	M1.086	III+14	1-3	IGHM	1	IGKV2-28	1	8.3	0.7	0.4	0.7	11.7	1.1	13.9	0.3	0.4	0.4			1.42E-06
L2286x2449	M1.086	III+14	3-9	IGHG1	0	IGKV1-12	1	10.9	0.5	0.7	0.7	12	0.4	13.1	0.1	0.1	0.1			5.04E-07
L2286x2431	M1.086	III+14	3-48	IGHG1	4	IGLV3-21	1	6.5	1.5	2.5	2	11.5	2.2	12.6	0.3	0.4	0.4			2.51E-06
L2286x2426	M1.086	III+14	3-33	IGHG1	4	IGKV3-11	1	4	0.9	0.6	8.2	0.5			0.3	0.3	0.3			

L2286x2425	M1.086	III+14	3-33	IGHM	6	IGKV1-9	1	0.7	1	0.6	1	0.7			0.2	0.2	0.2			
L2286x2424	M1.086	III+14	3-30	IGHG1	14	IGLV1-47	1	2.9	1.4	0.5	1.2	0.4			0.2	0.2	0.2			
L2286x2421	M1.086	III+14	3-9	IGHG1	3	IGLV1-40	1	11.7	1.2	0.9	1	11.9	1.4	13.4	0.3	0.3	0.3			4.10E-08
L2286x2412	M1.086	III+14	3-21	IGHG1	1	IGLV3-21	1	5.5	1.5	0.8	0.8	11.8	2.5	14	0.7	0.7	0.7			1.20E-07
L2286x2384	M1.086	III+14	3-9	IGHG1	2	IGLV1-51	1	11.8	1.9	0.8	1.2	11.9	1.4	13.5	0.2	0.2	0.2			2.80E-08
L2286x2377	M1.086	III+14	3-20	IGHG1	0	IGKV3-15	5	1.7	1	0.6	1	0.5			0.2	0.2	0.2			
L2286x2347	M1.086	III+14	3-49	IGHM	3	IGKV3-20	1	11.8	4.3	5	11.3	1.4			0.3	0.3	0.3	1.59E-06	3.33E-08	
L2286x2336	M1.086	III+14	3-33	IGHM	7	IGKV4-1	1	1.6	1	1.1	0.2	0.7			0.3	0.2	0.2			
L2286x2291	M1.086	III+35	3-74	IGHG1	10	IGLV4-69	1	0.6	1	0.6	0.5	0.6			0.2	0.2	0.2			
L2286x2268	M1.086	III+35	3-23	IGHG1	12	IGLV1-47	4	2.1	1.2	0.6	0.5	1.2			0.2	0.2	0.2			
L2286x2152	M1.086	III+35	3-23	IGHG1	3	IGKV1-13	1	11.3	0.5	0.4	0.7	11.7	1.1	13.8	0.2	0.2	0.2			1.64E-07
L2286x2106	M1.086	III+35	3-33	IGHG1	4	IGKV3-11	1	11	0.8	10.8	12.5	1			0.3	0.3	0.3	1.88E-05	3.54E-08	
L2286x2041	M1.086	III+35	3-7	IGHG1	17	IGLV1-47	1	2.2	1.2	0.8	0.5	0.9			0.9	0.9	0.9			
L2286x1984	M1.086	III+35	3-21	IGHG3	4	IGLV3-21	1	13.9	0.5	0.5	1	12	1.2	13.3	0.8	0.7	0.7			1.50E-08
L2286x1961	M1.086	III+35	3-23	IGHG2	11	IGLV4-69	1	11.1	11.7	11.2	12	11.2	11.2	0.2	0.3	0.3	0.2	1.25E-06	4.59E-07	2.48E-06

***mAbs- monoclonal antibodies; ID- mAb identification number; SHM- Somatic hyper-mutation count (base pair); aa- amino acid sequence; CDR- Complementarity determining region; AUC- Area under the curve; dsDNA- double stranded DNA; LPS- Lipopolysaccharide; K_D- Binding kinetics; ND- Not determined

Supplementary Table 3: C-CSP mAbs selected for blocking assay with their respective affinities.

mAbs	Affinity	C-CSP ELISA binding (AUC) of mAb 1710 or 1512 after blocking with indicated mAbs		7G8 FL-CSP (AUC)
		mAb 1710	mAb 1512	
L2356x3393	5.11E-10	15.48		1
L2649x1805	1.41E-09	21.54		1.3
L2356x4192	2.77E-09	18.35		0.8
L2351x3667	3.49E-09	22.46		1.4
L2263x3666	5.50E-09	50.69		2.9
L2251x0566	5.70E-09	18.1		0.6
L2649x2801	5.74E-09	42.07		0.6
L2271x4595	6.40E-09	19.76		10.1
L2649x1593	8.00E-09	19.72		0.5
L2649x2889	9.28E-09	18.09		0.6
L2271x4121	9.81E-09	36.09		12.7
L2251x0621	1.02E-08	40.09		1.6
L2263x3743	1.04E-08	22.59		0.7
L2650x3033	1.09E-08	17.49		13.4
L2660x3133	1.21E-08	18.4		0.6
L2256x1891	1.25E-08	48.59		0.9
L2356x3451	1.26E-08	69.77		0.8
L2256x0937	1.34E-08	28.11		1.4
L2286x1984	1.50E-08	26.99		1.3
L2660x3116	1.74E-08	23.48		0.9
L2356x4025	2.31E-08	145.8	28.33	13.2
L2271x4164	2.54E-08	25.04		0.5
L2676x3268	2.66E-08	41.77		1.8

L2356x4118	2.74E-08	149.3	45.37	10.8
L2659x2446	2.78E-08	46.61		1.5
L2286x2384	2.80E-08	45.21		0.8
L2251x3128	2.91E-08	26.48		2.4
L2271x4135	3.15E-08	47.63		2.2
L2650x2959	3.51E-08	143.9	75.75	13.1
L2251x0762	3.70E-08	41.61		0.8
L2286x2421	4.10E-08	69.39		1.4
L2251x0709	4.11E-08	144.4	27.04	13.1
L2263x3616	4.63E-08	49.29		0.6
L2286x2599	6.61E-08	31.44		1.1
L2263x0335	7.34E-08	51.57		0.5
L2664x3694	9.10E-08	155.2	68.04	13.5
L2664x3713	9.58E-08	55.03		0.6
L2676x3217	9.95E-08	42.57		12
mAb 1710 (scally <i>et al.</i> , 2017)	7.01E-08	53.74	183.6	0.2
mAb 1512 (Beutler <i>et al.</i> , 2022)	2.85E-10	156.8	21.53	NA

***mAbs- Monoclonal antibodies; mAb identification number; number; AUC- Area under the curve; K_D - Binding kinetics; ND- Not determined

Supplementary Table 4: C-CSP mAbs selected for sporozoite binding and inhibitory assays with their respective affinities and inhibitory capacities at indicated concentrations.

mAbs			Epitope specificity	Binding affinity	Av. SPZ. Binding (%)		Av. Traversal inhibition (%)
	ID	VH		VL	K _D (M)	100 µg/ml	1 µg/ml
L2356x3393	3-21	Vλ3-1	Th2R/Th3R	5.11E-10	0.8		4.1
L2251x0566	3-21	Vλ3-21	Th2R/Th3R	5.70E-09	0.4		-3.2
L2271x4121	3-30	Vλ1-36	Th2R/Th3R	9.81E-09	0.7		0.7
L2263x3743	3-9	Vλ2-23	Th2R/Th3R	1.04E-08	0.6		9.9
L2271x4135	3-21	Vλ6-57	Th2R/Th3R	3.15E-08	0.6		-8.3
L2356x4025	4-61	Vκ3-20	RII+	2.31E-08	1		3.5
L2271x4164	3-7	Vλ3-1	Th2R/Th3R	2.54E-08	0.7		-1.6
L2356x4118	3-23	Vλ7-43	RII+	2.74E-08	0.5		5.1
L2251x0709	3-48	Vκ3-11	RII+	4.11E-08	0.6		-12.8
L2286x2152	3-23	Vκ1-13	ND	1.64E-07	1		2
L2356x3764	3-33	Vκ2-30	C-linker	1.72E-07	77	0.9	-12.8
L2256x1061	4-59	Vλ1-47	Linear peptide	1.93E-07	0.9		-10.7
L2251x0590	1-3	Vλ3-21	ND	2.45E-07	0.6		-13.7
L2356x3750	1-3	Vκ1-33	ND	4.17E-07	0.8		16.3
L2286x2449	3-9	Vκ1-12	ND	5.04E-07	0.7		3.1

***mAbs- Monoclonal antibodies; ID- mAb identification number; VH- variable heavy chain segments; VL- Variable light chain segments; K_D - Binding Kinetics; Th2R/Th3R and RII+ specific mAbs as determined by blocking ELISA; C-linker and Linear peptide specific mAbs as determined by ELISA; ND- Not determined; Av.- Average; SPZ- Sporozoites.

Supplementary Table 5: PCR primers for amplification of Ig genes (First PCR) ²³⁰**Heavy chain**

Forward Primer	
Primer	Sequence
<i>hIGHV-1/7-066-fw</i>	ACAGGTGCCCACTCCCAGGTGCAG
<i>hIGHV-1/7-017-fw</i>	ATGGACTIONGGACCTGGAG
<i>hIGHV-1/7-041-fw</i>	TCCTCTTTGTGGTGGCAGCAGC
<i>hIGHV-2-035-fw</i>	TCCACGCTCCTGCTRCTGAC
<i>hIGHV-3-066-fw</i>	AAGGTGTCCAGTGTGARGTGCAG
<i>hIGHV-3-057-fw</i>	TAAAAGGTGTCCAGTGT
<i>hIGHV-4/6-066-fw</i>	CCCAGATGGGTCTGTCCCAGGTGCAG
<i>hIGHV-4-022-fw</i>	ATGAAACACCTGTGGTTCTTCC
<i>hIGHV-5-066-fw</i>	CAAGGAGTCTGTTCCGAGGTGCAG
Reverse Primer	
<i>hIGHA-111-rv</i>	GTCCGCTTTTCGCTCCAGGTCACT
<i>hIGHE-140-rv</i>	AAGGTCATAGTTGTCCCGTTGAGG
<i>hIGHG-137-rv</i>	GGAAGGTGTGCACGCCGCTGGTC
<i>hIGHM-082-rv</i>	GGAAGGAAGTCCTGTGCGAGGC

Kappa chain

Forward Primer	
Primer	Sequence
5' L-V κ 1/2	ATGAGGSTCCCYGCTCAGCTGCTGG
5' L-V κ 3	CTCTTCCTCCTGCTACTCTGGCTCCCAG
5' L-V κ 4	ATTTCTCTGTTGCTCTGGATCTCTG
Reverse Primer	
3' C κ 543	GTTTCTCGTAGTCTGCTTTGCTCA

Lambda chain

Forward Primer	
Primer	Sequence
5' L-Vλ1	GGTCCTGGGCCCAGTCTGTGCTG
5' L-Vλ2	GGTCCTGGGCCCAGTCTGCCCTG
5' L-Vλ3	GCTCTGTGACCTCCTATGAGCTG
5' L-Vλ4/5	GGTCTCTCTCSCAGCYTGTGCTG
5' L-Vλ6	GTTCTTGGGCCAATTTTATGCTG
5' L-Vλ7	GGTCCAATTCYCAGGCTGTGGTG
5' L-Vλ8	GAGTGGATTCTCAGACTGTGGTG
Reverse Primer	
3' hCl-057	CACCAGTGTGGCCTTGTTGGCTTG

Supplementary Table 6: PCR primers for amplification of Ig genes (Second PCR)

Forward Primer	
Primer	Sequence
hIGHV-pan-080-fw	AGGTGCAGCTGCTGGAGTCKGG
Reverse Primer	
hIGHA-076-rv	GGAAGAAGCCCTGGACCAGGC
hIGHE-070-rv	CCAGGCAGCCCAGAGTCACGG
hIGHG-074-rv	AGTCCTTGACCAGGCAGCCC
hIGHM-031-rv	GGGAATTCTCACAGGAGACGA

Second PCR (Kappa chain)

Forward Primer	
Primer	Sequence
5' Pan-Vk	ATGACCCAGWCTCCABYCWCCCTG
Reverse Primer	
3' Ck494	GTGCTGTCCTTGCTGTCCTGCT

Second PCR (Lambda chain)

Forward Primer	
Primer	Sequence
hIGLV-pa1-fw	CAGYCTGYSTGACTCA
hIGLV-pa2-fw	TCCTATGAGCTGACWCAG
Reverse Primer	
3' hCI-040-XhoI	CTCCTCACTCGAGGGYGGGAACAGAGTG

Supplementary Table 7: Specific PCR primers- The restriction sites are highlighted in bold green**Heavy chain**

Forward Primer	
Primer	Sequence
5' Agel VH1	CTGCA ACCGGT GTACATTCCCAGGTGCAGCTGGTGCAG
5' Agel VH1-18	CTGCA ACCGGT GTACATTCCCAGGTTTCAGCTGGTGCAG
5' Agel VH1-24	CTGCA ACCGGT GTACATTCCCAGGTCCAGCTGGTACAG
5' Agel VH1/5	CTGCA ACCGGT GTACATTCCGAGGTGCAGCTGGTGCAG
5' Agel VH3	CTGCA ACCGGT GTACATTCTGAGGTGCAGCTGGTGGAG
5' Agel VH3-9	CTGCA ACCGGT GTACATTCTGAAGTGCAGCTGGTGGAG
5' Agel VH3-23	CTGCA ACCGGT GTACATTCTGAGGTGCAGCTGTTGGAG
5' Agel VH3-33	CTGCA ACCGGT GTACATTCTCAGGTGCAGCTGGTGGAG
5' Agel VH4	CTGCA ACCGGT GTACATTCCCAGGTGCAGCTGCAGGAG
5' Agel VH4-34	CTGCA ACCGGT GTACATTCCCAGGTGCAGCTACAGCAGTG
5' Agel VH4-39	CTGCA ACCGGT GTACATTCCCAGCTGCAGCTGCAGGAG
5' Agel VH6-1	CTGCA ACCGGT GTACATTCCCAGGTACAGCTGCAGCAG
5' Agel VH7	CTGCA ACCGGT GTACATTCTCAGGTGCAGCTGGTGCAATCTGG
Reverse Primer	
3' Sall JH1/2/4/5	TGCGAAG TCGAC GCTGAGGAGACGGTGACCAG
3' Sall JH3	TGCGAAG TCGAC GCTGAAGAGACGGTGACCATTG
3' Sall JH6	TGCGAAG TCGAC GCTGAGGAGACGGTGACCGTG

Kappa chain

Forward Primer	
Primer	Sequence
5' Agel Vk1-5	CTGCA ACCGGT GTACATTCTGACATCCAGATGACCCAGTC
5' Agel Vk1-5b	CTGCA ACCGGT GTACATTCAGACATCCAGTTGACCCAGTCT
5' Agel Vk1-6	CTGCA ACCGGT GTACATTCTGCCATCCAGATGACCCAGTC
5' Agel Vk1-13	CTGCA ACCGGT GTACATTCTGCCATCCAGTTGACCCAGTC
5' Agel Vk1D-43	CTGCA ACCGGT GTACATTGTGCCATCCGGATGACCCAGTC

5' Agel Vκ2-24	CTGCA ACCGGT GTACATGGGGATATTGTGATGACCCAGAC
5' Agel Vκ2-28	CTGCA ACCGGT GTACATGGGGATATTGTGATGACTCAGTC
5' Agel Vκ2-30	CTGCA ACCGGT GTACATGGGGATGTTGTGATGACTCAGTC
5' Agel Vκ3-11	TTGTGCTGCA ACCGGT GTACATTCAGAAATTGTGTTGACACAGT
5' Agel Vκ3-15	CTGCA ACCGGT GTACATTCAGAAATAGTGATGACGCAGTC
5' Agel Vκ3-20	TTGTGCTGCA ACCGGT GTACATTCAGAAATTGTGTTGACGCAGTCT
5' Agel Vκ4-1	CTGCA ACCGGT GTACATTCGGACATCGTGATGACCCAGTC
Reverse Primer	
3' BsiWI Jκ1/4	GCCAC CGTACG TTTGTATYTCCACCTTGGTC
3' BsiWI Jκ2	GCCAC CGTACG TTTGTATCTCCAGCTTGGTC
3' BsiWI Jκ3	GCCAC CGTACG TTTGTATATCCACTTTGGTC
3' BsiWI Jκ5	GCCAC CGTACG TTTAATCTCCAGTCGTGTC

Lambda chain

Forward Primer	
Primer	Sequence
5' Agel Vλ1	CTGCT ACCGGT TCCTGGGCCAGTCTGTGCTGACKCAG
5' Agel Vλ2	CTGCT ACCGGT TCCTGGGCCAGTCTGCCCTGACTCAG
5' Agel Vλ3	CTGCT ACCGGT TCTGTGACCTCCTATGAGCTGACWCAG
5' Agel Vλ4/5	CTGCT ACCGGT TCTCTCTCSCAGCYTGTGCTGACTCA
5' Agel Vλ6	CTGCT ACCGGT TCTTGGCCAATTTTATGCTGACTCAG
5' Agel Vλ7/8	CTGCT ACCGGT TCCAATTCYCAGRCTGTGGTGACYCAG
Reverse Primer	
3' hCl-040-XhoI	CTCCTCA CTCGAG GGYGGGAACAGAGTG

C-CSP	NKNNQGNGQGHNMPNDPNRNVDENANANSAVKNNNNEEPSDKHIKEYLNK IQNSLSTEWSPCSVTCGNGIQVRIKPGSANKPKDEL DYANDIEKKICKMEKCS VFNVVNSS
C-linker	NKNNQGNGQGHNMPNDPNRNVDENANANSAVKNNNNEE
α -TSR	MGILPSPGMPALLSLVSLLSVLLMGCVAETGYVEFEP SDKHIKEYLNKIQNSL STEWSPCSVTCGNGIQVRIKPGSANKPKDEL DYANDIEKKICKMEKCPHHHH HHA
P1	NKNNQGNGQGHNMP
P2	QGHNMPNDPNRNVD
P3	PNRNVDENANANSA
P4	ANANSAVKNNNNEE
P5	NNNNEEPSDKHIKE
P6	DKHIKEYLNKIQNS
P7	NKIQNSLSTEWSPC
P8	TEWSPCSVTCGNGI
P9	TCGNGIQVRIKPGS
P10	RIKPGSANKPKDEL
P11	KPKDEL DYANDIEK
P12	ANDIEKKICKMEKC
P13	CKMEKCSSVFNVVN
P14	MEKCSSVFNVVNSS

9.0 ACKNOWLEDGEMENT

Writing and completing this dissertation marks the end of an epic adventure that began more than four years ago. Without the invaluable help of my family, friends, and co-workers, I doubt if this day would have come to fruition. First and foremost, I am grateful to God, the infinite and unfathomable, for helping me to successfully complete the demanding doctoral program. I would also like to thank my direct principal investigator, Prof. Dr. Hedda Wardemann, whose laboratory I was able to use for this amazing research. I am grateful for the new perspectives you opened up for me, for the scientific freedom to pursue my ideas, and, most importantly, for the encouragement you provided to help me grow professionally in every way. Also, I would like to thank Prof. Dr. Nina Papavasiliou, Prof. Dr. Benjamin Mordmuller, and Prof. Dr. Faith Osier, who were all on my thesis advisory committee, for their insightful critiques, recommendations, and constant scientific support and encouragement throughout my doctoral studies. Moreover, I want to thank Prof. Dr. Oliver Fackler once again for serving on and chairing my thesis defense committee. I would also like to express my gratitude Dr. Guoliang Cui, who graciously agreed to serve on my PhD defense committee.

Prof. Dr. Benjamin Mordmüller and the Tübingen clinical team, as well as the brave volunteers, deserve enormous gratitude for conducting the clinical trial presented in this thesis. In addition, I would like to express my gratitude to Dr. Giulia Costa and Dr. Elena Levashina for their assistance with the parasite inhibitory assays and passive immunization of the monoclonal antibodies. My heartfelt appreciation also goes to Dr. Rajagopal Murugan for his timely and informative scientific advice, thorough training, and unending patience with my many questions. Your enthusiasm and drive were crucial to the completion of my PhD program. Dr. Christian Busse is another person who deserves special recognition for his unwavering encouragement and generosity throughout my doctoral studies. I really appreciate how helpful you are; it really marks you out as a great person. Thank you to Dr. Peter Sehr for his scientific support in measuring the antibody affinities and for the unrestricted use of the SPR machine.

Having fantastic co-workers was also crucial to the successful completion of my sojourn as a PhD student. Specifically, I would like to thank Claudia, Dorien, Julia G., Christine, and Yasmin for their technical support with the orders and cell cultures. A big thank you to everyone in the division of B Cell Immunology, who contributed in one way or the other to this work, especially Josh, Sandro, Anna, Julia L., Zhe, Hannah, Money, Cassandra, Leo, Irene, Ilka, and Tim. The best parts of my PhD studies were the interesting conversations we had, your friendly personality, and your willingness to connect with others. Kindly accept my thanks for being the

glue that holds the lab together. One of the best experiences during my PhD was getting to know all of you during our stimulating conversations and random hangouts.

I would also like to thank my friends and families who have helped me, both literally and figuratively. Thank you for always being there for me, Tayo, a friend who has become more like a brother. Femi, knowing you are there has given me peace of mind. The Abizon family: you made me feel at home and supported me in a foreign land. My heartfelt gratitude also goes to my wonderful parents, Elder and Deaconess I.O. Dada, as well as my siblings, Mrs. Wumi Ogunkoya, Dr. Ayodele Oludada, and Dr. Tosin Dada, for their unwavering support throughout my PhD program. To my father and mother-in-law, Elder and Deaconess Adeyeye, I am immensely grateful for your unending love and prayers, and for blessing me with the most wonderful woman in the world to call my wife. My deepest gratitude goes to my lovely, charming princess, and adorable daughter, Tiwaloluwa. Thank you for sharing this experience with me and bringing happiness and joy into our lives. Daddy loves you. Last but not least, I want to thank my wife, Adewunmi, who is truly a priceless gem, for all the years she has shown me unconditional love, selfless dedication, and constant support. Your help and support in so many ways are indescribable. You boosted my confidence as I sailed to the successful completion of my PhD. I appreciate your perseverance and prayers during the difficult years. I love you, my darling. Finally, the unending journey ends with prestige and honour!!!